May 2020

Characterization of DNA Interstrand Cross-Linking Agents by Liquid Chromatograhy-Mass Spectrometry

Anahit Marina Campbell
University of Wisconsin-Milwaukee

CHARACTERIZATION OF DNA INTERSTRAND CROSS-LINKING AGENTS BY LIQUID CHROMATOGRAHY-MASS SPECTROMETRY

by

Anahit Marina Campbell

A Thesis Submitted in
Partial Fulfillment of the
Requirements for the Degree of

Master of Science
in Chemistry

at

The University of Wisconsin – Milwaukee
May 2020

ABSTRACT

CHARACTERIZATION OF DNA INTERSTRAND CROSS-LINKING AGENTS
BY LIQUID CHROMATOGRAHY-MASS SPECTROMETRY

by

Anahit Marina Campbell

The University of Wisconsin – Milwaukee, 2020
Under the Supervision of Professors Xiaohua Peng and Joseph H. Aldstadt III

This study is to characterize novel reactive oxygen species (ROS)-activated nitrogen mustard analogues and UV-activated alkylating agents by Liquid Chromatography-Mass Spectrometry (LC-MS). First, we optimized the instrument conditions to successfully ionize a few novel binapthalene analogues and methoxybenzene analogues by MS. The highest signal intensity for compounds **3**-**10** was observed when atmospheric pressure chemical ionization (APCI) with an optimized corona needle position of 5mm or 10 mm was used, which led to successful analysis of compounds **3**-**10** by MS. Second, we determined pharmacokinetic properties of a drug compound (**FAN-NM-CH$_3$),** including animal study, assay development, optimization of MS/MS instrumental parameter and the development of a calibration model, and finally quantification of **FAN-NM-CH$_3$** in different tissues, including blood, liver, and brain by LC-MS/MS. The results indicated that the methyl analogue **FAN-NM-CH$_3$** showed a $t_{1/2}$ of 8.84 min that is two times of the parent compound **CWB-20145** with a t1/2 of 4.92 min. The results suggested that introduction of an alkyl group (CH_3) greatly increases in vivo duration, which is an important guide for further modification. The rate of elimination for the parent compound **CWB-20145** in the blood is two times faster (E_{rate} = 0.141 min^{-1}) than that of **FAN-NM-CH$_3$** (E_{rate} = 0.078 min^{-1}). **FAN-NM-CH3** showed an area under the curve (AUC) of 16.25 μg•min/mL, which is significantly higher than

that of **CWB-20145** (10.88 µg•min/mL). Further *in vitro* microsomal stability studies revealed that **FAN-NM-CH$_3$** is significantly more stable in human ($t_{1/2}$ = 77.06 min) than in mouse ($t_{1/2}$ = 33.0 min). The human microsomal stability of **FAN-NM-CH$_3$** supports its design as a human therapeutic.

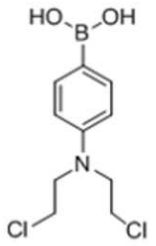

CWB-20145

1

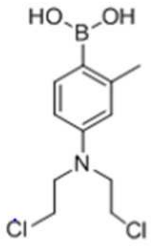

FAN-NM-CH3

2

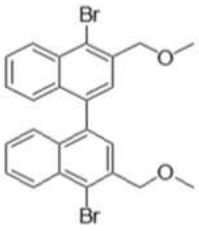

3

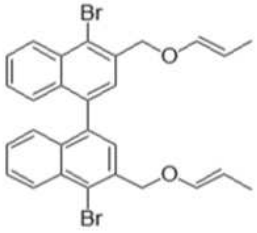

4

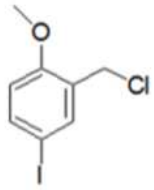

9

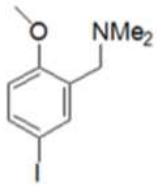

10

for Babu jan and Deda jan

TABLE OF CONTENTS

CHAPTER 1. INTRODUCTION 1

1.1 Halogenated ROS-Activated DNA Interstrand Cross-linking Agents 1
1.1.1 Background 1
1.2 Research Approach 6
1.2.1 Liquid Chromatography (LC) 6
1.2.2 Quantification by Mass Spectrometry (MS) 7
1.3. Characterization of Novel Halogenated Alkylating Compounds by Mass Spectrometry 8
1.3.1 Electrospray Ionization (ESI) 9
1.3.2 Atmospheric Pressure Ionization (APCI) 10
1.3.3 Dual Mode Ionization 11
I.4 Theory of In Vitro Microsomal Stability Studies and Pharmacokinetic Studies 12
1.4.1 In Vitro Microsomal Stability Study of Drug Compound 2 (FAN-NM-CH_3) 12
1.4.2 In Vivo Pharmacokinetic Study of Drug Compound 2 (FAN-NM-CH_3) 13
1.5 Instrumental Hyphenation 13
1.5.1 Analysis of HPLC-UV-NMR-MS Interfacing Scheme 13
1.5.2 LC-NMR Past Improvements 15
1.5.3 Brief Overview of NMR Theory 19
1.5.4 NMR Spectra 20
1.6 Research Goals 21
1.7 Figures and Tables 23
1.8 References 46

CHAPTER 2. EXPERIMENTAL 51

2.1 Experimental Conditions of Liquid Chromatography Mass Spectrometry (LCMS) 51
2.1.1 Chemical Reagents and Compounds 51
2.1.2 Sample Preparation 51
2.1.3 Mobile Phases for LC-MS 51
2.1.4 Instrumentation 53
2.2 Experimental Conditions of Microsomal Stability Assay 56
2.2.1 Chemical Reagents 56

2.2.2 Sample Preparation 56
2.2.3 Mobile Phases for LC-MS/MS 58
2.2.4 Instrumentation 58
2.3 Experimental Conditions of Pharmacokinetic Studies 59
2.3.1 Animal Model and Experimental Practices 59
2.3.2 Chemical Reagents 60
2.3.3 Sample Preparation 61
2.3.4 Mobile Phases in LC-MS/MS System 62
2.3.5 Instrumentation 63
2.4 Experimental Conditions of HPLC-UV-NMR Interfaced Scheme 64
2.4.1 Chemical Reagents 64
2.4.2 Mobile Phases used in Interfaced System 65
2.4.3 Sample Preparation 65
2.4.4 Instrumentation 65
2.5 Figures and Tables 67
2.6 References 77

CHAPTER 3. RESULTS AND DISCUSSION 78

3.1 Characterization of Novel Halogenated Alkylating Compounds by Liquid Chromatography Single Quadruple Mass Spectrometry 78
3.1.1 Mass Spectrometry Ionization Sources – An Overview of the Theory & Practice 78
3.1.2 Method Optimization 78
3.1.3 Characterization of Novel Compounds 79
3.2 Analysis of In Vitro Microsomal Stability Assay 82
3.2.1 Method Optimization 82
3.2.2 Calculations for the Determination of Drug Stability - An Overview of the Theory & Practice 84
3.3 Analysis of In Vivo Pharmacokinetic Studies 86
3.3.1 An Overview of the Theory & Practice 86
3.3.2 Blood Plasma Sample Analysis 86
3.3.3 Liver Sample Analysis 86
3.3.4 Brain Sample Analysis 87
3.4 Analysis of HPLC-UV-NMR Interfacing Scheme 88
3.4.1 HPLC, UV, and NMR - An Overview of the Theory and Practice 88
3.4.2 NMR Component Optimization 88
3.4.3 Interfacing LC-NMR: Flow Injection Manifold Design 89
3.5 Figures and Tables 92
3.6 References 138

CHAPTER 4. CONCLUSION 139

LIST OF FIGURES

CHAPTER 1.

Figure 1-1. Schematic diagram of a single quadrupole MS …… 23

Figure 1-2. Schematic diagram of a triple quadruple MS (MS/MS) ……. 24

Figure 1-3. The electrospray ionization process ……. 25

Figure 1-4. Schematic diagram of an atmospheric pressure chemical ionization source …..…. 26

Figure 1-5. A guide to the polarity regions most appropriate for each ionization source …….. 27

Figure 1-6. A schematic showing the DUIS ionization source ……..……..…. 28

Figure 1-7. Comparative data of DUIS mode ionization …….……...…. 29

Figure 1-8. A graphical depiction of first-order half-life ……. 30

Figure 1-9. Schematics of in-series (LC-NMR-MS) and in-parallel LC-NMR/MS hyphenation (Adapted from Gebretsadik, T., et al) ……... 31

Figure 1-10. Timeline of historical developments with hyphenated NMR techniques ...…… 32

Figure 1-11. LC-NMR/MS work by Lommen et al. to measure glycosides …… 33

Figure 1-12. A schematic demonstrating in-series and in-parallel hyphenation ……...……. 34

Figure 1-13. A schematic of LC-NRM coupled with ion-trap MS detection …….……. 35

Figure 1-14. A schematic of LC- ion-trap MS coupled with NMR …….…… 36

Figure 1-15. A study depicting information obtained from NMR and MS to determine the structure of a drug metabolite. A. is a 500 MHz proton NMR spectrum, B. is a spectrum obtained ESI MS, and finally C. is MS/MS ……...…… 37

Figure 1-16. A schematic of LC-NRM-MS/MS detection ……. 38

Figure 1-17. The first novel example of LC-NMR ……..……. 39

Figure 1-18. A diagram of a novel NMR Teflon probe ……..…….……. 40

Figure 1-19. A diagram of a stain-less steel NMR probe ……..……... 42

Figure 1-20. A schematic diagram of an on-line flow system developed for the LC-NMR method ……..……..…… 42

Figure 1-21. A schematic diagram of a novel microcoil NMR flow probe …….…… 43

Figure 1-22. Spectra of a WET stopped-flow experiment involving a 10 mM sucrose in CH3CN:D2O (50:50). While the spectrum at the stop depicts unsuppressed spectrum with significant solvent resonance at 1.95 ppm, the bottom spectrum includes the WET technique of solvent suppression ……..……..…… 44

Figure 1-23. A depiction of a spinning nuclei under an applied field ……. 45

CHAPTER 2.

Figure 2-1 a and b. Schematic diagram of Shimadzu 8020 LC-MS/MS (adapted from Shimadzu) and Schematic diagram of Shimadzu 8040 LC-MS/MS ……..……..…… 67

Figure 2-2 a and b. Image of the corona discharge needle setting on the MS instrument. 1 = distance intervals (mm) for the adjustment of the corona discharge needle. 2 = the corona discharge needle sample inlet and Image of the corona discharge needle (3) on the MS instrument ……..……..……..…. 68

Figure 2-3. Schematic diagram of Shimadzu 8040 LC-MS/MS (Adapted from Shimadzu …… 69

Figure 2-4. Diagram of the picoSpin NMR components ……. 70

Figure 2-5. Diagram of the picoSpin NMR inlet port and components and Image of the picoSpin NMR inlet port ……...……. 71

Figure 2-6. Schematic of the DVSP instrument (Adapted from Digital Valve Sequence Programmer Instruction Manual ……..……..…… 72

Figure 2-7 a and b. Diagram depicting the terminal strip connections used for the DVSP (Adapted from Digital Valve Sequence Programmer Instruction Manual) and Image of the terminal strip connections used for the DVSP ……..…… 73

Figure 2-8. Diagram of the six-port valve that interfaced the HPLC and NMR ……...……. 74

Figure 2-9. Diagram of the Agilent 1100 HPLC instrument and components ……...……. 75

CHAPTER 3:

Figure 3-1. A diagram depicting compatible ionization sources for particular compound characteristics such as size molecular mass and polarity ……..…… 92

Figure 3-2 a and b. A labeled chromatogram defining the signals produced at critical time points (t_m) and (t_R) and An experimentally acquired chromatogram that labels the terms (t_m) and (t_R) as noted above ……...……... 93

Figure 3-3 a, b, and c. PDA plot of compound 2 using a column, under APCI mode, MS spectrum of compound 2 by flow injection, under APCI mode, and MS spectrum region of interest for compound 2, depicting the Cl isotopic peaks of m/z = 176 and 178, at a 3:1 ratio, under APCI mode ……..…… 94, 95

Figure 3-4 a, b, and c. PDA plot of compound 2 using a column, under APCI mode, MS spectrum of compound 2 by flow injection, under APCI mode, and MS spectrum region of interest for compound 2, depicting the Cl isotopic peaks of m/z = 176 and 178, at a 3:1 ratio, under APCI mode ……..…… 96, 97

Figure 3-5 a-i. Flow injection chromatograph and MS spectrum in APCI mode with corona

discharge needle set to 2-10 mm ……. 98-106

Figure 3-6. A summary of the relative signals produced at different corona discharge needle settings in APCI mode for compound 2 ……. 107

Figure 3-7 a and b. PDA plot of uniodinated compound 10 and An MS spectrum of uniodinated compound 10, in APCI mode with the corona discharge needle set to 5 mm ……..…… 108

Figure 3-8 a and b. PDA plot of iodinated compound 10 and An MS spectrum of iodinated compound 10, in APCI mode with the corona discharge needle set to 5 mm ……..……. 109, 110

Figure 3-9 a and b. A chromatograph of compound 8 and An MS spectrum of compound 8, in APCI mode with the corona discharge needle set to 10 mm …...……. 111

Figure 3-10. An expected MS spectrum, with emphasis on the isotopic peak ratio for compound 8 ……. 112

Figure 3-11 a and b. A chromatograph of compound 11 and An MS spectrum of compound 11, in dual ionization mode with the corona discharge needle set to 10 mm …….…….… 113

Figure 3-12 a and b. A chromatograph of unknown compound and An MS spectrum of unknown compound, in dual ionization mode with the corona discharge needle set to 10 mm ……... 114

Figure 3-13 a and b. MRM spectrum for compound 2, in positive mode and MRM spectrum for compound 2, in negative mode ……..…… 115

Figure 3-14 a and b. Total CE optimization for compound 2 under MRM and CE optimization for compound 2 under MRM, in positive mode …… 116

Figure 3-15 a, b, and c. Chromatograph of first attempt at gradient programming, with an 8 min column run, The gradient programing time events for the first method for gradient programming, with an 8 min column run, and Gradient conditions for the first method for gradient programming …….. 117

Figure 3-16 a, b, and c. Chromatograph of second method at gradient programming, with a 9 min column run, The gradient programing time events for the first method for gradient programming,

with a 9 min column run, and Gradient conditions for the second method for gradient programming ……..…… 118

Figure 3-17 a, b, and c. Chromatograph of third method at gradient programming, with a 4 min column run, The gradient programing time events for the third method for gradient programming, with a 9 min column run, and Gradient conditions for the third method for gradient programming …… 119

Figure 3-18 a and b. Chromatograph depicting peaks detected using a MeOH organic mobile phase and Chromatograph depicting peaks detected after switching to ACN as the organic mobile phase ……..……. 120

Figure 3-19 a and b. 5 nM IS + 500 nM IS compound prepared in MeOH, no water and 5 nM IS + 500 nM compound prepared in 1:3 water:MeOH …….…….……...……. 121

Figure 3-20 a, b, and c. Precision of the IS concentration added to each standard for the microsomal stability assay calibration curve, A calibration curve with compound 2 and no IS, and A calibration curve with compound 2 and 10 nM IS …….. 122

Figure 3-21 a, b, c, and d. The microsomal stability assay calibration curve standard concentrations and respective concentrations for three trials, mean and standard deviation as determined by manual calculation by comparison of area integration and the calculations as acquired from LabSolutions software, Precision of the IS concentration added to each standard for the microsomal stability assay calibration curve as established by using the amended standard concentrations, A microsomal stability study calibration curve with the amended standard concentrations with compound 2 and no IS, and A microsomal stability study calibration curve with the amended standard concentrations with compound 2 and 10 nM IS ……..…….. 123, 124

Figure 3-22 a and b. 125 nM compound 2 + IS with an injection volume of 50 uL and 5 nM compound 2 + IS with an injection volume of 50 uL …… 125

Figure 3-23 a and b. 125 nM compound 2 + IS with an injection volume of 20 uL and 5 nM compound 2 + IS with an injection volume of 20 uL …… 126

Figure 3-24. A depiction of graphical half-life determination for first-order kinetics ….……. 127

Figure 3-25 a and b. Microsomal stability assay for compound 2 results depicting concentration (ppb) at various time points min, for human and mouse microsomes and Microsomal stability assay for compound 2 results depicting percentage ln concentration ratio at various time points min, for human and mouse microsomes……..…… 128

Figure 3-26 a and b. Graph of pharmacokinetic study on plasma compound concentration (ng/mL) vs. time (min) for compound 1 (A.) and compound 2 (B) ...…… 129

Figure 3-27 a and b. Graph of pharmacokinetic study on plasma compound concentration (ng/mL) vs. time (min), experiment 1 and Graph of pharmacokinetic study on plasma compound concentration (ng/mL) vs. time (min), experiment 2 ...…….. 130

Figure 3-28. Graph of pharmacokinetic study on liver compound concentration (ng/mL) vs. time (min) ...……...……. 131

Figure 3-29. Graph of pharmacokinetic study on brain compound concentration (ng/mL) vs. time (min) ...……...……. 132

Figure 3-30. An NMR spectrum of a 10 mM sample of toluene in deuterated chloroform injected into the NMR instrument and analyzed at 62 scans ..……...…….. 133

Figure 3-31 a and b. An NMR spectrum of a 10 mM sample of toluene in deuterated chloroform injected into the NMR instrument and analyzed at 62 scans and An NMR spectrum of a 10 mM sample of toluene injected into the NMR instrument and analyzed at 512 scans …...…...…… 134

Figure 3-32. An integrated NMR spectrum (512 cans) of chloroform (10 mM) in toluene 135

Figure 3-33. An integrated NMR spectrum (512 cans) of chloroform (10 mM) in toluene ….. 136

LIST OF TABLES

CHAPTER 1.

Table I. Studies of anti-cancer drug metabolites using ESI MS …. 46

CHAPTER 2.

Table I. A comparison of the properties of picoSpin models 45 and 80 (Adapted from ThermoFisher Scientific) ……..……...……. 76

CHAPTER 3.

Table I. A table of H-NMR shifts for various solvents ……..…….…… 137

ACKNOWLEDGEMENTS

This work would not be possible without my wonderful family including my loving grandparents, brother, mom and dad; my mom who has set an example of a strong woman in STEM and my dad who has been my math tutor, writing editor, and personal advisor since I was in the first grade.

I am forever appreciative to my advisors. I would like to thank Dr. Xiaohua Peng for believing in me, pushing me to think beyond, being patient with me, always being honest with me, and always supporting me. You are nothing short of the person I hope to someday become and my respect for you is beyond measure. And I thank to Dr. Joseph Aldstadt for his guidance and for all that he has have taught me. You have trained me how to think and this skill has shaped me to become the scientist I am today. And lastly, thank you to my committee member Dr. Andy Pacheco for serving on my committee, your support, and genuine kindness.

I am incredibly grateful to my amazing and inspirational labmates, classmates, and friends in the department. Each of them has inspired me, supported me in many ways, and in have made my time at UWM more pleasant. Thank you especially to Veronica Marco Alvarez, Lisa Kendhammer, and Heli Fan. Thank you to my chemistry family: Qi Zhang, Asad Zaman, Nurul Setu, Taufeeque Ali, Eron Saxon. Thank you to my classmates who have helped me with my work and been an immense resource: Dan Knutson, Elliot DiMilo, Roni Rashid, Milad Momtez, and Mohiminul Islam. Thank you to my past and present analytical group: Liv Heinderlich, Lexie Lanphere, Malati Thapa, Shawn Salske, Garrett Finn.

I thank Dr. Mark Dietz for his on-going support of me since taking his Chem 221 course back in 2012. I also thank Dr. Alan Schwabacher for sharing with his students the love of learning. Thank you to Dr. Anna Benko for help assistance with my mass spectrometry project.

Thank you to all other classmates, friend, and family who have supported me throughout my time completing my Masters.

CHAPTER 1. INTRODUCTION

Mass spectrometry (MS) is perhaps the most widely used analytical method in the pharmacological context of drug development. It is an analytical technique where ions are separated and then detected by means of their mass to charge ratio (m/z). The popularity of MS is due to the fact that it is highly sensitive, selective, and can be hyphenated to other techniques such as liquid chromatography (LC), ultra violet (UV) absorption spectroscopy, nuclear magnetic resonance (NMR) spectroscopy, and several others. This work will focus on the application of single quadrupole (MS) and triple quadrupole (MS/MS) mass spectrometry for analysis of DNA alkylating agents.

LC-MS analysis of the drug compounds consists of sample pretreatment, separation, and detection. Each component has effects on factors such as accuracy, precision, selectivity, and sensitivity of the results (*1*). While sample preparation and separation are generally similar processes among various drug compounds, the difficulty lies in the detection of the compounds because of the fact that the compounds must be ionized for detection to occur with MS. This work will describe the challenges pertaining to the ionization of alkylating agents containing halogens, experimental design for *in vitro* and *in vivo* MS/MS analysis, and finally the design of a novel LC-NMR/MS method that will allow for the high-throughput determination of drug compounds while providing complimentary structural information by NMR as well as MS.

1.1 Halogenated ROS-Activated DNA Interstrand Cross-linking Agents

1.1.1 Background

During WWI, alkylating agents were used not as therapeutic drug compounds but as a warfare agent known as nitrogen mustard gas. Nitrogen mustard reacts with the N7 position of purine bases guanine and adenine in the double strands of DNA and induces DNA interstrand cross-links (ICLs), thus preventing the separation of DNA double helix. Nitrogen mustard has been used as a chemotherapy drug in the 1940s. Early examples of such drugs had been modified for decreased toxicity including chlorambucil and busulfan, which have been approved by the FDA to treat various types of cancer (*2*).

Most cancer diseases have to be treated with systematic chemotherapy or radiotherapy, which has negative adverse effects for the patient due to its lack of selectivity towards the tumor cell. Targeting tumor-specific conditions, such as reactive oxygen species (ROS), can result in a drug that is more selective to tumor cells and reduce adverse effects. Many tumor cells are under oxidative stress and have higher level of ROS than healthy cells (*3*). Recently, Peng's group has developed a series of H_2O_2-activated DNA interstrand cross-linking agents that showed selective cytotoxicity towards cancer cells but spared the normal cells. For example, compound **1** (**CWB-20145)** and compound **2** (**FAN-NM-CH$_3$)** (Scheme 1) are activated by H_2O_2 to induce DNA interstrand cross-link (ICL) formation. Moreover, the compounds discussed are neutrally charged, thus improve cell membrane diffusion and drug efficacy (*4*-*7*). Peng's group also developed a series of photo-activated DNA ICL agents. For example, compounds **3** and **4** (Scheme 2) can be activated by 350 nm light (hv) to generate free radicals that are then oxidized to the carbocations directly producing DNA ICLS (*7*). Regardless, both types of triggers result in the compounds with better DNA cross-linking efficiency (*4*-*7*).

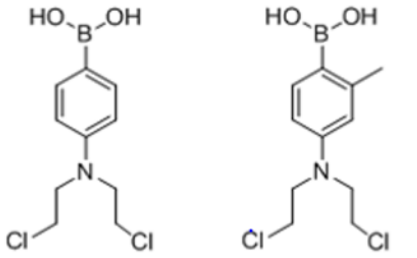

CWB-20145 **FAN-NM-CH3**

1 **2**

Scheme 1: The structures of Modified Nitrogen Mustard Analogues **1 (CWB-20145)** and **2 (FAN-NM-CH3)**.

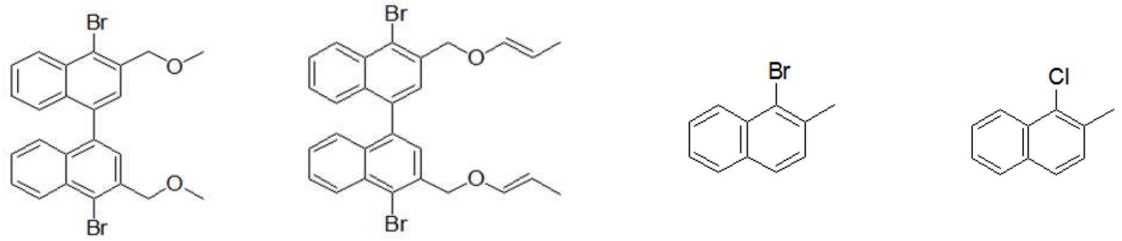

3 **4** **5** **6**

Scheme 2: The structures of Binapthalene Analogues **3**, **4**, **5**, and **6** (including naphthalene precursors **5** and **6**).

The general mechanism of function for these DNA ICL agents is to block DNA transcription and replication by cross-linking the DNA double helix strands. This in turn results in the death of cancer cells (*8*). Compounds **1** and **2** consist of a H_2O_2-responsive moiety (a trigger, boronic acid or ester) that reacts with H_2O_2 and an effector that acts as DNA cross-linker (e.c. nitrogen mustard). The effector is deactivated by the electron withdrawing boronate ester

group. However, this deactivation can be reversed if the boron group is replaced by a donating OH group in the presence of H_2O_2, therefore increasing the electron density of the aromatic ring and activating the nitrogen mustard. This facilitates DNA ICL formation.

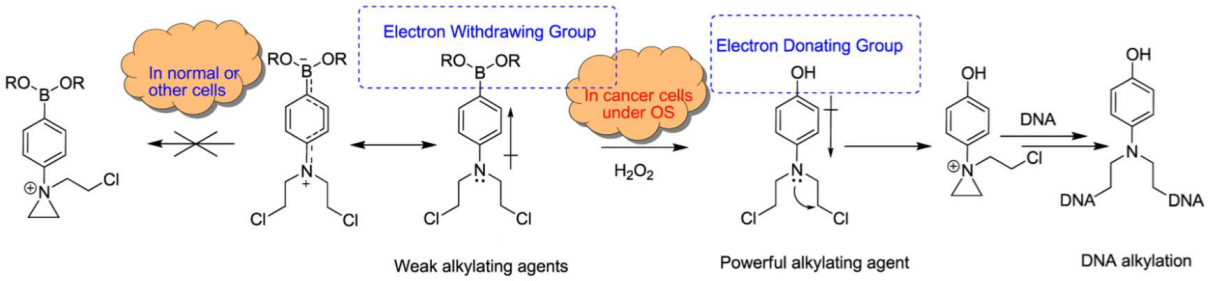

Figure 1. Activation Mechanism of 1 by H_2O_2 to form DNA ICLs, where OR = OH (*5*).

Although there are many examples of FDA-approved ICL prodrugs, many still contain low selectivity (and thus adverse effects), poor efficacy, among other shortcomings. In the case of the compounds developed by previous collaborators in our group, it was found that compound **1** and compound **2** hold promising potential for cancer cell lines such as SR (leukemia), NCI-H460, (non-small-cell lung cancer), and MDA-MB-468 (breast cancer). It was also determined that the aromatic substituents on compound **1** greatly affected the ICL efficiency. The results suggested that avoiding a bulky protecting group and introduction of a weak electron donating group is beneficial for selectivity (*5*).

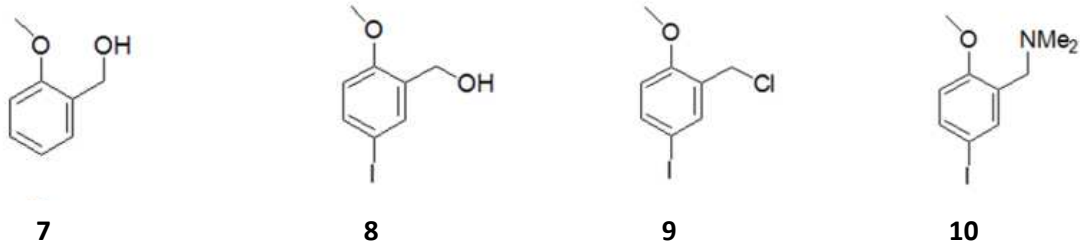

7 **8** **9** **10**

Scheme 3: The structure of Methoxybenzene Analogues **7**, **8**, **9**, and **10**.

In addition, compound **1** and compound **2** show potential as being a more effective treatment option for triple negative breast cancer (TNBC) than FDA approved drugs such as chlorambucil (7). Furthermore, while there have been great strides in the development of ROS activated prodrugs, especially towards their in vitro cytotoxicity and selectivity, little work has been done on the in vivo efficacy as well as selectivity. Lastly, in vivo studies provide that there are no adverse effects from the therapeutic dosing of compound **1** and compound **2**, which is not the case for the FDA approved drugs such as chlorambucil or melphalan. Lastly, **7**, **8**, **9**, and **10** (Scheme 3) are precursors for some new novel photo-activated DNA cross-linking agents (*5*), the mass of which were confirmed by mass spectrometry, during this study. Further information on ROS-activated prodrug analogues developed by group collaborators can be found in the references (*4-7*).

1.2 Research Approach

This study presents the LC-MS quantification of several alkylating agents synthesized by

collaborators in the group. We describe the analytical challenges associated with compounds **1** and **2** and present solutions that enable ionization to occur. Additionally, we present pharmacokinetic data of compound **2** that showed advantages over the parent compound **1**, such as longer duration time, slower elimination rate, and higher absorption. Lastly, this work will describe in detail a proposed hyphenated instrumental design that allows for the high-throughput, convenient, and information-rich analysis of such drug compounds using LC, NMR, and MS.

1.2.1 Liquid Chromatography (LC)

LC is the most common and versatile method of separation for biological analysis in the context of drug development due to its orthogonality. Although HPLC methods are commonly used, UPLC (ultra-high pressure liquid chromatography) is becoming more common because it is more efficient. The most common type of LC used in pharmaceutical investigations is reversed-phase liquid chromatography (RPLC). This type of separation involves the elution of the liquid sample which is pumped at high pressures through an injection port that leads the sample into a heated column where it is separated. The detector then processes the signal and displays the peaks in a spectrum by the order of elution which for RPLC, more polar compounds elute first and more non-polar compounds elute last. RPLC-MS mobile phases typically consist of water, methanol, or acetonitrile and often times additives that promote positive ionization, such as ammonium acetate, ammonium formate, acetic acid, and formic acid or additives that promote negative ionization such as ammonium hydroxide (*9*). It is the ionization of these compounds that is key to mass spectrometry and a challenge that will be discussed in this work.

1.2.2 Quantitation by Mass Spectrometry (MS)

MS detection is well suited to function with reversed-phase UPLC (hereafter referred to as LC), due to the fact that compatible solvents to elute the sample and additives in the solvent assist the ionization process (*9*). A mass spectrometer is a detector that is selective, sensitive, and can be used to analyze a variety of compounds. In addition to single quadruple mass spectroscopy (see Figure 1-1), tandem mass spectrometry (see Figure 1-2) is one of the most powerful tools for the analysis of drug compounds. A single quadrupole MS has four parallel rods, two positive and two negative. The opposing rods are attracted to one another and when a radio frequency (RF) voltage and direct current (DC) are applied to a pair of opposing rods, the charged ions travel between the rods. Ions of a particular m/z will make it to the detector for a certain voltage to RF ratio. Other ions will collide with the rods ad not reach the detector. Triple quadruple MS (MS/MS) includes three sets of the quadruples, the first set (Q1) serving as a mass filter, the collision cell (Q2) where the ions collide with neutral gas for fragmentation, which then enter the second (Q3) serving to filter fragment ions based on the parent peak selected in the first set. Other components include sample separation (HPLC) and a detector The instrument is operated in multiple reaction monitoring (MRM) mode which can determine the molecular mass of the ion as well as the fragment ions. Because of this additional layer of information, the instrument has higher sensitivity as well as selectivity than just a single MS (*9*).

For quantitation, an internal standard is typically used to correct for instrument variations. A suitable internal standard (IS) is one that is structurally similar and in the same mass range as the analyte, so that the IS undergoes a similar ionization process as the analyte. One major issue that plagues mass spectrometry is ion suppression, which is caused by less volatile compounds that affect the droplet formation and evaporation process. This phenomenon thus varies the

amount of charged ions that are produced and therefore causes errors in the analysis. Ion suppression can be avoided by carefully selecting various additives to use in the LC mobile phase. Weaker acids (acetic, formic, etc.) can be used in the place of stronger acids (TFA), for example (*10*).

Other considerations include the fact that sample, especially biological samples, cannot be injected directly into the LC-MS instrument and instead must undergo sample preparation to remove matrix effects, preconcentrate the sample, and otherwise ensure that the sample that can be analyzed. Of the methods available, solid-phase extraction (SPE), is commonly used because it is versatile a wide range of cartridges and solvent systems are commercially available. Another option is liquid–liquid extraction (LLE) followed by rotoevaporation to remove the organic phase. A detailed discussion of sample preparation for the analysis of alkylating agents is discussed in the next section. sample preparation for the analysis of alkylating agents is discussed in the next section.

1.3 Characterization of Novel Halogenated Alkylating Compounds by Mass Spectrometry

Alkylating agents, as expressed previously, bind to nucleophilic moieties and are cytotoxic to cancer cells once they cross-links DNA strands. Literature has demonstrated a variety of sample preparation and analysis conditions for particular types of alkylating agent. For example, SPE (C_{18} cartridges) were used to extract cyclophosphamide and its metabolites from human plasma in a study. A faster and simpler method of LLE (methanol□acetonitrile) was used for protein precipitation and resulted in high recoveries (89%–100%) of cyclophosphamide and 4□hydroxycyclophosphamide from plasma samples. Limits of detection of 0.2 ng/mL of agents

(cyclophosphamide and ifosfamide) have been achieved in urine (*11-14*). When it comes to analysis of an unstable compound as well as one that lacks chromophores, oxazaphosphorines, LC-MS was the appropriate choice for the analysis as compared to GCMS or LC-UV (*15*). In the case of chlorambucil, a nitrogen mustard derivative, although several LC-UV methods have been presented, LC□MS/MS methods have proven to be not only more rapid, but at least 10x more sensitive in plasma and urine samples (*1*).

In the case of our group's novel alkylating agents, another issue needed to be considered- is ionization. Even after adequate sample preparation, solvent system optimization, and instrument consideration, the challenge was achieving ionization of the compounds. Experimental design for alkylating agents requires the careful selection and corona needle optimization, as described in the following section on ESI, APCI, and DUIS ionization modes.

1.3.1 Electrospray Ionization (ESI)

Electrospray ionization (ESI) (see Figure 1-3) is an ionization technique for MS where a liquid sample is converted into nebulized aerosol composed of tiny charged droplets which are then charge separated. The droplets undergo high electric potential between the liquid sample (in a capillary) and the counter electrode. In this stage the radius of the droplets will decrease as the solvent evaporates, and due to the Rayleigh limit, Coulombic forces overcome the surface tension of the droplet resulting in "Coulombic fission." In this manner, the ions enter the gas-phase. Advantages of ESI include the "soft" ionization (resulting in multi-charging and thus an advantage for large molecules), high ion transmission, and high sensitivity even at low flow rates (*16*).

The basis of ESI was first described in the context of MS in the 1960s by Dole in his group's analysis of polystyrene. Variations of the method evolved, but in the 1980s, Fenn successfully developed an efficient ESI interface to MS for the first time, earning him the Nobel Prize in Chemistry in 2002 (*16*). Further advances included Bruins' addition of a nebulizing gas to create a charged aerosol in 1987 (*17*) and most recently, the coupling of APCI with ESI (*18*).

1.3.2 Atmospheric Pressure Ionization (APCI)

Atmospheric pressure chemical ionization (APCI), see Figure 1-4, is an ionization technique for MS consisting of an inlet capillary within a nebulizer capillary. It is in this heated capillary that nebulization occurs with the auxiliary gas serving to prevent interactions between the wall and the analyte. A corona discharge needle causes the ionization process to occur. The ionization can occur in positive mode where a proton transfer, charge transfer, or adduct formation can occur. The ionization can also occur in negative mode where proton abstraction, electron capture or anion attachment can occur (*9*). There are advantages and disadvantages to the APCI mode of ionization. One advantage is that since APCI is a "soft" ionization technique in that the mass spectra are relatively simple (*16*). In addition, matrix effects are not as pronounced as is the case in ESI. However, selection of a solvent system to use with APCI can be difficult because of preferential ionization of solvents with high proton affinity (*19*).

Shahin was the first to utilize APCI as an ionization source for MS in the 1960s, where a platinum wire was used as the anode in a discharge chamber (*20*). In the 1970s, Horning and co-workers developed the corona discharge needle when the LC was coupled to MS (*21*) which is the interface familiar today (the heated tube nebulizer was introduced later). Finally in the 1990s,

dual ionization mode (ESI and APCI) was achieved by switching between the two ionization modes in the same experiment (*22*). Recent advancements in APCI include various interface heating methods. Such designs include gradient heating to prevent the ion source from recirculating the atmosphere (*23*).

The theory of APCI is that the most stable reagent ion will be formed, which in turn will ionize the analytes of interest. If the reagent ion is more stable than the ionized analyte, the analyte ion will not form because the reaction will not be favored. In positive mode, RH+ is the reagent ion and B denotes an analyte:

$$\mathbf{RH^+ + B \rightleftharpoons BH^+ + R}$$

The protonation of the analyte will only proceed if the gas phase basicity (GB) for B is higher than the GB for the reagent ion RH^+ . The gas phase basicity is defined as the change in Gibbs free energy for the reaction (*16*):

$$\mathbf{B + H^+ \rightleftharpoons BH^+}$$

Thus the solvent system can influence ion stabilities and therefore ionization efficiency. For example, in reference to proton affinities (positive mode) or gas-phase acidity (negative mode) of solvents (and additives), methanol has a lower proton affinity than acetonitrile (754 kJ mol^{-1} vs 779 kJ mol^{-1}, respectively. Therefore, methanol would be a more suitable choice as an LC solvent if the proton affinity of the analyte is low (*24*).

1.3.3 Dual Mode Ionization

Different types of samples require different ionization modes. For example, for non-polar compounds, APCI is a better choice because in ESI, the non-polar compounds tend to not

evaporate and thus will not undergo the ionization process. For polar compounds, ESI is a more appropriate ionization choice because APCI occurs in the gas-phase, and thus the solvent does not need to be polar for ionization to occur as in ESI. A diagram of the polarity regions most appropriate for each ionization source is depicted in Figure 1-5 as well as Table I (*1*), depicting various studies with their respective ionization conditions. Some compounds or mixtures require dual-mode ionization, i.e., both ESI and APCI simultaneously, as illustrated in Figure 1-6 and depicted in Figure 1-7 as described from a case study (*25*). The disadvantage however is that the degree of sensitivity is less than when they are used individually (*26*).

1.4 Theory of In Vitro Microsomal Stability Studies and Pharmacokinetic Studies

1.4.1. In Vitro Microsomal Stability Study of Drug Compound 2 (FAN-NM-CH_3)

In-vitro stability studies allow for the prediction of a drug compound's potential metabolic clearance by liver enzymes, but without the cost and demands of an in vivo animal study (*2*). To calculate first-order rates, we calculate the half-life (t_0) using the following equation:

$$\mathbf{(t_0)_{min} = \ln(2)/k = 0.693/k}$$

where *k* is the first-order rate constant. We then linearize the data with the following transformation:

$$\mathbf{(t_0)}$$

In the case of first-order half-life, the half-life decay is constant, as seen in Figure 1-8 in an example diagram (*27*). The hepatic metabolism is a key initial step as it is a good indicator of in

vivo pharmacokinetics. The assumption is that hepatic metabolic clearance is the major mechanism of clearance (*28*), as in the case shown below with **2**.

1.4.2 In Vivo Pharmacokinetic Study of Compound 2 (FAN-NM-CH_3)

The experiments after the in-vitro stability study dealt with in-vivo pharmacokinetics (PK), or the determination of how the in-vivo model handles a drug compound in the context of absorption, distribution, metabolism, and elimination. In the case of compounds derived from nitrogen mustard drugs, a slower clearance of the drug is desired (*28*). Such studies can help assess the concentration-time curve using the following ratio:

AUC/MIC

where *AUC* is "area under the curve" and *MIC* is the "minimal inhibitory concentration". This ratio is a key measure of drug efficacy (*29*).

1.5 Instrumental Hyphenation

1.5.1 Analysis of HPLC-UV-NMR-MS Interfacing Scheme

As this work has already presented, MS is a critical tool in the drug development process. It allows for compounds to be accurately determined. However, MS has the disadvantage of lacking structural data. On the other hand, proton NMR is also a powerful tool for drug development as it a non-destructive method to provide structural information to allow distinguish

stereo-isomers however NMR has limitations as it is a tool that cannot compare to the sensitivity and selectivity that MS can offer and is not a suitable method if the analyte's functional groups are NMR-silent (i.e., lacking protons or able to exchange protons with the solvent) (*30*). It can be concluded then that NMR and MS are complimentary techniques, and both are necessary in the study of drug compounds. Yet drug development requires high-throughput capabilities and adds an additional challenge because of the complexity of the samples. Therefore, much research has occurred in the past several decades to interface NMR and MS.

More recently, splitting the flow to the NMR and MS while coupling preconcentration methods (e.g., SPE) upstream, and in-parallel analysis (*31*). There are two types of methods of hyphenation, the first being in-series hyphenation, which is one detector after another, while in-parallel hyphenation introduces the sample to the detectors simultaneously. With in-series hyphenation, the disadvantages include greater difficulty in ascribing the results to a given detector and more frequent leaks because of the large pressure difference between the NMR and MS. With in-parallel hyphenation, advantages include that the analysis can occur simultaneously although there is a delay with completing the NMR measurement (*32-33*). Examples of both coupling method schematics are found in Figure 1-9 from work by Gebretsadik et al (*34*). Summarizing timelines (Figure 1-10 (a) and (b)) of the historical developments of hyphenated NMR are presented (*31*).

LC-NMR has several advantageous when compared to conventional NMR. Proton NMR spectra can be acquired quickly and without spectral interferences if the analyte is isolated in pure form. There are however, obvious concerns about a hyphenated LC-NMR method (*35*). One major concern with coupled NMR and MS is that there can be significant solvent suppression of the NMR signal if either non-deuterated solvents are used or if the suppression is not mitigated

through some other means such as preconcentration. Additionally, if the solvent contains solvent additives, there may be adverse effects such as the deposition of salts in the NMR flow cell, e.g., with the use of sodium phosphate or TFA (trifluoroacetic acid) which may result in ion suppression for acidic compounds. Formic acid is an additive that avoids these issues because it promotes positive ionization. Simply using deuterated solvents holds issues as well because H/D exchange with the analyte may occur, which would result in inaccurate measurements (*32*).

1.5.2: **LC-NMR Past Improvements**

Coupling LC to both NMR and MS, whether in-series or in-parallel, offers the potential for an immense amount of information to be gathered in a single experiment. In reality however, there are difficulties because of the large sensitivity difference ($10^3 – 10^6$) between the two detectors, because the MS is far more sensitive than the NMR. In addition, the acquisition time for the MS is far shorter than for the NMR (*36*). Furthermore, there are trade-offs to choosing an in-series or an in-parallel instrumental design. Lommen et al. were able to overcome these challenges in an experiment, the data for which is shown in Figure 1-11 (*37*). In this experiment, the parent mass as well as the fragments were determined selectively by MS as compared to UV. The first inset chromatograph depicts a spectrum by UV analysis. Directly below is a mass spectrum of the m/z = 301 of only quercetine fragments (below),

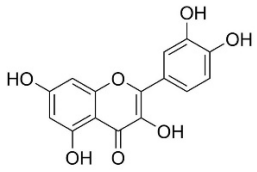

selected by an NMR measurement. The last inset depicts the loss of an ion of m/z = 162, thus only peaks with a C6 sugar appear in the spectrum. It can be concluded that NMR and MS data

are complimentary, and by following up with further NMR analysis post MS analysis, co-eluting peaks such as those of compounds glucopyranosid and galactopyrandosid, was determined (*37*).

Nevertheless there have been successful applications of LC-NMR-MS in drug studies. For example, Paracetamol (acetomeaphen) (below)

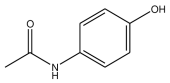

was determined in urine using RPLC-UV-NMR-MS, where NMR and MS spectra were collected in parallel. The mobile phase solvents were non-deuterated acetonitrile in D_2O with deuterated trifluoroacetic acid and the LC eluent was split 98:2 to the NMR:MS. A schematic of the in-parallel instrumental coupling including NMR and MS can be seen in Figure 1-12 (*33*). The authors used a combination of two measurements to deduce information about the endogenous drug metabolites. These experiments included an initial run with identification of the pseudo-molecular ion (MD^+) at m/z 334 and then a second run with the addition of methanol:acetic acid to enable the deuterons to exchange with the hydrogen atoms. MH^+ ions were produced for all of the fragments of the analyte and the exchanged hydrogens distinguished by the mass difference (*33*).

There have also been studies of dihydroquinoxalinecarboxylate (below),

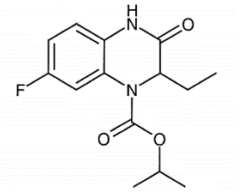

a drug used to treat HIV, in urine. The method used gradient elution RPLC (acetonitrile in D_2O with acetic acid), and LC fractions were collected on-line in a loop collector, and run in-series to a proton NMR and then to an ion trap MS. The schematic diagram depicting in-series NMR and

MS with a fraction collector down-stream is presented in Figure 1-13 (*38*). The same group also carried out the measurement in reverse, i.e., RPLC-ion trap MS-NMR (Figure 1-14) (*39*). The LC-MS-NMR design was studied with a drug used to treat bipolar disorder called triazolopyridine. By determining the masses of the peaks of interest, the fractions could then be stored for stopped-flow analysis with the NMR, on-line (*39*).

LC-NMR-MS/MS has also been reported by Scarfe and co-workers. Once again, a solvent gradient of acetonitrile in D_2O with acetic acid was employed along with an ion trap and ESI MS/MS. The authors determined the major metabolite in the urine sample to be a sulphate conjugate, which are considered "NMR-silent" (due to a lack of protons) and in addition MS could not determine the actual position of substitution of the aromatic ring of the metabolite, that NMR could if the compound was not silent. This case proves clearly how beneficial hyphenated methods can be because neither HPLC-NMR nor HPLC-MS alone were able to determine the metabolites. Instead it was the complimentary information from the HPLC-NMR-MS method that allowed for accurate determination (*30*). Another study showed how stereochemistry could be determined by the NMR in a hyphenated system, in which ibuprofen in urine was metabolized to glucuronide diastereomers, which were not distinguishable by MS but were by NMR, the results of which can be found in Figure 1-15 (40) and the in-parallel schematic diagram for this work is shown in Figure 1-16 (*40*).

NMR is a powerful analytical tool that provides vital information to aid in the prediction of the chemical structure of a compound (*9*). LC-NMR was first described in the 1970s, and there has been an increasing interest in it over the last two decades because of improvements made to NMR instruments. For example, Watanabe and Niki first reported a successful LC-NMR design in 1978 (Figure 1-17) (*41*) by using a thin-walled Teflon tube (1.4 mm in inner

diameters) to serve as a continuous-flow cell. The authors used deuterated solvents to evade solvent suppression to measure various drug compounds. The study also presented various areas that needed improvement including sensitivity, as the sample had to be run hundreds of times to achieve an equivalent signal to noise ratios for samples of different concentration (*41*). Two years later, the first design of on-flow LC-NMR was reported by Dorn *et al.* using a novel NMR flow cell insert (Figure 1-18) (*42*) to analyze jet fuel sample mixtures. The optimized insert had a vertical orientation to prevent air bubbles from becoming trapped in the cell. The cell was also tapered at both ends of the insert to prevent eddy diffusion by minimizing particle size (*42*). Building upon this work, Laude and Wilkins (1984) further optimized the insert design by incorporating a stainless-steel column, minimizing the transfer line and thus increasing resolution and sensitivity due to the minimization of dead volume, as seen in Figure 1-19 (*43*).

Another problem that had to be resolved that of the mobile phase, which earlier had been fairly non-complex in order to avoid potential interfere with the sample with the use of two solvent resonance changes during a gradient elution, and of course the detection limit. Smallcombe in 1995 reported a technique to overcome these issues by WET ("water suppression enhanced through T1 effects"), where selective pulses are applied at the solvent's resonance and then this is followed by field gradients that are pulses to diphase (or minimize) the residual magnetization produced by the solvent. This allows for the selection of a particular magnetization and not of others. This can be seen in the spectra results in Figure 1-20 (*44*), with the unsuppressed and suppressed resonance of acetonitrile solvent (*44*).

Low sensitivity and issues with solvent complexity was also addressed through the implementation of smaller flow cells and the use of cryogenic probes. This was reported by Sweedler et al. in the late 1990's with their development of a microcoil flow cell probe, which is

depicted in Figure 1-21 (*45*). For the cryogenic microcoil probes, the NMR cell was cooled to 20° C, thereby improving sensitivity (Figure 1-22) (*45*). This first demonstration of continuous-flow technique was used to analyze an amino acid and peptide mixture and was able to detect analyte concentrations of 750 ng/mL (ppb). In addition, separation was achieved in under 10 min and NMR spectra were collected with 12 s of time resolution. Lastly, the authors also performed stopped-flow experiments to collect 2D COSY spectra (*45*).

Not only are there various instrument coupling methods, but the connection of the LC component to the NMR or other instrument is much more than just connecting some capillary tubing from the LC column, but instead requires an automated way to ensure the most reproducible and reliable results in addition to ease of use. A switching value interface can involve continuous flow of the sample through the NMR as the signal is acquired, or "on-flow," or it can be measured while the flow is stopped and the sample is in the NMR cell. There are two types of designs for this purpose: "(direct) stop-flow" and "loop storage/loop transfer". In "stop-flow," the chromatographic separation is interrupted for an NMR measurement whereas with "loop storage/loop transfer," the chromatographic peaks are stored as they elute into a loop system until a measurement is taken with the NMR. In the case of the design research reported herein, we combine "on-flow," "stop-flow," and a "loop transfer" to capture the eluted sample in the NMR flow cell, and then acquire the spectra while the sample is static within the NMR cell and divert the rest of the LC eluent to waste (*36*).

1.5.3 Brief Overview of NMR Theory

Nuclei spin at an angular momentum "p" and thus this charged nucleus creates a

magnetic field. A magnetic moment "μ" is positioned along the spin's axis and is equal to p:.

$$\boldsymbol{\mu = \gamma p}$$

where γ is the proportionality constant specific to the nucleus. If a magnetic field "B_0" is applied to a spinning nucleus, μ becomes oriented in either of the directions of the field. When B_0 is absent, the quantum states of the nucleus are the same. Thus the strength of the magnetic field is a principle component to NMR and its strength dictates the strength of the observed signal:

$$\boldsymbol{(N_j/N_0) = 1 - (vhB_0)/(2\pi kT)}$$

where N_j and N_0 are the number of protons present in the higher and lower energy states, respectively, v is the frequency, h is Plank's constant, B_0 is the applied field strength, k, again, is Boltzmann's constant, and T is absolute temperature. A depiction of the nuclei under the conditions described above can be found in Figure 1-23 (*9*).

The advantages of using NMR are plentiful. First, NMR is non-destructive and can detect low molecular weights of molecules. In addition, NMR provides complimentary information to the MS such as chemical shifts, multiplicity, integrals, intermolecular relationships, and dynamic processes (*46*). The disadvantages include the sensitivity of NMR, which means that large amounts of analyte are required as compared to MS. For example, NMR would require at least μg/mL concentrations whereas MS only requires ng/mL concentrations to produce an adequate signal. As noted above, this issue can be addressed by splitting the flow from the LC to separate tubing of different diameter to direct > 99% of the eluting volume to the NMR while 1% would be directed to the MS (*34*).

1.5.4 NMR Spectra

One advantage of proton NMR is that the peak area can be directly quantified as the amount of nuclei that produce the peak, provided of course that this peak does not overlap with another peak. The solvent plays the role of a standard shift, since the rest of the peaks can be standardized to that of the known solvent peak, for the purpose of quantification.

Chemical shifts arise from the fact that hydrogens have different environments and number of hydrogens that belong to each signal can be determined by the integration of the peaks.

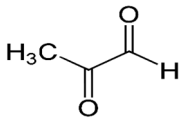

For example, the molecule shown has two different proton environments and thus two distinct For a simple example, consider Methyl Glyoxal shown above, which has two different proton environments and thus two distinct signals in its NMR spectrum — one for the hydrogens on the CH_3 and one for the terminal CH. Following the "n+1 rule," the neighboring carbon to the CH_3 is a C with no hydrogens. Thus the signal produced for the CH_3 would be a 0+1 or a singlet "s" with an integration of 3 hydrogens. The other signal from the CH would also be a singlet, however with an integration of 1 hydrogen. Both signals would be found down-field on the spectrum because the electronegatively of their environments are high from the nearby oxygens, and therefore different magnetic fields are necessary to achieve resonance at a set frequency (*9*).

1.6 Research Goals

The goals of this project were to:

1.Develop an LC-MS method to analyze the novel FAN-NM-CH_3 compound.

2. Modify the method for the analysis of pharmacokinetic samples.

3. Design an on-line LC-NMR-MS system.

1.7 Figures and Tables

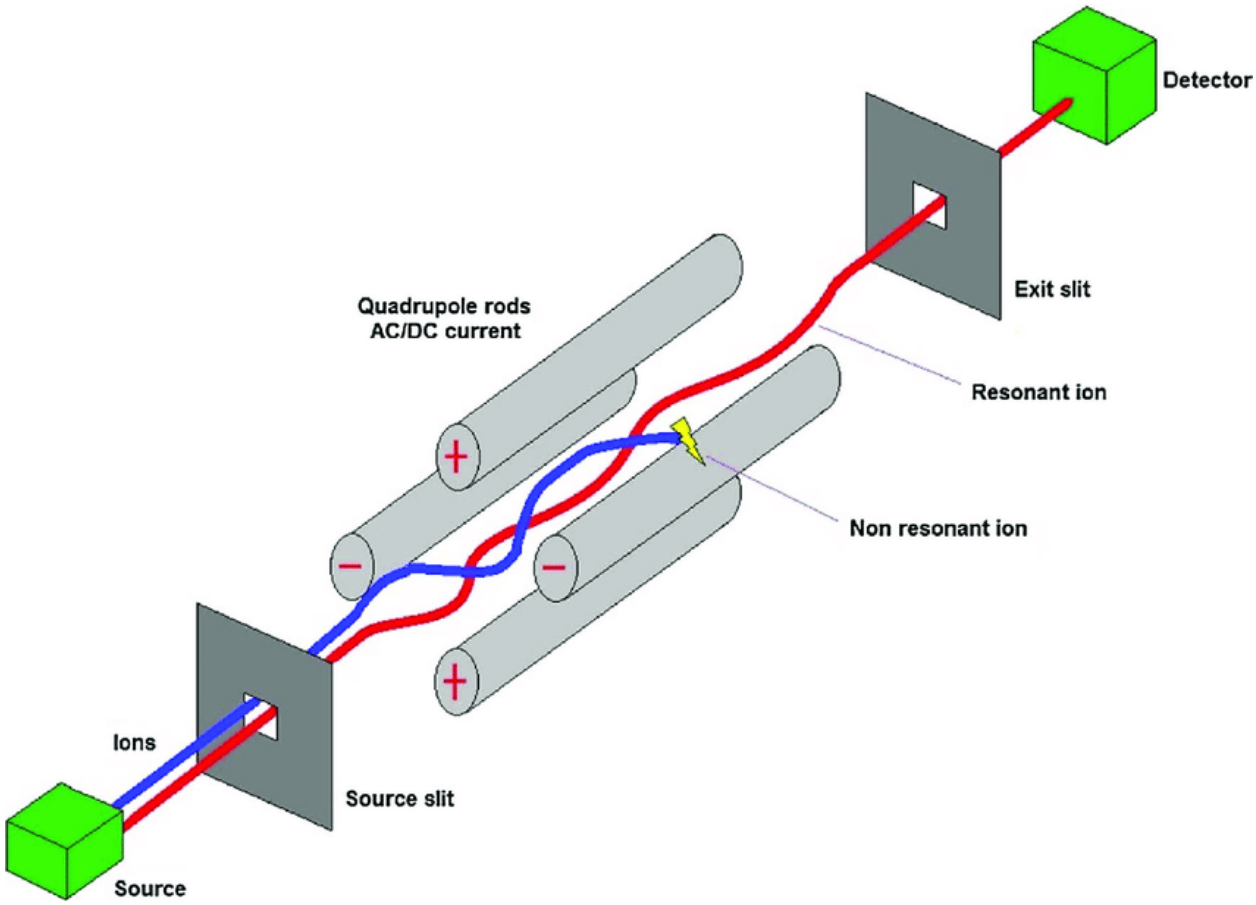

Figure 1-1. Schematic diagram of a single quadrupole MS (*48*).

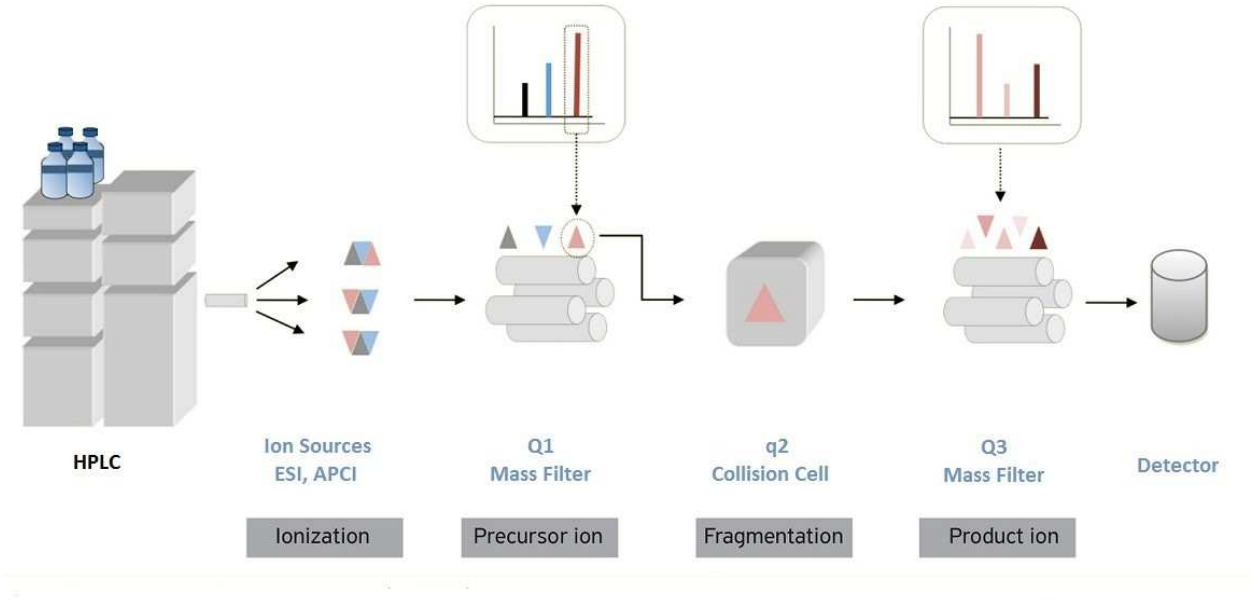

Figure 1-2. Schematic diagram of a triple quadruple MS (MS/MS) (*47*).

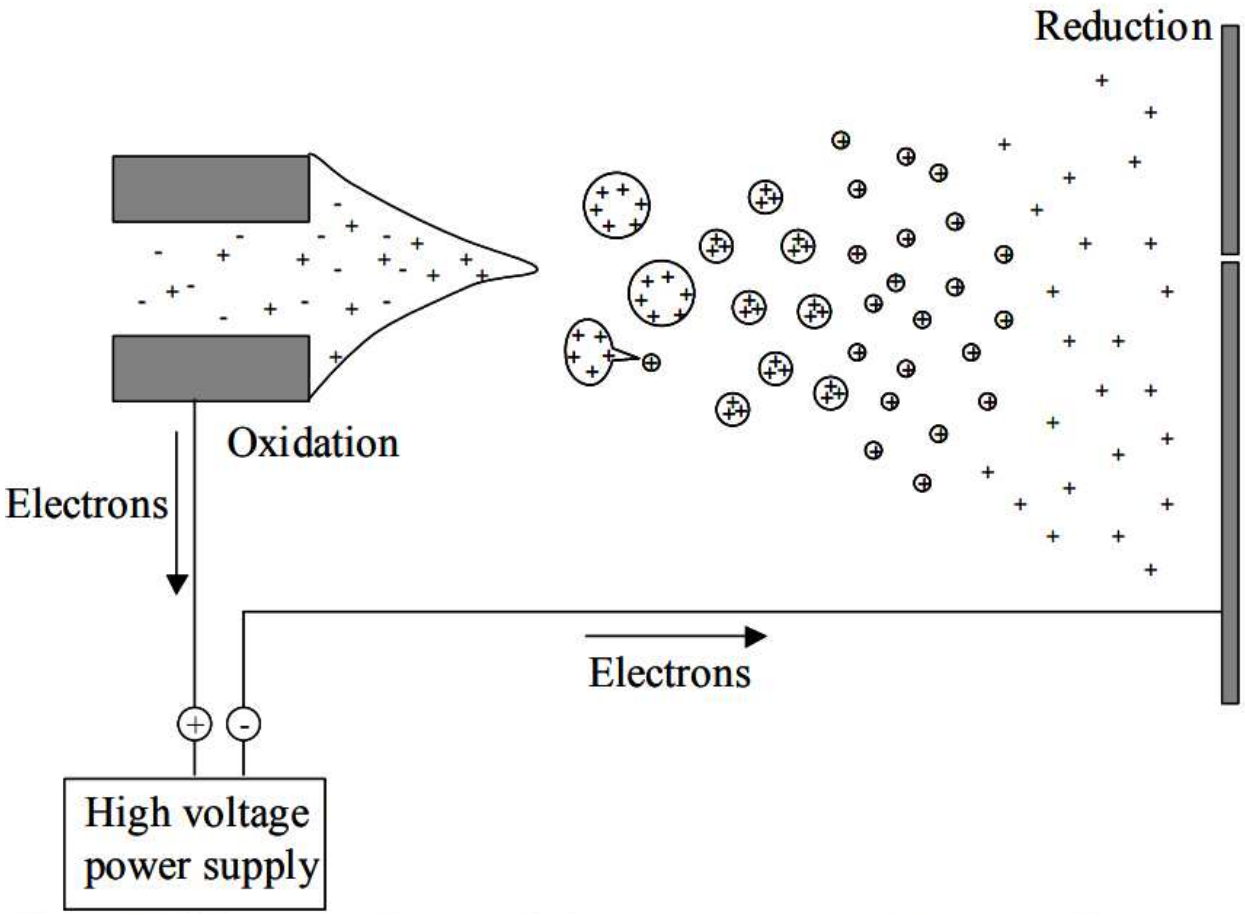

Figure 1-3. The electrospray ionization process (*18*).

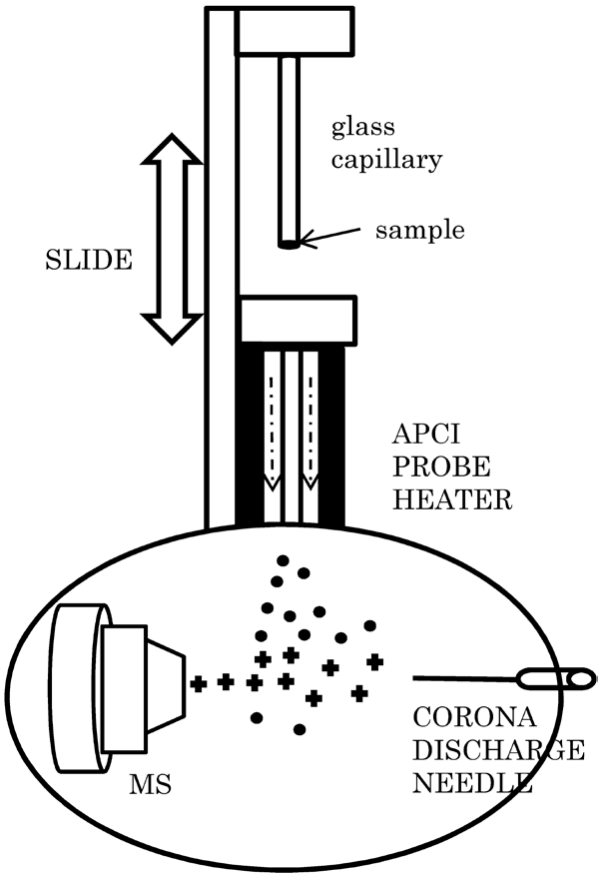

Figure 1-4. Schematic diagram of an atmospheric pressure chemical ionization source (*49*).

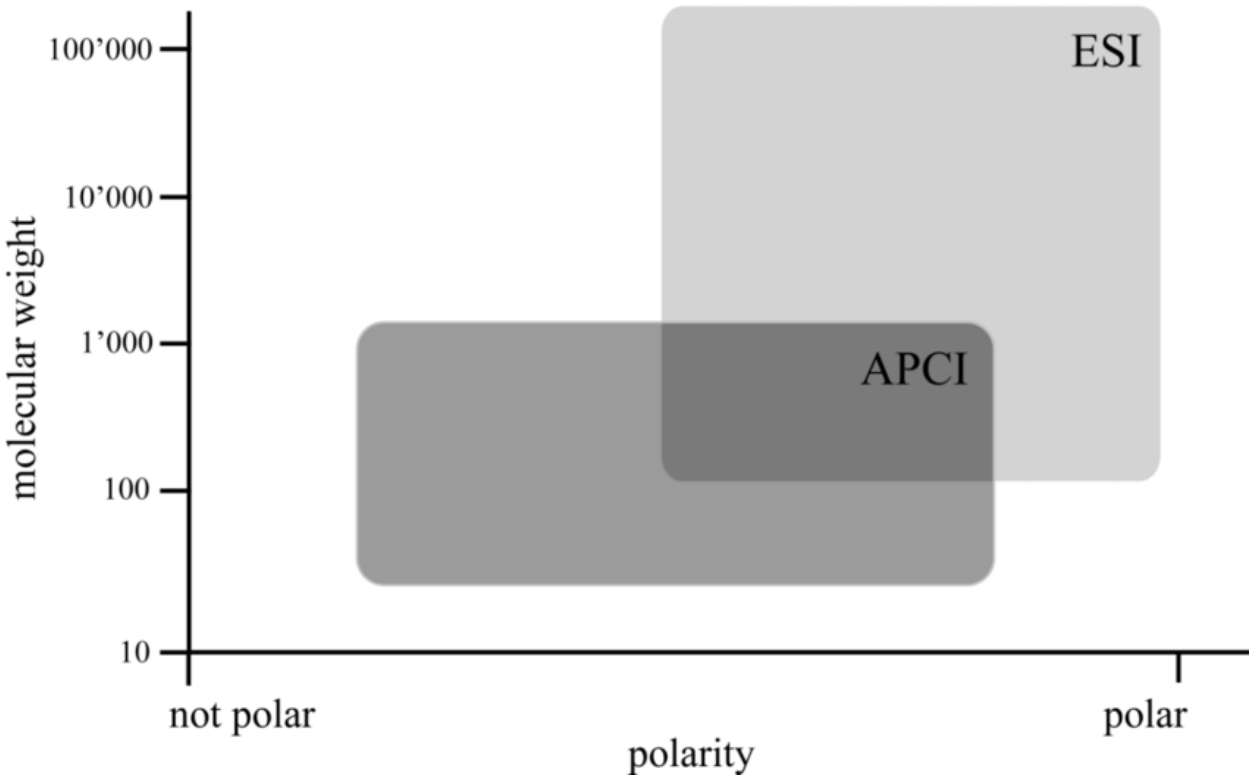

Figure 1-5. A guide to the polarity regions most appropriate for each ionization source (*51*).

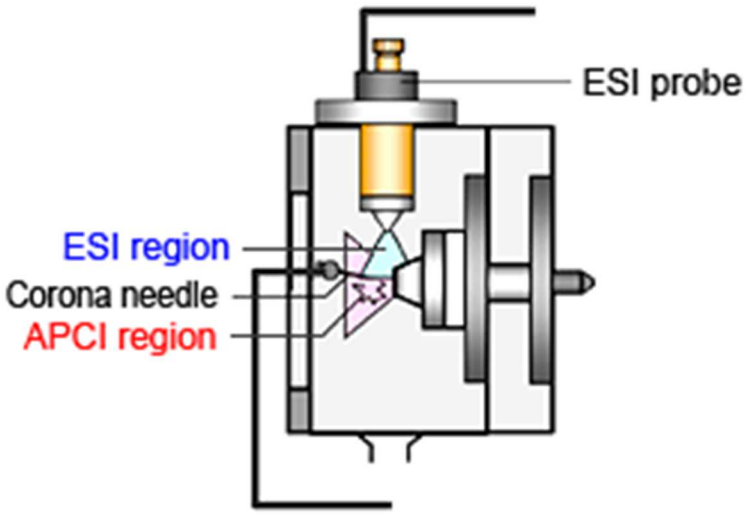

Figure 1-6. A schematic showing the DUIS ionization source (*29*).

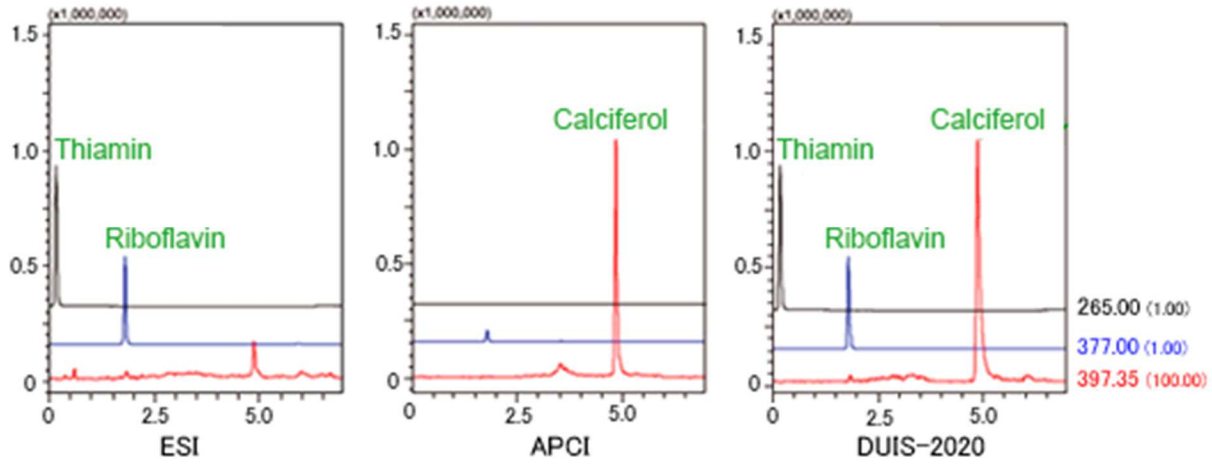

Figure 1-7. Comparative data of DUIS mode ionization (*25*).

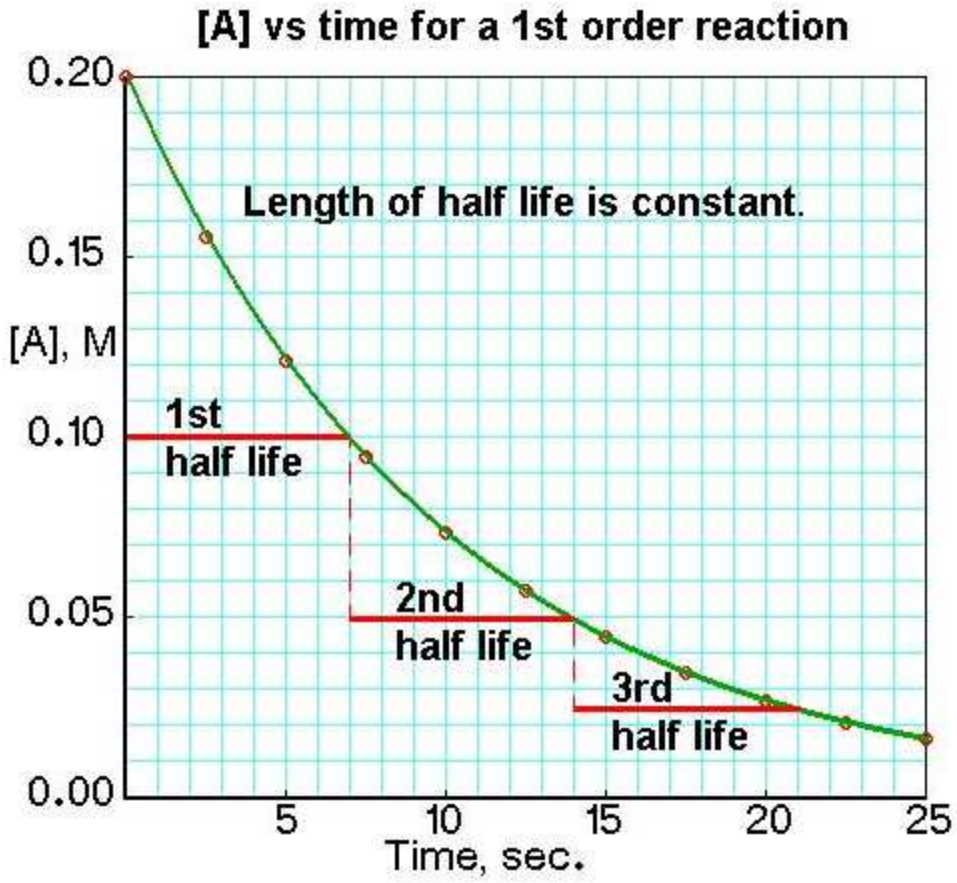

Figure 1-8. A graphical depiction of first-order half-life (*29*).

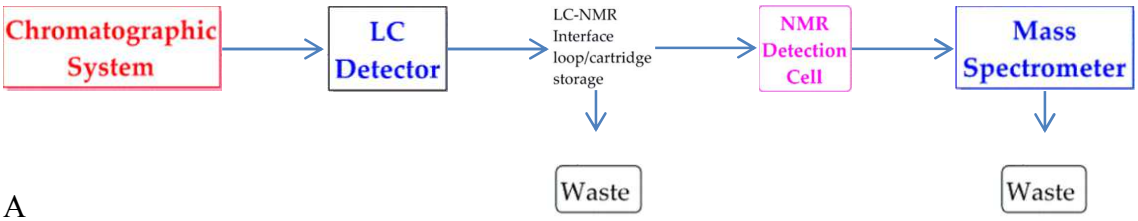

A

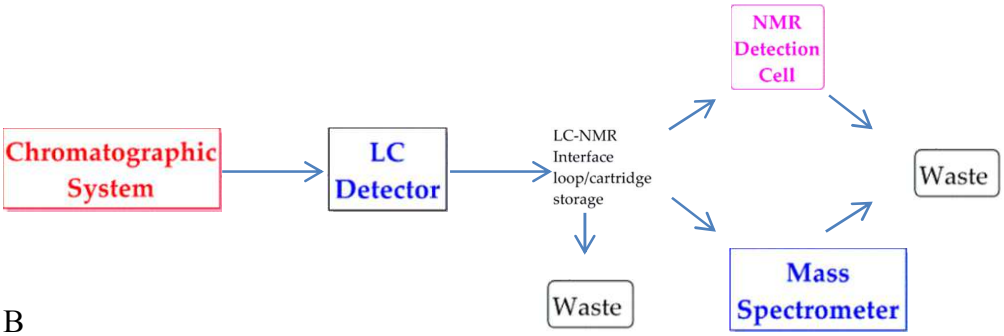

B

Figure 1-9 (a) and (b). Schematics of in-series (LC-NMR-MS) and in-parallel LC-NMR/MS hyphenation (Adapted from Gebretsadik, T, et al) (*34*).

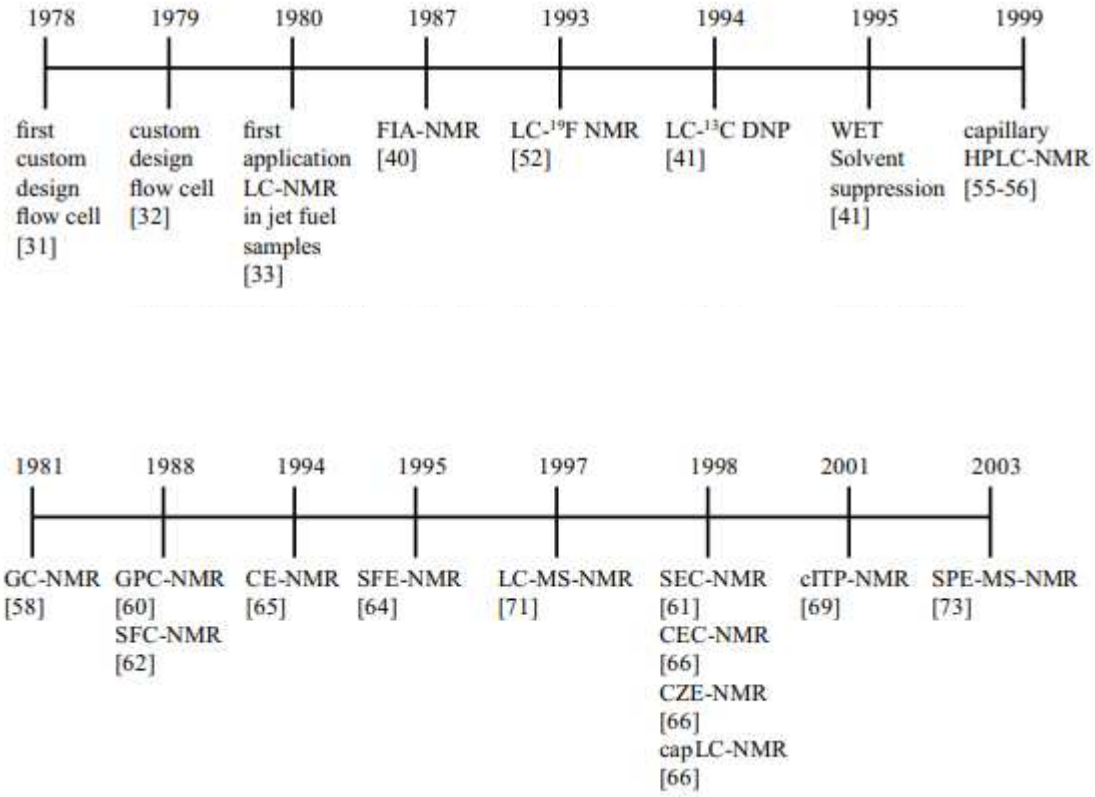

Figure 1-10 (a) and (b). Timeline of historical developments with hyphenated NMR techniques (*31*).

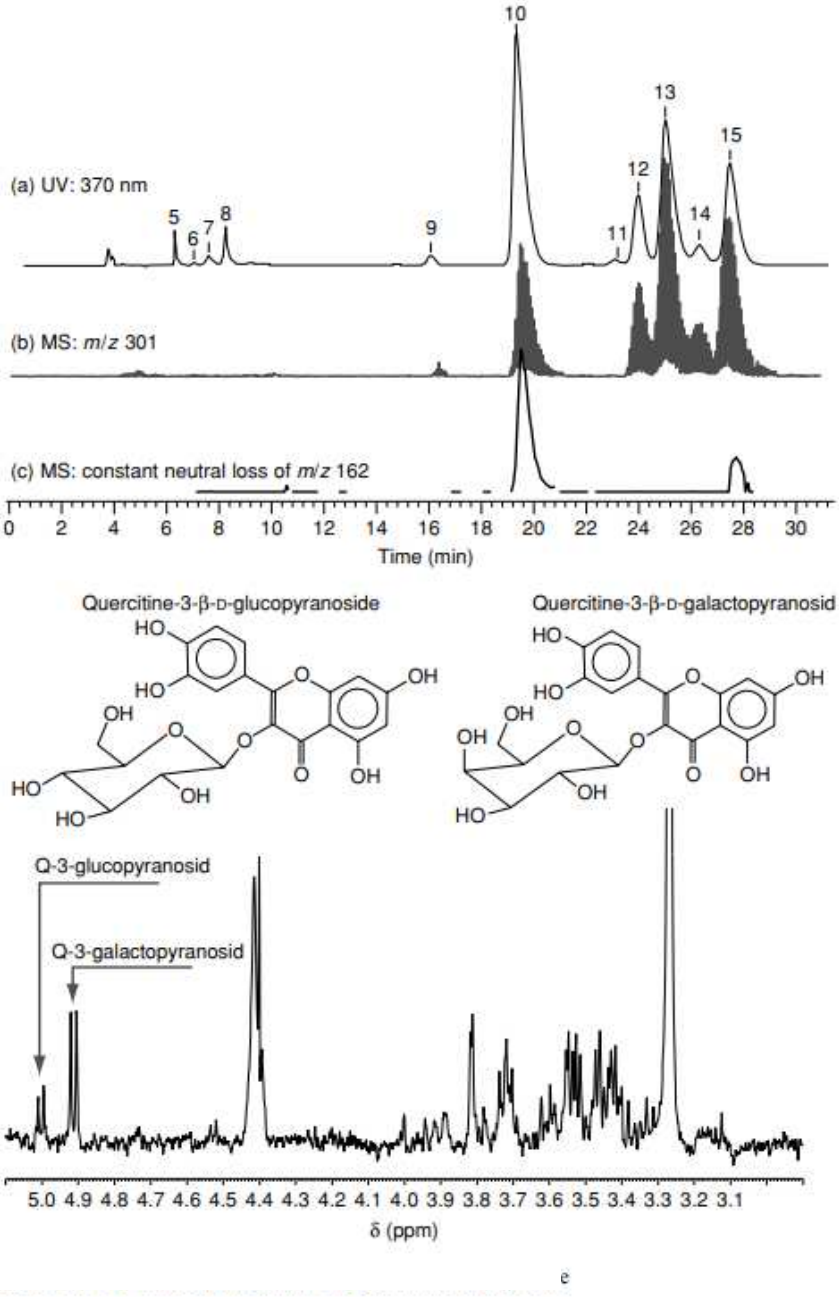

Figure 1-11. LC-NMR/MS work by Lommen et al. to measure glycosides (*37*).

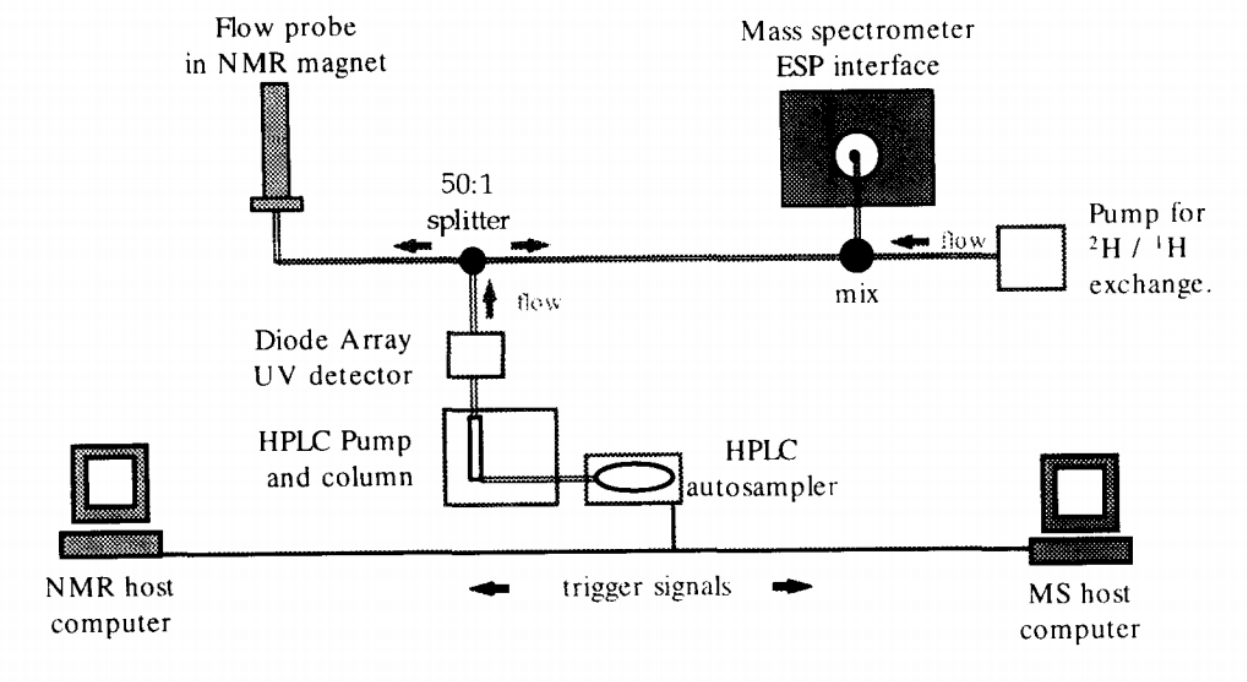

Figure 1-12. A schematic demonstrating in-series and in-parallel hyphenation (*33*).

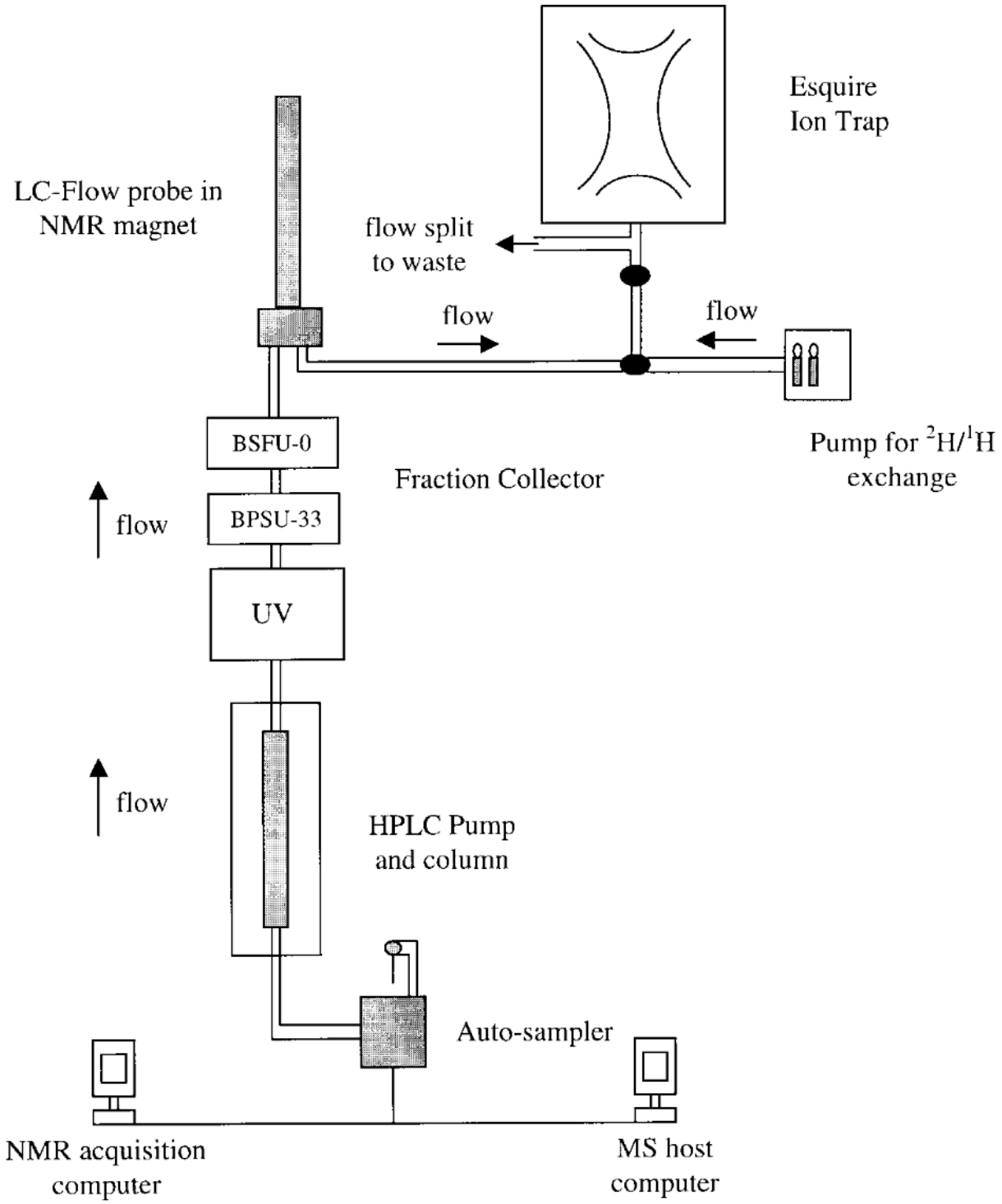

Figure 1-13. A schematic of LC-NRM coupled with ion-trap MS detection (*38*).

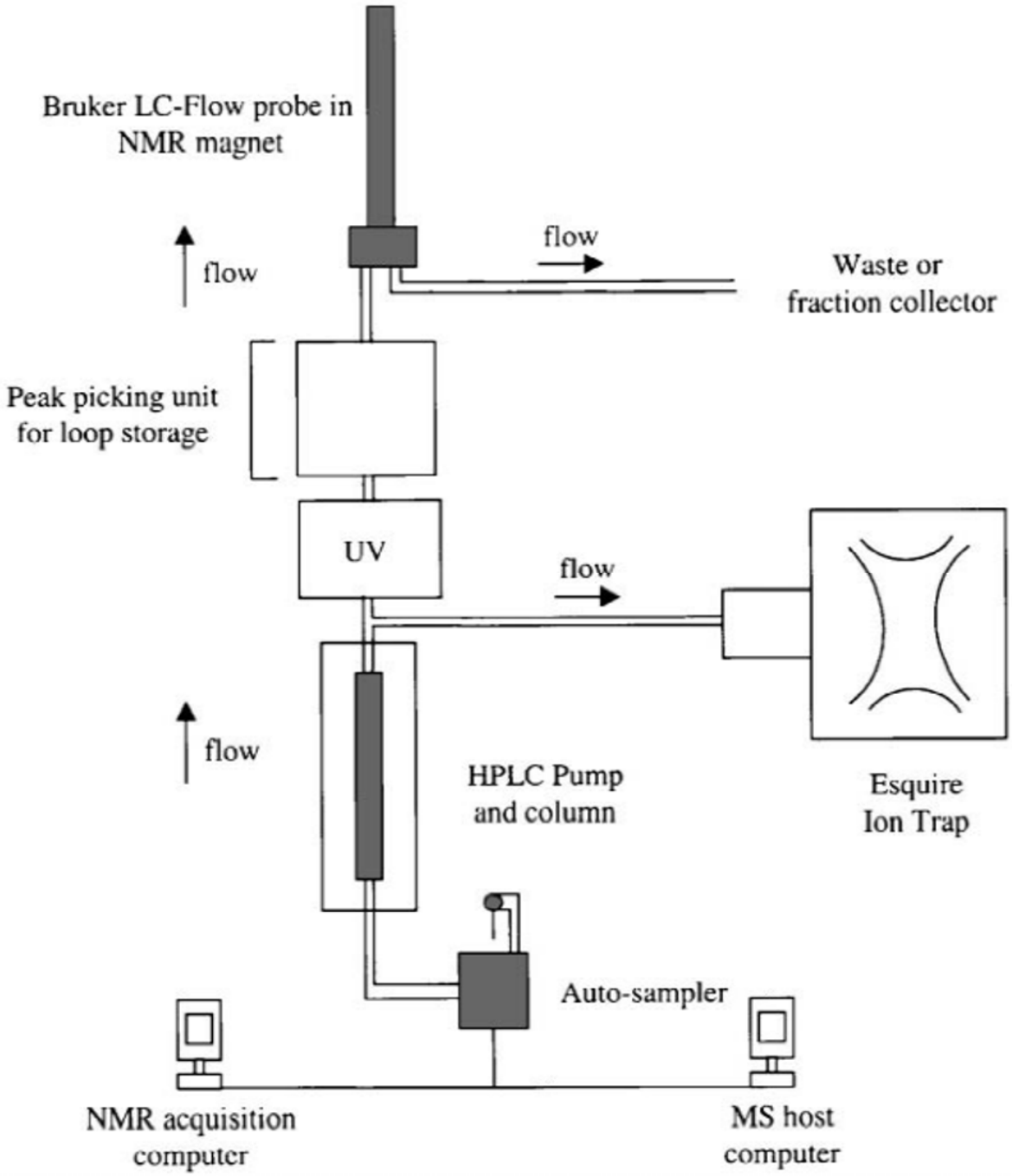

Figure 1-14. A schematic of LC- ion-trap MS coupled with NMR (*39*).

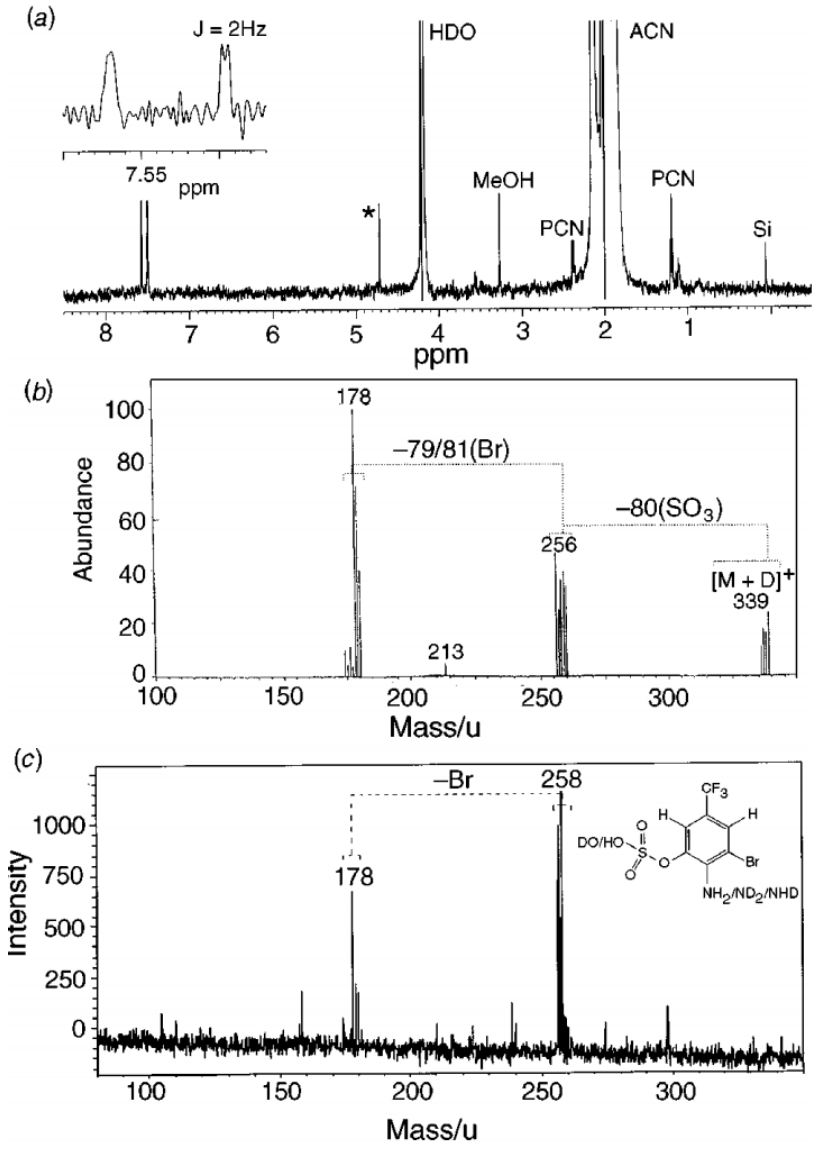

Figure 1-15. A study depicting information obtained from NMR and MS to determine the structure of a drug metabolite. A. is a 500 MHz proton NMR spectrum, B. is a spectrum obtained ESI MS, and finally C. is MS/MS (*40*).

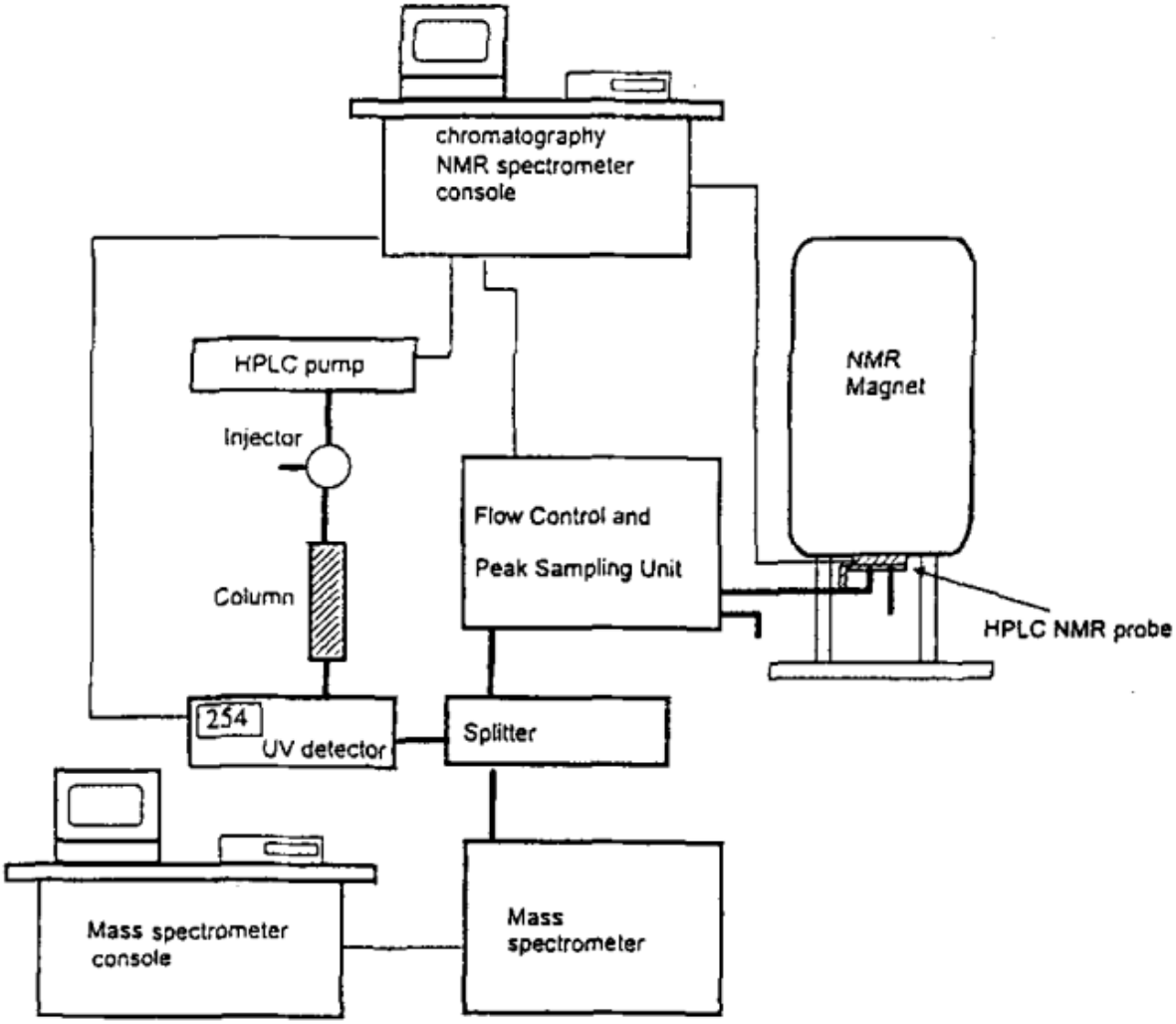

Figure 1-16. A schematic of LC-NRM-MS/MS detection (*40*).

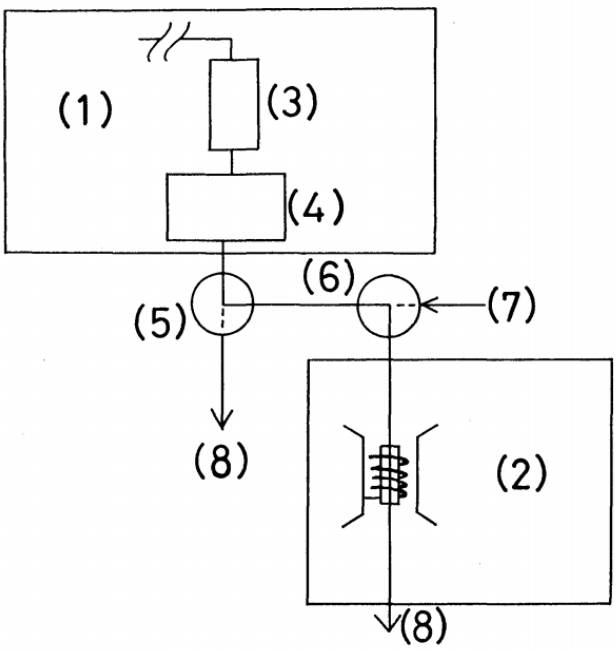

Schematic diagram of LC-NMR direct-coupling. (1) HPLC, (2) FT-NMR, JEOL FX-60, (3) column, (4) dielectric constant detector, (5) three-way valve-1, (6) three-way valve-2, (7) injection port for resolution etc., (8) drain.

Figure 1-17. The first novel example of LC-NMR (*41*).

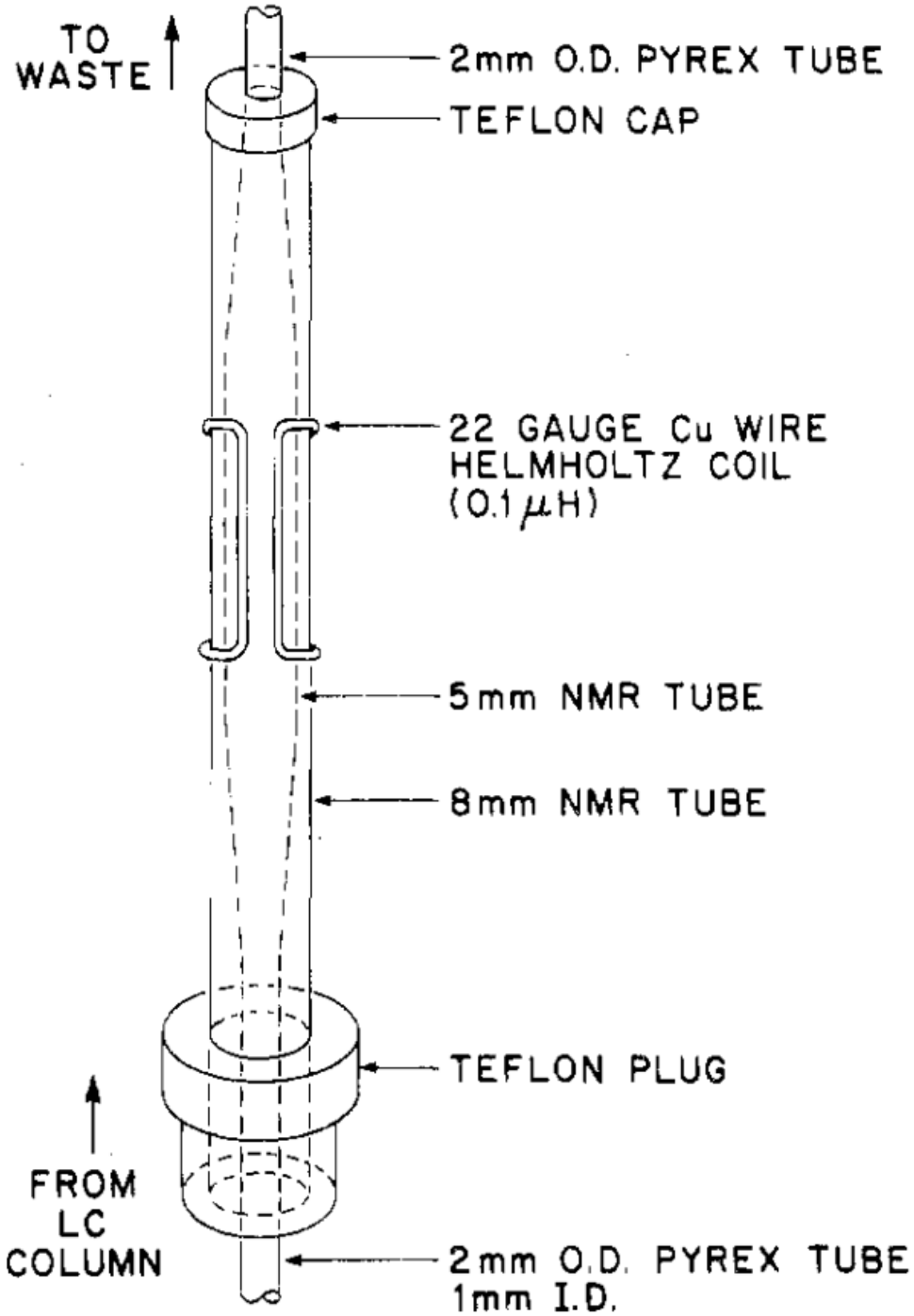

Figure 1-18. A diagram of a novel NMR Teflon probe (*42*).

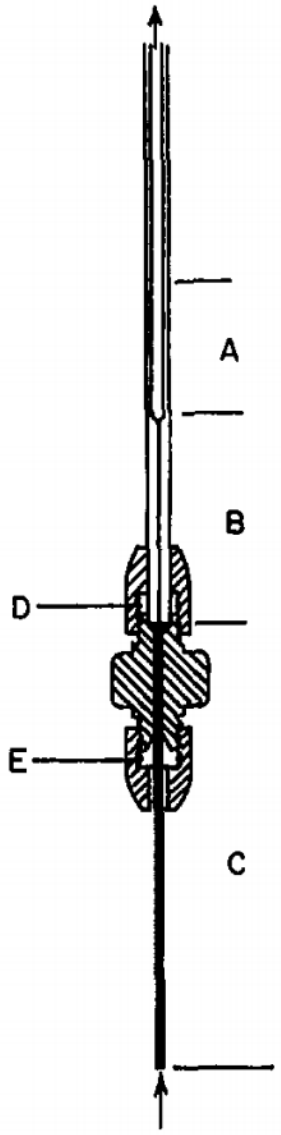

Diagram of the NMR flow cell and interface: (A) glass observe region; (B) glass capillary; (C) stainless-steel capillary; (D) Teflon® gasket; (E) Teflon® ferrule. The arrows indicate the direction of flow.

Figure 1-19. A diagram of a stain-less steel NMR probe (*43*).

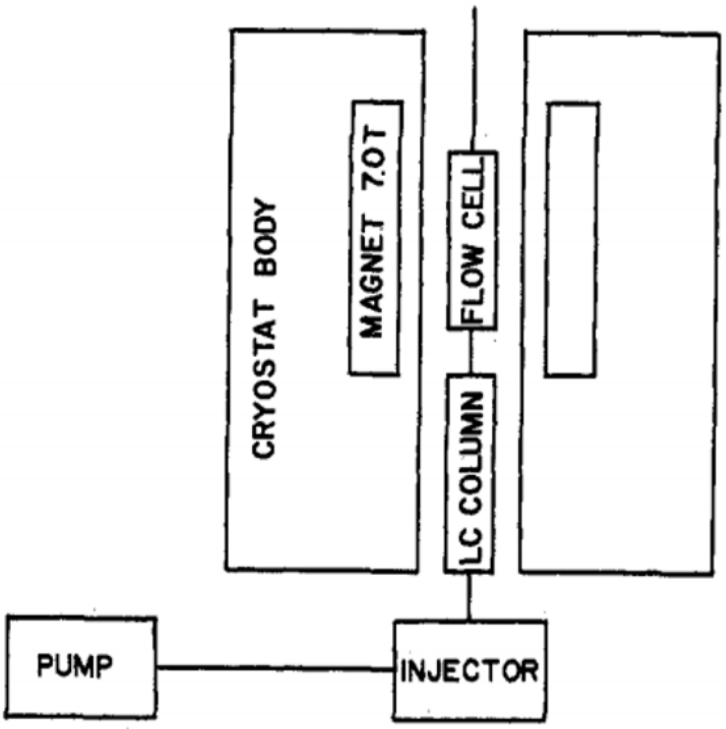

Figure 1-20. A schematic diagram of an on-line flow system developed for the LC-NMR method (*45*).

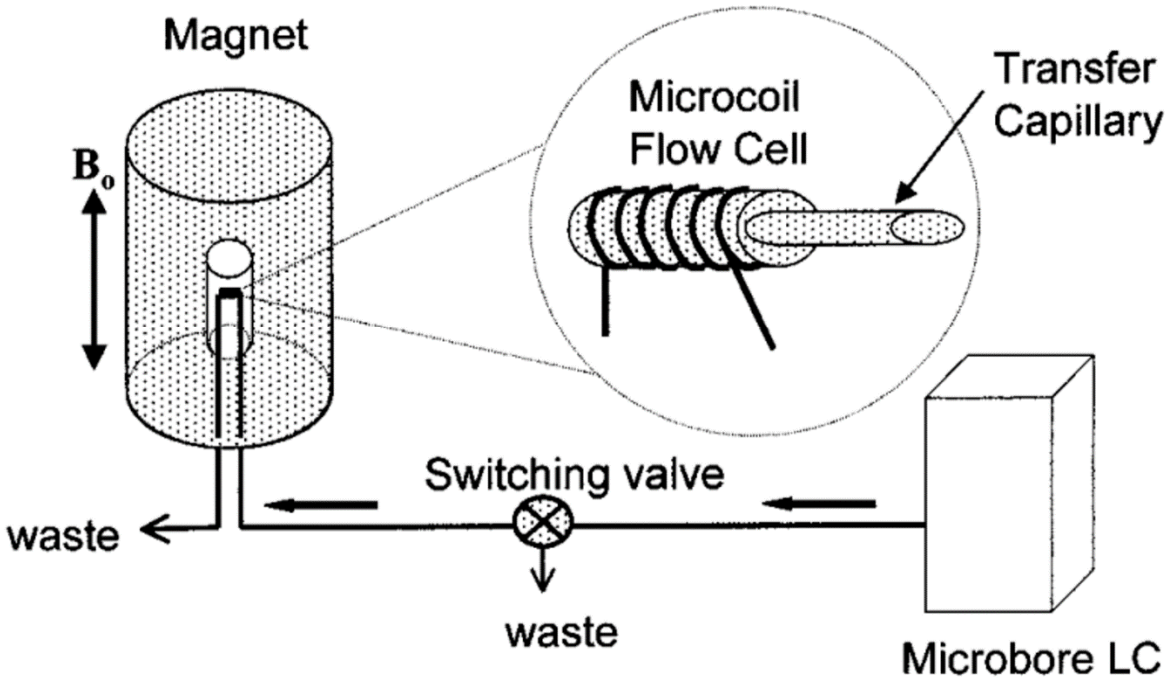

Figure 1-21. A schematic diagram of a novel microcoil NMR flow probe (*45*).

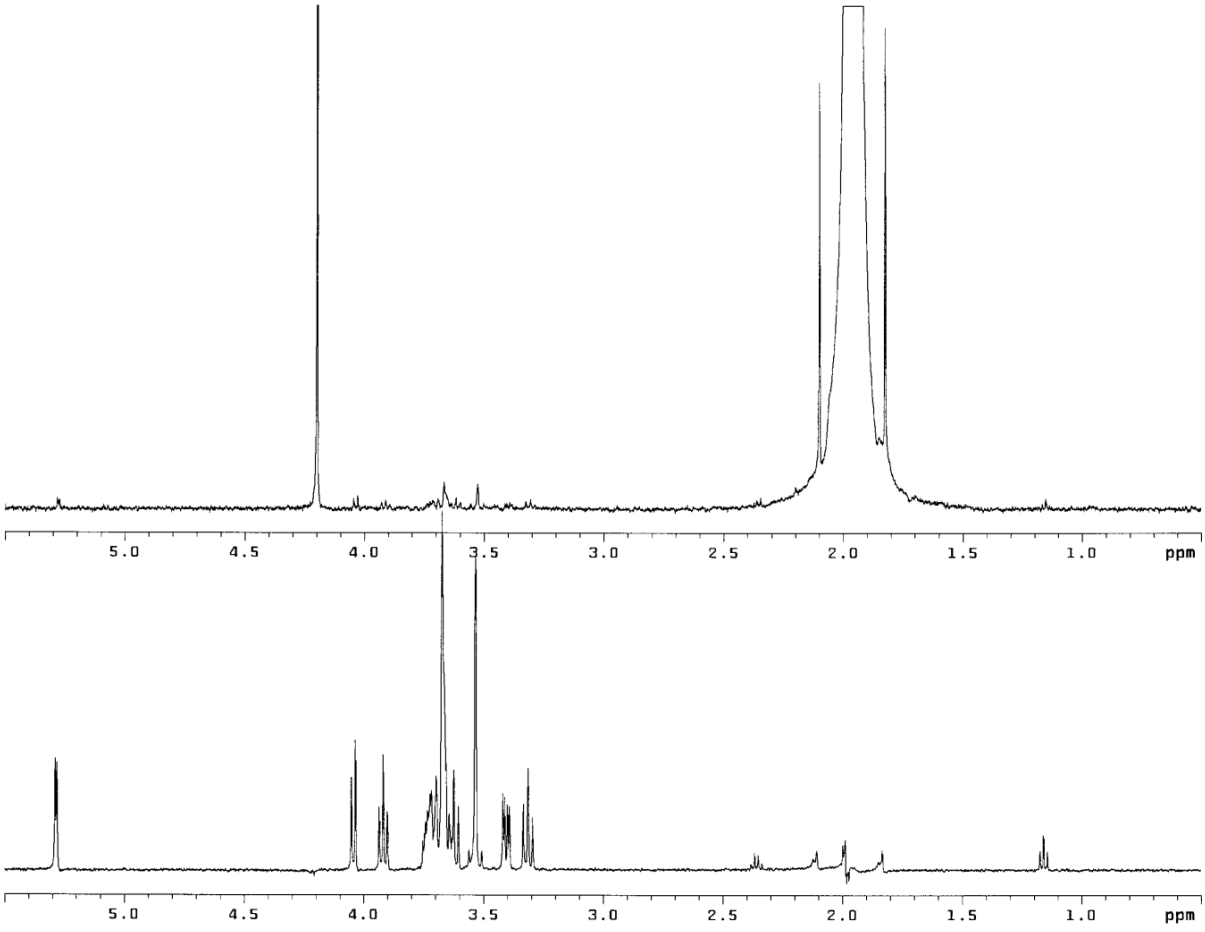

Figure 1-22. Spectra of a WET stopped-flow experiment involving a 10 mM sucrose in CH3CN:D2O (50:50). While the spectrum at the stop depicts unsuppressed spectrum with significant solvent resonance at 1.95 ppm, the bottom spectrum includes the WET technique of solvent suppression (*44*).

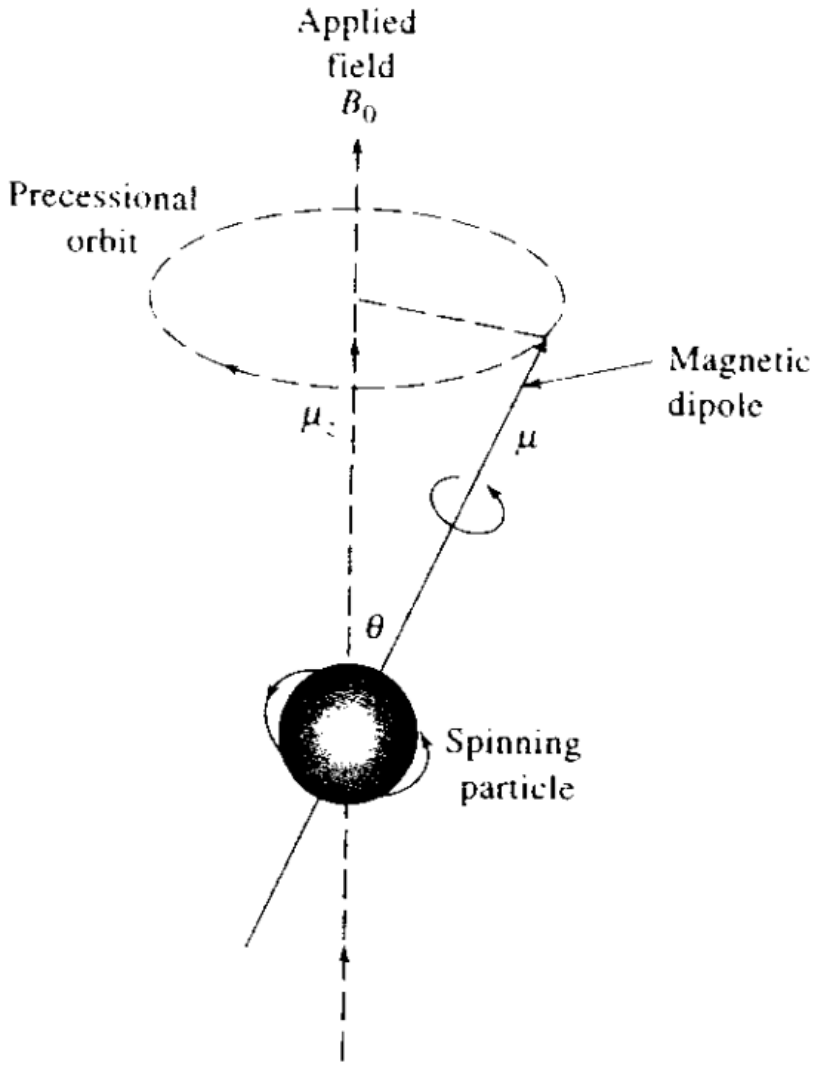

Figure 1-23. A depiction of a spinning nuclei under an applied field (*9*).

Table I: *Studies of anti-cancer drug metabolites using ESI MS* (*1*).

Compound	Matrix	Sample (µL)	Sample Pretreatment	LC	Interface	MS mode	IS	LLOQ (ng/mL)	Run time (min)	Met. Quan.	Remarks	Ref.
Cyclophosphamide	Human urine	5000	LLE	I: M-AA pH4	ESI (+)	MRM	None	0.2	10	No	Monitoring hospital personnel	Turci et al., 2002
Ifosfamide	Human urine	5000	LLE	I: M-AA pH4	ESI (+)	MRM	None	0.2	10	No		
Cyclophosphamide	Human plasma	450	SPE	I: M-AA,HA	ESI (+)	SIM	An.	50	20	Yes		Baumann et al., 1999
Cyclophosphamide	Human plasma	100	PP	G: A-AH	ESI (+)	MRM	An.	200	9	Yes		de Jonge et al., 2004
Thiotepa	Human plasma	100	PP	G: A-AH	ESI (+)	MRM	An.	5	9	Yes		
Cyclophosphamide	Mouse plasma	250	PP	I: A-W-F	ESI (+)	MRM	An.	3.1	2.5	Yes		Sadagopan et al., 2001
Cyclophosphamide	Mouse spleen	25 mg	PP	I: A-W-F	ESI (+)	MRM	An.	1250 ng/g	2.5	Yes		
Phosphoramide mustard	Human plasma	500	PP	I: M-AA pH4	ESI (+)	SIM	SIL	660	7	-	Metabolite of cyclophosphamide	Kalhorn et al., 1999
Chlorambucil	Human plasma	200	Aut. SPE	I: A-W-F	ESI (+)	MRM	SIL	4	2.5	Yes		Davies, Allonson & Causon, 1999
Chlorambucil	Human serum	200	Aut. SPE	I: A-W-F	ESI (+)	MRM	SIL	4	2.5	Yes		
Melphalan	Human plasma	200	Aut. SPE	I: A-W-F	ESI (+)	MRM	SIL	2	2.5	No		Davies, Allonson & Causon, 2000
Melphalan	Human serum	200	Aut. SPE	I: A-W-F	ESI (+)	MRM	SIL	2	2.5	No		
Thiotepa-mercapturate	Human urine	90	None	I: A-AA pH4.8	ESI (+)	Q1	Other	1000	14	-	Metabolite of thiotepa	van Maanen & Beijnen, 1999
Busulfan	Human plasma	200	LLE	I: M-AA	ESI (+)	SIM	SIL	5	10	No		Quernin et al., 2001
Busulfan	Human plasma	200	LLE	G: A-AA,HA	ESI (+)	SIM	SIL	5	11	No		Mürdter et al., 2001
MTIC	Rat plasma	70	PP	I: M-AA,F	ESI (+)	MRM	An.	10	4.5	No		Chowdhurry et al., 1999
MTIC	Dog plasma	70	PP	I: M-AA,F	ESI (+)	MRM	An.	10	4.5	No		

Abbreviations:

A	Acetonitrile	I	Isocratic elution	Ref.	References
AA	Ammonium acetate in water	IS	Internal standard	SIL	Stable isotopically labeled internal standard
AF	Ammonium formate in water	LC	Liquid Chromatography	SIM	Selective ion monitoring mode
AH	Ammonium hydroxide in water	LLOQ	Lower limit of quantitation	SPE	Solid phase extraction
An.	Structural analogue	LLE	Liquid-liquid extraction	W	Water
Aut.	Automated	M	Methanol		
ESI	Electrospray ionization	Met. Quan.	Metabolites quantified		
F	Formic acid	MRM	Multiple reaction monitoring mode		
G	Gradient elution	MS	Mass spectrometry		
HA	Acetic acid	PP	Protein precipitation		

1.8 References

1. Stokvis, E.; Rosing, H.; Beijnen, J. H. Liquid Chromatography-Mass Spectrometry for the Quantitative Bioanalysis of Anticancer Drugs. *Mass Spectrometry Reviews* **2005**, *24* (6), 887–917.
2. Nassar, A. F.; Wisnewski, A.V.; Wu T.; Lam T. T.; King, I. Development and Validation of LC–MS-MS Assay for the Determination of the Emerging Alkylating Agent Laromustine and Its Active Metabolite in Human Plasma. *Journal of Chromatographic Science* **2018**, *57* (3), 195–203.
3 Weinstain, R.; Savariar E. N.; Felsen C. N.; Tsien R. Y. In vivo targeting of hydrogen peroxide by activatable cell-penetrating peptides. *J Am Chem Soc* **2014**, *136*, 874-877.
4. Lin, Z.; Fan, H.; Zhang, Q.; Peng, X. Design, Synthesis, and Characterization of Binaphthalene Precursors as Photoactivated DNA Interstrand Cross-Linkers. *The Journal of Organic Chemistry* **2018**, *83* (16), 8815–8826.
5. Chen, W.; Balakrishnan, K.; Kuang, Y.; Han, Y.; Fu, M.; Gandhi, V.; Peng, X. Reactive Oxygen Species (ROS) Inducible DNA Cross-Linking Agents and Their Effect on Cancer Cells and Normal Lymphocytes. *Journal of Medicinal Chemistry* **2014**, *57* (11), 4498–4510.
6. Wang, Y.; Lin, Z.; Fan, H.; Peng, X. Corrigendum: Photoinduced DNA Interstrand Cross-Link Formation by Naphthalene Boronates via a Carbocation. *Chemistry - A European Journal* **2017**, *23* (46), 11175–11175.
7. Chen, W.; Fan, H.; Balakrishnan, K.; Wang, Y.; Sun, H.; Fan, Y.; Gandhi, V.; Arnold, L. A.; Peng, X. Discovery and Optimization of Novel Hydrogen Peroxide Activated Aromatic Nitrogen Mustard Derivatives as Highly Potent Anticancer Agents. *Journal of Medicinal Chemistry* **2018**, *61* (20), 9132–9145.
8. Huang, Y.; Li, L. DNA crosslinking damage and cancer - a tale of friend and foe, *Transl Cancer Res* **2013**, *2*, 144-154.
9. Skoog, D. A.; Holler, F. J.; Crouch, S. R. *Principles of instrumental analysis*; Cengage Learning: Boston, MA, 2018.
10. Annesley, T. Ion Suppression in Mass Spectrometry. *Clinical Chemistry* **2003**, *49* (7), 1041–1044.
11. Baumann, F.; Lorenz, C.; Jaehde, U.; Preiss, R. Determination of Cyclophosphamide and Its Metabolites in Human Plasma by High-Performance Liquid Chromatography–Mass Spectrometry. *Journal of Chromatography B: Biomedical Sciences and Applications* **1999**, *729* (1-2), 297–305.
12. De Jonge, M. E.; Van Dam, S. M.; Hillebrand, M. J.; Rosing, H.; Huitema, A. D.; Rodenhuis, S.; Beijnen, J. H. Simultaneous Quantification of Cyclophosphamide, 4-Hydroxycyclophosphamide,N,N′,N″-Triethylenethiophosphoramide(Thiotepa) And N,N′,N″-Triethylenephosphoramide(Tepa) in Human Plasma by High-Performance Liquid Chromatography Coupled with Electrospray Ionization Tandem Mass Spectrometry. *Journal of Mass Spectrometry* **2004**, *39* (3), 262–271.
13. Turci, R.; Sottani, C.; Ronchi, A.; Minoia, C. Biological Monitoring of Hospital Personnel Occupationally Exposed to Antineoplastic Agents. *Toxicology Letters* **2002**, *134* (1-3), 57–64.
14. Bahr, U.; Schulten, H. R. Isolation, Identification and Determination of Cyclophosphamide and Two of Its Metabolites in Urine of a Multiple Sclerosis Patient by High Pressure Liquid Chromatography and Field Desorption Mass Spectrometry. *Biological Mass*

Spectrometry **1981**, *8* (11), 553–557.
15. Davies, I. D.; Allanson, J.P.; Causon, R.C. Rapid Determination of the Anti-Cancer Drug Chlorambucil (Leukeran™) and Its Phenyl Acetic Acid Mustard Metabolite in Human Serum and Plasma by Automated Solid-Phase Extraction and Liquid Chromatography–Tandem Mass Spectrometry. *Journal of Chromatography B: Biomedical Sciences and Applications* **1999**, *732* (1), 173–184.
16. Bokman, C. F. Analytical Aspects of Atmospheric Pressure Ionization in Mass Spectrometry. Ph.D. Dissertation. Uppsala University, Uppsala, Sweden, 2002.
17. Bruins, A. P.; Covey, T. R.; Henion, J. D. Ion Spray Interface for Combined Liquid Chromatography/Atmospheric Pressure Ionization Mass Spectrometry. *Analytical Chemistry* **1987**, *59* (22), 2642–2646.
18. Wolff, J. C.; Eckers, C.; Sage, A. B.; Giles, K.; Bateman, R. Accurate Mass Liquid Chromatography/Mass Spectrometry on Quadrupole Orthogonal Acceleration Time-of-Flight Mass Analyzers Using Switching between Separate Sample and Reference Sprays. 2. Applications Using the Dual-Electrospray Ion Source. *Analytical Chemistry* **2001**, *73* (11), 2605–2612.
19. Chu, J.; Fang, S.; Xin, P.; Guo, Z.; Chen, Y. Quantitative Analysis of Plant Hormones Based on LC-MS/MS. *Hormone Metabolism and Signaling in Plants* **2017**, 471–537.
20. Shahin, M. M. Ion—Molecule Interaction in the Cathode Region of a Glow Discharge. *The Journal of Chemical Physics* **1965**, *43* (5), 1798–1805.
21. Horning, E. C.; Carroll, D. I.; Dzidic, I.; Haegele, K. D.; Horning, M. G.; Stillwell, R. N. Atmospheric Pressure Ionization (API) Mass Spectrometry. Solvent-Mediated Ionization of Samples Introduced in Solution and in a Liquid Chromatograph Effluent Stream. *Journal of Chromatographic Science* **1974**, *12* (11), 725–729.
22. Tabei, K.; Siegel, M. M. 47th ASMS Conference on Mass Spectrometry, 1999, Dallas, TX, June 13-17, 1999, NO 234.
23. Covey, T.; Jong, R.; Javahari, H.; Liu, C.; Thomson, C.; LeBlanc, Y. 49th ASMS Conference on Mass Spectrometry, 2001, Chicago, IL, May 27-31, 2001, TPC077.
24. Kostiainen, R.; Kauppila, T. J. Effect of Eluent on the Ionization Process in Liquid Chromatography–Mass Spectrometry. *Journal of Chromatography A* **2009**, *1216* (4), 685–699.
25. LCMS-2020. https://www.shimadzu.com/an/lcms/lcms2020/duis.html (accessed Nov 20, 2019).
26. Loos, G.; Van Schepdael, A.; Cabooter, D. Quantitative Mass Spectrometry Methods for Pharmaceutical Analysis. *Philosophical Transactions of the Royal Society A: Mathematical, Physical and Engineering Sciences* **2016**, *374* (2079), 20150366.
27. Robinson, B. https://www.chem.purdue.edu/gchelp/howtosolveit/Kinetics/Halflife.html (accessed Nov 7, 2019).
28. Masimirembwa, C. M.; Bredberg, U.; Andersson, T. B. Metabolic Stability for Drug Discovery and Development. *Clinical Pharmacokinetics* **2003**, *42* (6), 515–528.
29. Zhao, M.; Lepak, A. J.; Andes, D. R. Animal Models in the Pharmacokinetic/Pharmacodynamic Evaluation of Antimicrobial Agents. *Bioorganic & Medicinal Chemistry* **2016**, *24* (24), 6390–6400.
30. Scarfe, G. B.; Wilson, I. D.; Spraul, M.; Hofmann, M.; Braumann, U.; Lindon, J. C.; Nicholson, J. K. Application of directly coupled high-performance liquid chromatography-nuclear magnetic resonance-mass spectrometry to the detection and characterization of the metabolites of 2-bromo-4-(trifluoromethyl)aniline in rat urine. *Anal. Commun.* **1997**, *34*, 37-39.

31. Elipe, M. V. S. *LC-NMR and other hyphenated NMR techniques overview and applications*; Wiley: Hoboken, NJ, 2012.
32. Down, S. A Primer on LC/NMR/MS. https://www. spectroscopynow.com/details/education/sepspec10145education/A-Primer on-LCNMRMS.html?1,1=& (accessed Nov 11, 2019).
33. Burton, K.I.; Everett, J. R.; Newman, M. J.; Pullen, F. S.; Richards, D. S.; Swanson, A. G. On-line liquid chromatography coupled with high-field NMR and mass spectrometry (LC-NMR-MS): a new technique for drug metabolite structure elucidation. *J. Pharm. Biomed. Anal.* **1997**, *15*, 1903-1812.
34. Gebretsadik, T.; Linert, W.; Thomas, M.; Berhanu, T.; Frew, R. LC-NMR for Natural Products Analysis: A Journey from an Academic Curiosity to a Robust Analytical Tool. *Sci* **2019**, *1* (1), 31.
35. Walker, G. S.; Oconnell, T. N. Comparison of LC-NMR and Conventional NMR for Structure Elucidation in Drug Metabolism Studies. *Expert Opinion on Drug Metabolism & Toxicology* **2008**, *4* (10), 1295–1305.
36. Albert, K. *On-line LC-NMR and related techniques*; John Wiley & Sons: Chichester, 2002.
37. Lommen, A.; Godejohann, M.; Venema, D. P.; Hollman, P. C. H.; Spraul, M. Application of Directly Coupled HPLC−NMR−MS to the Identification and Confirmation of Quercetin Glycosides and Phloretin Glycosides in Apple Peel. *Analytical Chemistry* **2000**, *72* (8), 1793–1797.
38. Dear, G. J., Ayrton, J.; Plumb, R.; Sweatman, B. C.; Ismail, I. M.; Fraser, I. J.; Mutch, P. J. A rapid and efficient approach to metabolite identification using nuclear magnetic resonance spectroscopy, liquid chromatography/mass spectrometry and liquid chromatography/nuclear magnetic resonance spectroscopy/sequential mass spectrometry. *Rapid Commun. Mass Spectrom.* **1998**, *12*, 2023-1930.
39. Dear, G. J., Plumb, R.; Sweatman, B. C.; Ayrton, J.; Lindon, J. C.; Nicholson, J. K.; Ismail, I. M. Mass directed peak selection, an efficient method of drug metabolite identification using directly coupled liquid chromatography-mass spectrometry-nuclear magnetic resonance spectroscopy. *J. Chromatogr. B* **2000**, *748*, 281-293.
40. Clayton, E.; Taylor, S.; Wright, B.; Wilson, I. D. The application of high-performance liquid chromatography, coupled to nuclear magnetic resonance spectroscopy and mass spectrometry (HPLC-NMR-MS), to the characterization of ibuprofen metabolites from human urine. *Chromatographia* **1998**, *47*, 264-270.
41. Watanabe, N.; Niki, E. Direct-Coupling of FT-NMR to High Performance Liquid Chromatography, *Proc. Jpn. Acad. Ser. B. Phys. Biol. Sci.* **1978**, *54* 194–199.
42. Haw, J.; Glass, T.; Dorn, H. Continuous Flow High Field Nuclear Magnetic Resonance Detector for Liquid Chromatographic Analysis of Fuel Samples. *Analytical Chemistry* **1981**, *53* (14), 2327–2332.
43. Laude, D.; Wilkins, C. Direct-Linked Analytical Scale High-Performance Liquid Chromatography/Nuclear Magnetic Resonance Spectrometry. *Analytical Chemistry* **1984**, *56* (13), 2471–2475.
44. Smallcombe, H.; Patt, S.; Keifer, P. WET Solvent Suppression and Its Applications to LC NMR and High-Resolution NMR Spectroscopy. *Journal of Magnetic Resonance, Series A* **1995**, *117* (2), 295–303.
45. Subramanian, R.; Kelley, W. P.; Floyd, P. D.; Tan, Z. J.; Webb, A. G.; Sweedler, J. V. A

Microcoil NMR Probe for Coupling Microscale HPLC with On-Line NMR Spectroscopy, *Anal. Chem.* **1999**, *71*, 5335–5339.
46. Corcoran, O.; Spraul, M. LC–NMR–MS in Drug Discovery. *Drug Discovery Today* **2003**, *8* (14), 624–631.
47. Creative Proteomics. Triple Quadrupole Mass Spectrometry. https://www.creative-proteomics.com/technology/triple-quadrupole-mass-spectrometry.htm (accessed Nov 12, 2019).
48. Santoiemma, G. Recent Methodologies for Studying the Soil Organic Matter. *Applied Soil Ecology* **2018**, *123*, 546–550.
49. Ito, S.; Chikasou, M.; Inohana, S.; Fujita, K. Analysis of Processed Foods Containing Oils and Fats by Time of Flight Mass Spectrometry with an APCI Direct Probe, *Food Hygiene and Safety Science* ***2016***, *57* (5), 2016, 160–165.

CHAPTER 2. EXPERIMENTAL

2.1 Experimental Conditions of Halogenated Aromatic Compounds as UV/ROS-Activated DNA Interstrand Cross-linking Agents by Liquid Chromatography Single Quadruple Mass Spectrometry

2.1.1 Chemical Reagents and Compounds

All solvents used in this work (including water) were LC-MS grade and were used without further purification. Water, acetonitrile (MeCN), methanol (MeOH), and formic acid (HCOOH) were obtained from Fisher Scientific (Pittsburgh, PA, USA). Lastly, 2 mL glass MS autosampler vials were purchased from (Shimadzu Corp., Kyoto, Japan).

2.1.2 Sample Preparation

All compounds analyzed were provided by other group members.

Binapthalene Analogues **3**, **4**, **5**, and **6** (including naphthalene precursors **5** and **6**)

A concentration of ~0.5 mg/mL sample of **3** and **4** was prepared for LC-MS analysis. This was done by dissolving the respective compound in a 2:1 ratio of LC-MS grade MeCN:MeOH and vortexing the solution for 10 s, then sonicating the solution for 10 min and vortexing for another 10 s. A dilution of the100 μM sample was prepared for LC-MS analysis. After the samples were prepared in vials, the vials were wrapped in aluminum foil to prevent photodegradation of the compound.

A 1.0 mM sample of **5** and **6** was prepared for LC-MS analysis. This was done by dissolving the compound in LC-MS grade acetonitrile and vortexing the solution for 10 s, then

sonicating the solution for 10 min and vortexing again for 10 s. Dilutions of 250 µM and 100 µM were prepared from the stock.

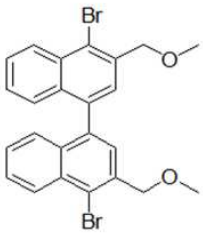

3

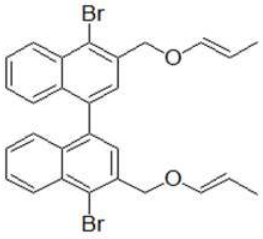

4

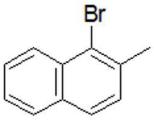

5

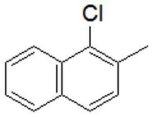

6

Methoxybenzene Analogues **7**, **8, 9**, and **10**

A 1.00 mM sample of **7**, **8**, **9**, and **10** was prepared for LC-MS analysis. This was done by dissolving the compound in LC-MS grade MeOH and vortexing the solution for 10 s, then sonicating for 10 min and then vortexing again for 10 s. Dilutions of 100 µM and 10 µM were also prepared, however they were not concentrated enough to achieve a distinct signal on the MS instrument.

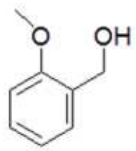

7

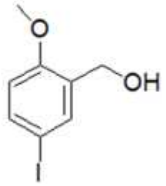

8

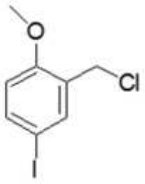

9

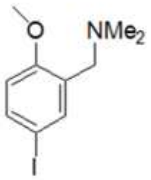

10

2.1.3 Mobile Phases for LC-MS

Naphthalene precursors **5** and **6**

The mobile phase was composed of water with 0.1% HCOOH (v/v) (A) and MeCN (B). The gradient programming was the following: 50% B (0.0 min) → hold at 100% MeCN B (6 min) → return to 50% B (2.5 min) → hold at 50% MeCN B (3.5 min). The column ttempérature was 40 °C.

Binapthalene Analogues **3**, **4**

The mobile phase was composed of water with 0.1% HCOOH (v/v) (A) and MeCN (B). The gradient programming was the following: 10% B (0.0 min) → 100% MeCN (8.0 min) → hold at 100% B (12.0 min) → return to 10% B (20.1 min) → hold at 10% B (18 min). The column temperature was 40 °C.

2-Methoxy Analogues and Starting Material **7**, **8**, **9**, and **10**

The mobile phase was composed of water with 0.1% HCOOH (v/v) (A) and MeOH (B). The gradient programing was the following: 20% B (0.0 min) → 40% MeOH (1.0 min) → 60% B (2.0 min) → 80% MeOH (3.0 min) → hold at 90% B (2.0 min) → return to 20% B (7.0 min). The column temperature was 40 °C.

2.1.4 Instrumentation

Naphthalene precursors **5** and **6**

Qualitative LC-MS (Shimadzu Model 2020, Shimadzu Corp., Kyoto, Japan) (Figure 2-1 (a)) analysis was employed to confirm the identity of the compounds. An Agilent TC-C18

column (4.6 mm x 250 mm, 5 µm particle size, Agilent Technologies, Santa Clara, CA, USA) was used for separation. The ionization sources for the 2020 model include ESI, APCI, and dual mode (DUIS), as seen in Figure 2-1b. The sample (10 µL) was injected into the LC-MS instrument in APCI mode, with the corona discharge needle set to an optimal position of 5 mm. Images of the corona discharge needle setting can be seen in Figure 2-2 (a) and (b). The MS was operated with the following method factors:

- heat block temperature at 400 °C
- drying gas flow rate of 15 L/min
- desolvation line temperature of 250 °C
- nebulizing gas flow rate of 1.5 L/min
- interface voltages of 4.5 kV
- positive or negative: APCI modes

The LC and column were operated with the following factors:

- gradient elution flow rate of 0.7 mL/min
- column oven temperature of 40 °C
- 200-400 nm UV-VIS molecular absorption detection

All experiments were conducted in duplicate with blank solvent injections in between each set of duplicate trials.

Binapthalene Analogues **3** and **4**

Qualitative LC-MS (Shimadzu 2020, Shimadzu Corp., Kyoto, Japan) analysis was employed to confirm the identity of the compounds. 10 µL of the sample was injected into the LC-MS instrument. The ionization mode was ESI. The MS was operated with the method

parameters as described for *Brominated and Chlorinated Naphthalene Analogues*.

2-Methoxy Analogues and Starting Material **7**, **8**, **9**, and **10**

Qualitative LC-MS (Shimadzu 2020, Shimadzu Corp., Kyoto, Japan) analysis was employed to confirm the identity of the compound. An ultra-high pressure column, (ACQUITY CSH C18, 2.1 mm × 50 mm, 1.7 μm particle size, Waters Corp, Milford, MA, USA), was used for separation. The sample (5 μL) was injected into the LC-MS instrument. The ionization mode was optimized to be dual ESI/APCI mode with the corona discharge needle set to an optimized position of 10 mm.

- heat block temperature at 400 °C
- drying gas flow rate of 15 L/min
- desolvation line temperature of 250 °C
- nebulizing gas flow rate of 1.5 L/min
- interface voltages of 4.5 kV
- positive or negative: DUIS (dual mode ionization)

The LC and column were operated with the following factors:

- gradient elution at a flow rate of 0.5 mL/min
- column oven temperature of 40 °C
- 190-700 nm UV-VIS molecular absorption detection

All experiments were conducted in triplicate with blank solvent injections in between each set of triplicate trials.

2.2 Experimental Conditions of Microsomal Stability Assay

2.2.1 Chemical Reagents

The solvents were LC-MS grade and were used without further purification. Water, acetonitrile (MeCN), methanol (MeOH), formic acid (HCOOH), and potassium phosphate buffer were obtained from Fisher Scientific (Pittsburgh, PA, USA). The NADPH (Nicotinamide adenine dinucleotide phosphate) Regenerating System Solution A and B were purchased from Corning Life Science (Corning, NY, USA). Human and mouse (CD-1) microsomes were purchased from Thermo Fisher Scientific (Waltham, MA, USA). Dimethyl sulfoxide (DMSO) was purchased from Cambridge Isotope Laboratories (Tewksbury, MA, USA). Spin-X HPLC filter tubes (0.22 □m) were purchased from Corning Inc. (Corning, NY, USA). Lastly, 2 mL glass MS autosampler vials were purchased from (Shimadzu Corp., Kyoto, Japan).

2.2.2 Sample Preparation

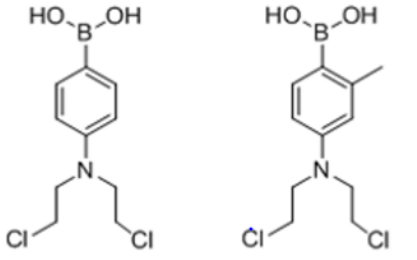

CWB-20145 **FAN-NM-CH3**

1 **2**

A stock mix was prepared containing 282 µL of deionized water (18.2 mΩ-cm, 80 µL of potassium phosphate buffer (0.5 M, pH 7.4), 20 µL of NADPH Regenerating System

Solution A, 4 µL of NADPH Regenerating System Solution B, and 10 µL of human or mouse microsomes (for a final microsomal concentration of 0.5 mg/mL). The stock mix was pre-incubated at 37 ºC for 5 min. Directly after pre-incubation, 4 µL of the drug compound (1 mM in DMSO) was added to initiate the reaction and upon the addition of the drug compound, the duration of the reaction was recorded. The reaction mixture was then allowed to incubate at 37 ºC. After the incubation was complete, aliquots of 50 uL of the reaction mixture were retrieved at various time intervals (without compound): 0, 10, 20, 30, 40, 50, and 60 min. These aliquots were added to 100 µL of ice-cold MeCN that contained 3 µM of internal standard (IS), and then the mixture was immediately sonicated for 10 s and centrifuged at 10,000 rpm for 5 min. Compounds **1** and **2** served as the IS for each other, thus when **1** was the target analyte, **2** was the respective IS, and vice versa. Next 100 µL aliquots of the supernatant were transferred to Spin-X HPLC filter tubes and centrifuged at 13,000 rpm for 5 min. Finally, 50 µL of the filtrate was diluted 1:20 with MeOH (950 µL) and transferred to a 2 mL
l glass auto sampler vial for analysis.

Standards for the assay were prepared to establish a calibration model. Standard concentrations for the analysis were: 1, 10, 50, 100, 200 nM, and the IS compounds were each at a concentration of 10 nM. To minimize solvent effects, the diluent was composed of a 1:1 ratio of water with 0.1% (v/v) HCOOH and MeCN.

2.2.3 Mobile Phases for LC-MS/MS

The mobile phase was composed of water with 0.1% HCOOH (v/v) (A) and MeOH (B) (to prevent the formation of adducts). The gradient programming was the following: 30% B

(0 min) → 40% MeCN (1.5 min) → 90% B (2.0 min) → hold at 90% B (0.5 min) → return to 35% B (0.5 min) → hold at 35% B (2 min). The column temperature was 40 °C.

2.2.4 Instrumentation

The samples prepared as described above were analyzed by quantitative LC-MS/MS (Shimadzu 8040, Shimadzu Corp., Kyoto, Japan) (Figure 2-3) to monitor product ion values and establish a calibration model. The sample (10 µL) was injected into the LC-MS instrument equipped with an ACQUITY CSH C18 column (2.1 mm × 50 mm with 1.7 µm particle size) obtained from Waters Corp. (Milford, MA, USA). The ionization mode was APCI mode with the corona discharge needle set to an optimal position of 5 mm. The MS was operated with the following method parameters:

- heat block temperature at 400 °C
- drying gas flow rate of 15 L/min
- desolvation line temperature of 250 °C
- nebulizing gas flow rate of 2.0 L/min
- interface voltages of 4.5 kV
- positive ESI modes

The LC and column were operated with the following factors:

- gradient elution at a flow rate of 0.6 mL/min
- column oven temperature of 40 °C
- 254 nm UV-VIS detection

All experiments were conducted in triplicate with blank solvent injections in between each set of

triplicate trials.

The following ion pair transitions are monitored in multiple reaction monitoring (MRM) mode for **1** and **2** (IS), respectively: m/z 275.90 —> 164.10, m/z 275.90 —> 213.10, m/z 275.90 —> 146.10 and m/z 262.10 —> 150.10, m/z 262.10 —> 199.10, m/z 262.10 —> 132.10. Collision energies were optimized for each transition for sensitivity.

The system control and data acquisition for the LC-MS/MS was performed on a Dell desktop computer (Round Rock, TX, USA) and using *LabSolutions* software version 6.2 SP1 (Shimadzu Corp, Kyoto, Japan). All experiments represent two independent days in triplicate.

2.3 Experimental Conditions of Pharmacokinetic Studies

2.3.1 Animal Model and Experimental Practices

Female CD-1 mice (Charles River Laboratory, Wilmington, MA, USA) that were four-six weeks old were used for the determination of the drug compound's pharmacokinetic properties. Each trial of the study was performed in triplicate. All animal experiments were performed in compliance with the University of Wisconsin−Milwaukee or Columbia University Institutional Animal Care and Use Committees (IACUC). Such a protocol stipulated that the animals were housed in conditions that are free of specific pathogens and under controlled standard environmental conditions such as humidity, temperature, and lighting (a 12 hr light and dark cycle). The lab animals also had free access to both food and water. Before the commencing of the experiment, the animals were allowed to adapt to their caging environment for a period of

~5 days, to ensure their comfort.

2.3.2 Chemical Reagents

The solvents used were LC-MS grade and were used without further purification. Water, methanol (MeOH), and formic acid (HCOOH), were obtained from Fisher Scientific (Pittsburgh, PA, USA). The phosphate-buffered solution (PBS) and PEG400 were acquired from Fisher Scientific (Pittsburgh, PA, USA). Dimethyl sulfoxide DMSO was purchased from Cambridge Isotope Laboratories (Tewksbury, MA, USA). Herapin was purchased from Fisher Scientific (Pittsburgh, PA, USA). Spin-X HPLC filter tubes were purchased from Corning Incorporated (Corning, NY, USA). 384-well optical bottom plates and 96-well plates were purchased from Nunc (Roskilde, Denmark). Lastly, 2 mL glass MS autosampler vials were purchased from Shimadzu Corp. (Kyoto, Japan). For organs, the hand held LabGEN 7b Series Portable Homogenizer; 220 VAC was obtained from Cole-Palmer (Vernon Hills , IL, USA). CellTiter-Glo® Luminescent Cell Viability Assay was purchased from Promega (Madison, WI, USA). Matrigel® solution (protein mixture of type IV collagen, laminin, and heparan sulfate proteoglycan) was obtained from Corning Life Science (Corning, NY, USA).

2.3.3 Sample Preparation

Blood Plasma Pharmacokinetics

Female CD-1 mice (~20 -22 g) were dosed with either drug compound **1** or **2**, at a concentration of 10 mg/kg, that was formulated in PBS/PEG400/DMSO (19:19:2) and

administered intraperitoneally (IP), with three mice to a group. After the drug administration and after the animal was placed under terminal CO_2, blood was periodically drawn by cardiac puncture and collected into tubes containing 50 μL of herparin (1 mg/mL in water) to prevent coagulation. The blood samples were then stored in liquid nitrogen until analysis was performed.

To prepare the samples for LC-MS/MS analysis, the blood samples were thawed slowly on ice and vortexed for 10 s. Next, a 100 μL aliquot was taken and added to 300 μL cold MeOH that was premixed with 133.3 ng/mL of internal standard (IS). This mixture was then vortexed again for 30 s and centrifuged at 14,000 rpm for 5 min. The supernatant layer was then spin-filtered through Spin-X HPLC filter tubes. Finally 150 μL samples of the filtrate was transferred to a 2 mL glass autosampler vials for analysis.

Liver Pharmacokinetics

Female CD-1 mice (~20 -22 g) were dosed with either drug compound **1** or **2**, at a concentration of 10 mg/kg, that was formulated in PBS/PEG400/DMSO (19:19:2) and administered by IP, with three mice to a group. Samples were then treated as described above.

The samples were removed from the liquid nitrogen and thawed slowly on ice. The organ was then removed from the vial and placed on a tray, where it was rinsed with water to remove excess blood, gently dried, and placed in a new vial. The organ was then homogenized for 10 s on a setting that did not allow the homogenizer probe to get too hot. Careful rinsing of the homogenizer probe was done between each sample to minimize contamination.

In the next step, 300 μL of cold MeOH containing 133.3 ng/mL of IS was added to the homogenized organ. This mixture was then vortexed for 30 ss and centrifuged at 14,000 rpm for 5 min. The supernatant layer was then spin-filtered through Spin-X HPLC filter tubes and the

remaining contents of the vial were discarded. Finally, 150 µL samples of the filtrate were transferred to a 2 mL glass autosampler vials for analysis.

Brain Pharmacokinetics

The preparation of the sample for the brain pharmacokinetics was the same as described for the *Liver Pharmocokinetics* section. Note that the brain was the harvested organ.

2.3.4 Mobile Phases for LC-MS/MS

Blood Plasma Pharmacokinetics, Liver Pharmacokinetics, Brain Pharmacokinetics

The mobile phase was composed of water with 0.1% HCOOH (v/v) (A) and MeOH (B). The gradient programing was the following: 35% B (0) → 35% MeOH (0.5 min) → 40% B (1.0 min) → hold at 40% B (1.5 min) → 90% MeOH (2.0 min) → hold at 90% B (2.5 min) → return to 35% B (3.0 min) → hold at 35% B (4.0 min). The column temperature was 40 °C.

2.3.5 Instrumentation

Blood Plasma Pharmacokinetic Analysis

Quantitative LC-MS/MS (Shimadzu 8040, Shimadzu, Kyoto, Japan), analysis employed to monitor product ion values, as depicted in Figure 2-1. 10 µL of the sample was injected into the LC–MS/MS (Shimadzu 8040, Shimadzu Corp., Kyoto, Japan) instrument equipped with ACQUITY CSH C18 column (2.1 mm × 50 mm, 1.7 µm particle size) (Waters Corp, Milford, MA, USA. The MS was operated with the following method parameters:

- heat block temperature at 400 °C
- drying gas flow rate of 15 L/min
- desolvation line temperature of 250 °C
- nebulizing gas flow rate of 2.0 L/min
- interface voltages of 4.5 kV
- positive ESI mode

The LC and column were operated with the following factors:

- gradient elution at a flow rate of 0.6 mL/min
- column oven temperature at 40 °C
- 254 nm UV-VIS detection

All experiments were conducted in triplicate with blank solvent injections in between each set of triplicate trials.

The following ion pair transitions are monitored in multiple reaction monitoring (MRM) mode for **1** (IS) and **2**, respectively: m/z 275.90 > 164.10, m/z 275.90 > 213.10, m/z 275.90 > 146.10 and m/z and 262.10 > 150.10, m/z 262.10 > 199.10, m/z 262.10 > 132.10. Collision energy was optimized for each transition to obtain optimal sensitivity, via the instrument computer software.

The system control and data acquisition for the LC-MS/MS was performed on a Dell desktop computer (Round Rock, TX, USA) using *LabSolutions* software version 6.2 SP1 (Shimadzu Corp., Kyoto, Japan). All experiments represent two independent days in triplicate.

Liver Pharmacokinetic Analysis

The preparation of the sample for the liver pharmacokinetic analysis was the same

as described for the *Blood Plasma Pharmacokinetic Analysis* section.

Brain Pharmacokinetic Analysis

The preparation of the sample for the brain pharmacokinetic analysis was the same as described for the *Blood Plasma Pharmacokinetic Analysis* section.

2.4 Experimental Conditions of HPLC-UV-NMR Interfaced Scheme

2.4.1 Chemical Reagents

The solvents were LC-MS grade and were used without further purification. Water, acetonitrile (MeCN), and formic acid (HCOOH), were obtained from Fisher Scientific (Pittsburgh, PA, USA). Chloroform-d was purchased from Cambridge Isotope Laboratories (Tewksbury, MA, USA). Lastly, LC-MS grade toluene was purchased from Sigma-Aldrich (St. Louis, MO, USA).

2.4.2 Mobile Phases used in Interfaced System

The mobile phase was composed of water with 0.1% HCOOH (v/v) (A) and MeCN (B). The gradient programing was the following: 0% MeCN B (0.0 min) → 15% MeCN (5.0 min) → 30% MeCN B (3.0 min) → 45% MeCN B (3.0 min) → return to 0% MeCN (3.0 min) → hold at 0% MeCN B (6.0 min).

2.4.3 Sample Preparation

A 100 μM sample solution of toluene in chloroform-d was prepared from a 1 mM stock solution. The sample was transferred to a 2 mL glass autosampler vial for analysis. Lastly, 2 mL glass MS autosampler vials were purchased from (Shimadzu Corp., Kyoto, Japan).

2.4.4 Instrumentation

NMR

PicoSpin Model 45 and Model 80 benchtop NMR instruments (Thermo Fisher Scientific, Madison, WI) were used. A diagram of the components of the NMR instrument is found in Figure 2-4. The instrument was shimmed with LC-MS grade water twice weekly and water was injected in the instrument holding cell, during storage. All samples, including those for shimming, were injected via the inlet port, a diagram of which is depicted in Figure 2-5.

Digital Valve Sequence Programmer

The Digital Valve Sequence Programmer (Model DVSP-4, Valco Instruments, Houston, TX, USA) (Figure 2-6) was wired as described in the manual (*4*). The depicting of the terminals and their wiring can be found in Figure 2-7a (*4*) with an image in Figure 2-7b. The six-port, two -position valve (Figure 2-8) was connected to the DVSP (three wires — black, red, and green). Next, the black (INJECT) wire was corrected to the NO ("normally open") terminal of the A relay. The red (LOAD) wire was connected to the NO terminal of the C ("common") relay. Lastly, the green (GROUND) wire was connected to the C terminal of the C relay. Times were set on the DVSP to synchronize the elution time of the analyze from the column, i.e., to

automatically switch the FIA from LOAD to INJECT.

HPLC

A separation of the sample was performed using the Agilent 1100 HPLC (Santa Clara, CA, USA) (Figure 2-9) (5). The sample (10 μL) was injected into the HPLC instrument. The HPLC was operated with the following method parameters:

- Agilent TC-C18 column (4.6 mm x 250 mm, 5 μm particle size) (Agilent Technologies, Santa Clara, CA, USA)
- gradient elution at a flow rate of 0.3 mL/min
- column oven temperature at 40 °C
- 190-700 nm UV-VIS detection

2.5 Figures and Tables:

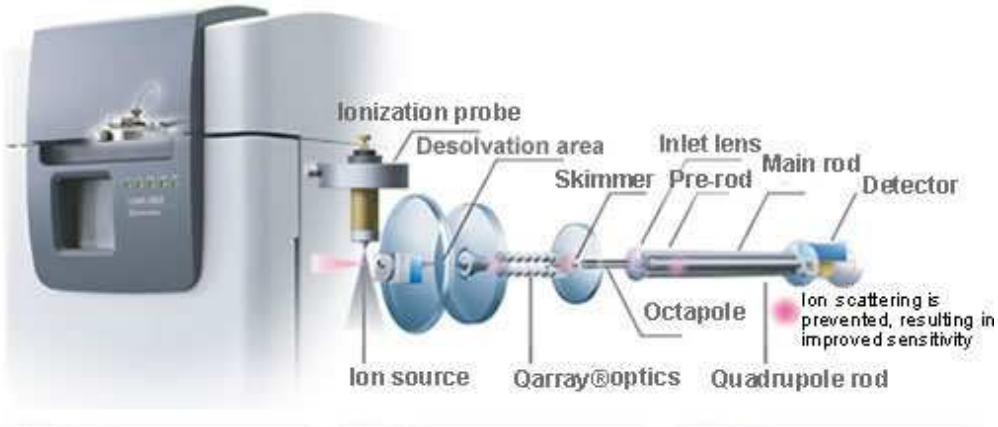

Figure 2-1a. Schematic diagram of Shimadzu 8020 LC-MS/MS (adapted from Shimadzu) (1).

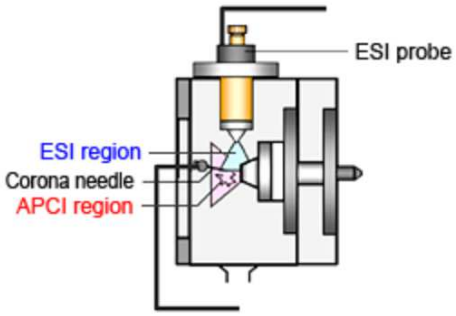

Figure 2-1b. Schematic diagram of Shimadzu 8040 LC-MS/MS (*1*).

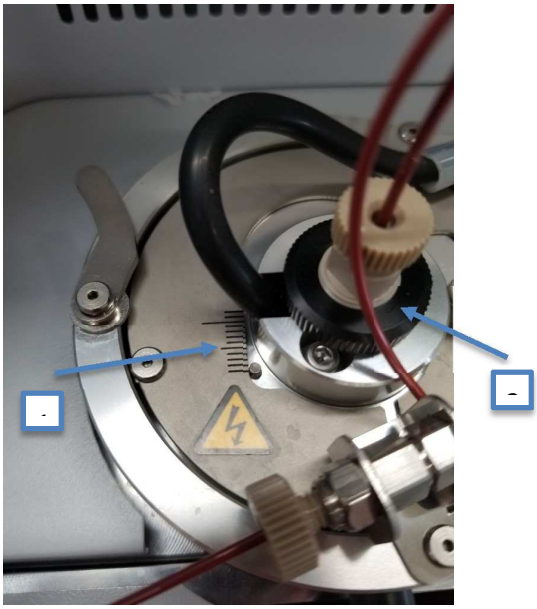

Figure 2-2a. Image of the corona discharge needle setting on the MS instrument. 1 = distance intervals (mm) for the adjustment of the corona discharge needle. 2 = the corona discharge needle sample inlet.

Figure 2-2b. Image of the corona discharge needle (3) on the MS instrument.

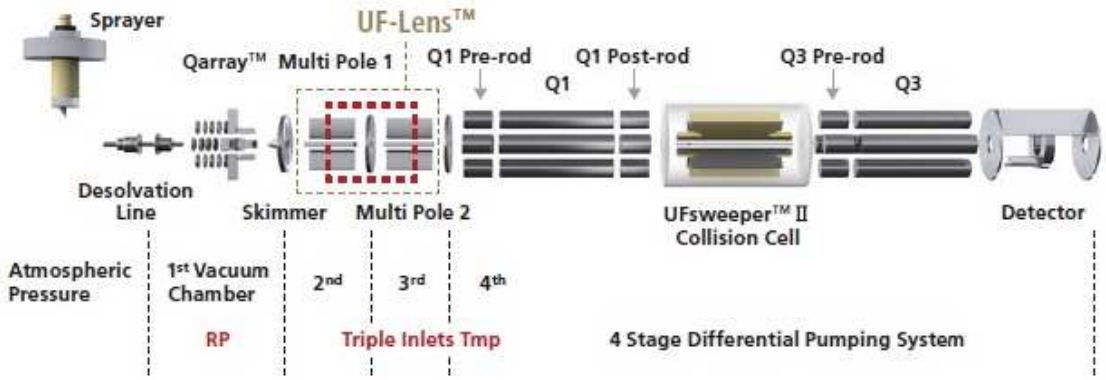

Figure 2-3. Schematic diagram of Shimadzu 8040 LC-MS/MS (Adapted from Shimadzu) (*1*).

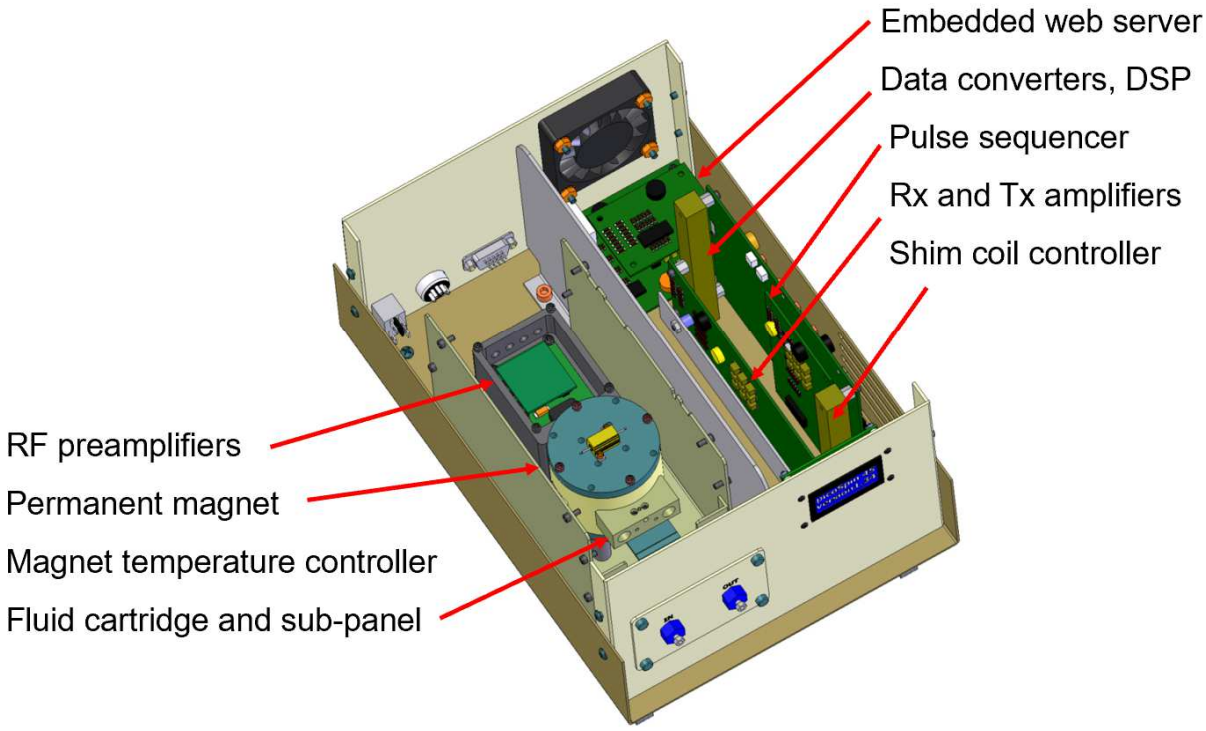

Figure 2-4. Diagram of the picoSpin NMR components (*3*).

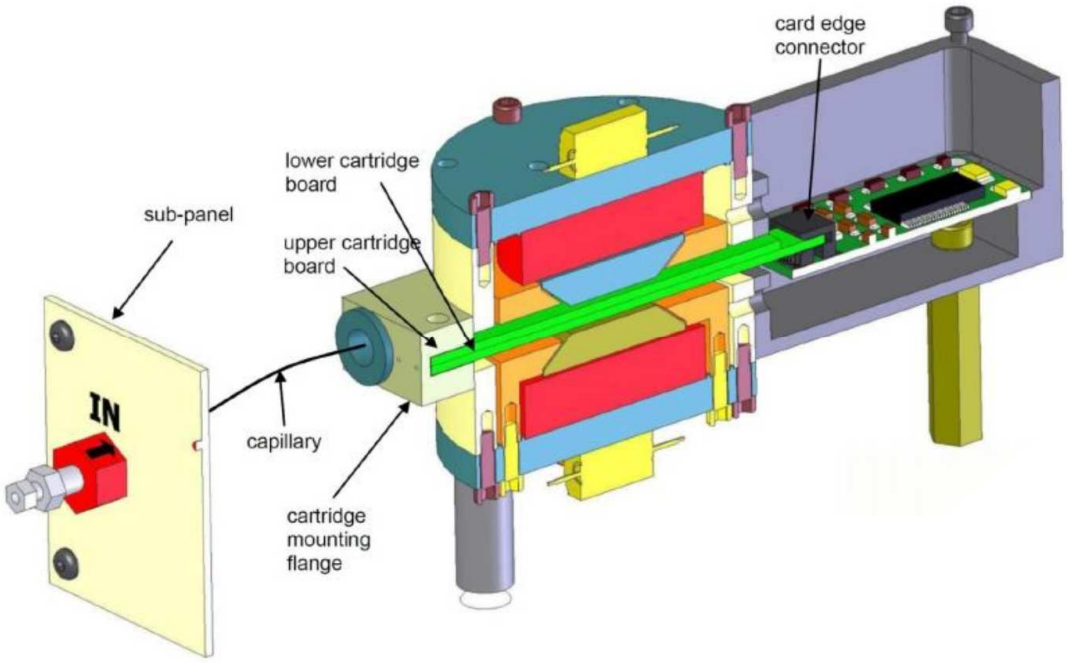

Figure 2-5. Diagram of the picoSpin NMR inlet port and components (*3*).

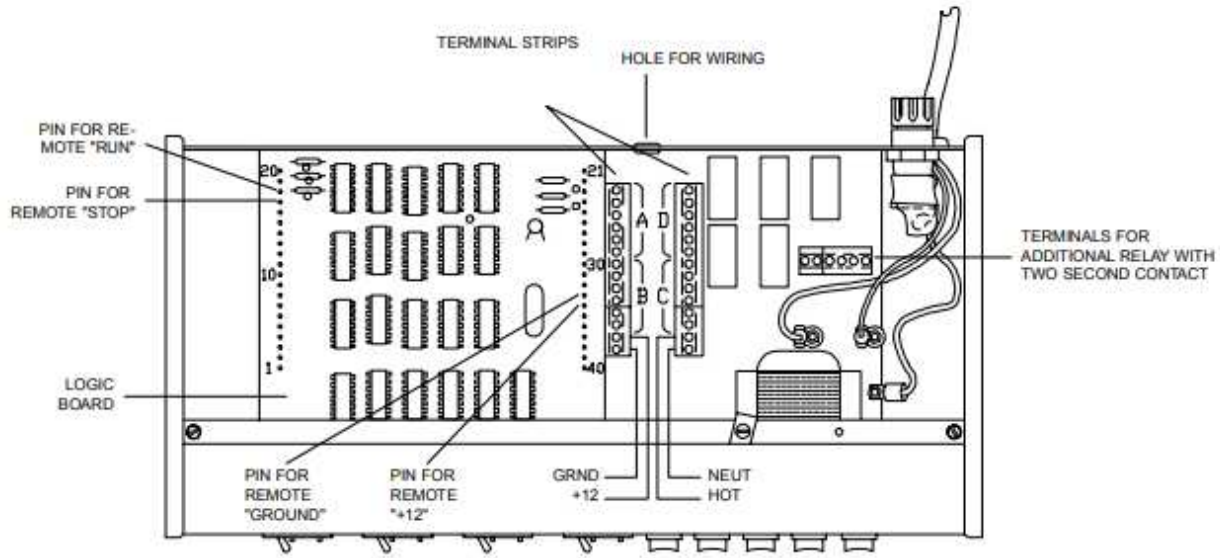

Figure 2-6. Schematic of the DVSP instrument (Adapted from Digital Valve Sequence Programmer Instruction Manual) (*4*).

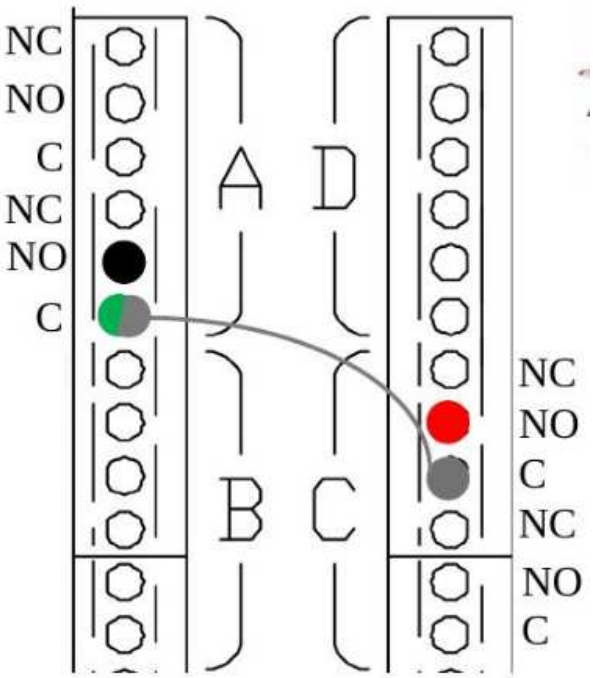

Figure 2-7a. Diagram depicting the terminal strip connections used for the DVSP (Adapted from Digital Valve Sequence Programmer Instruction Manual) (*4*).

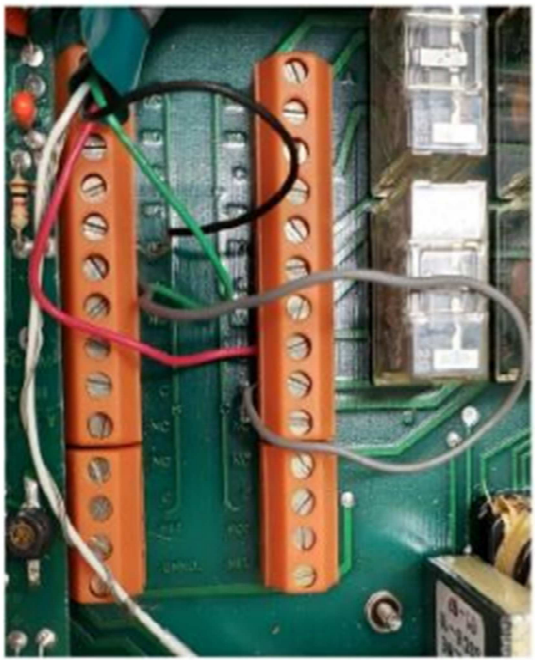

Figure 2-7b. Image of the terminal strip connections used for the DVSP.

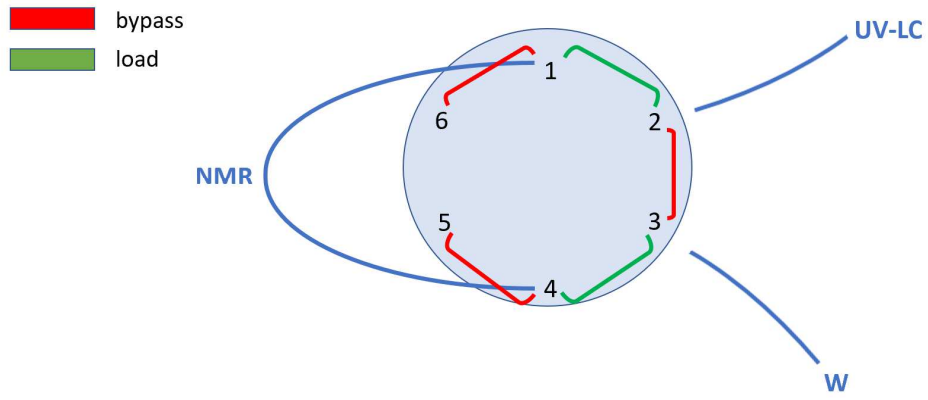

Figure 2-8. Diagram of the six-port valve that interfaced the HPLC and NMR.

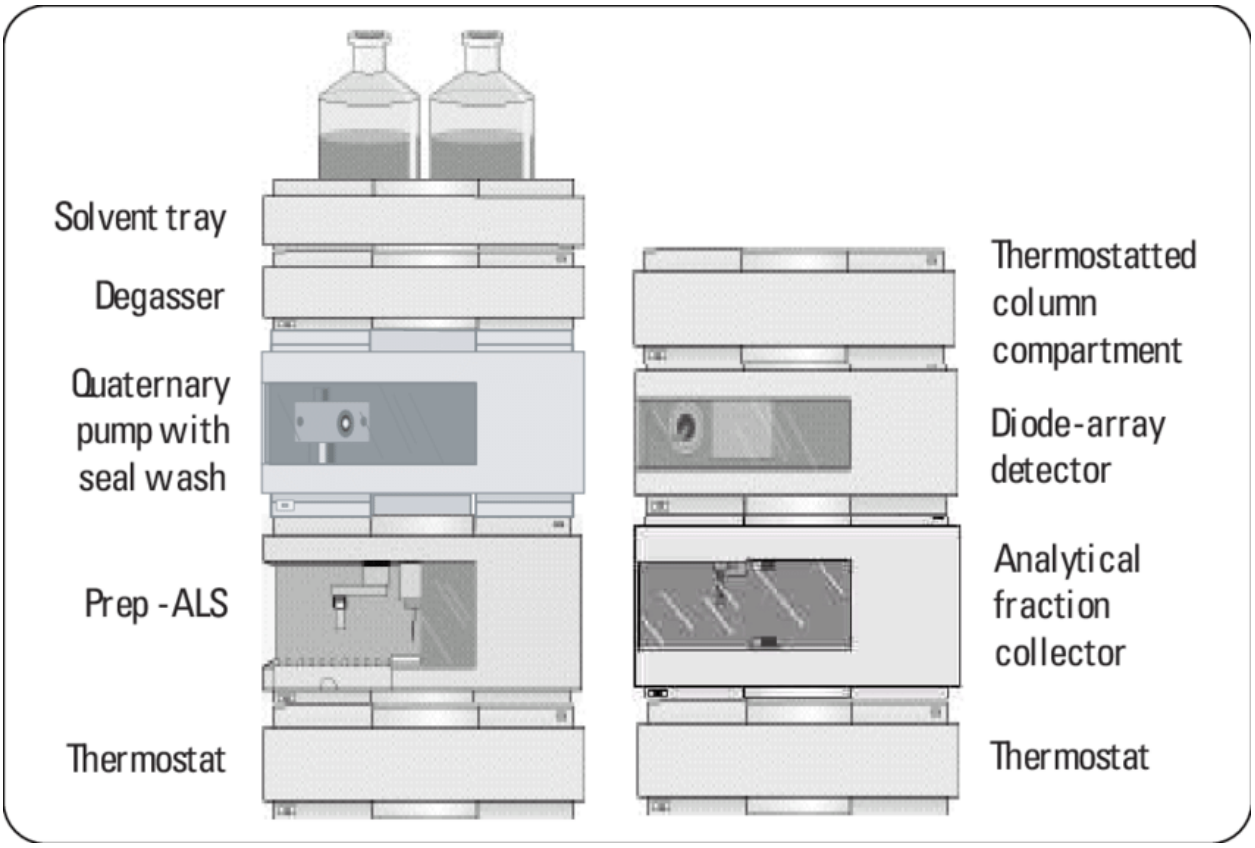

Figure 2-9. Diagram of the Agilent 1100 HPLC instrument and components (*5*).

Table I. A comparison of the properties of picoSpin models 45 and 80 (Adapted from ThermoFisher Scientific) (*3*).

	picospin 45	**picospin 80**
Weight	10.5 lb	43 lb
Larmor Frequency	45 ± 1 MHz	82 ± 2 MHz
Type	Proton	Proton
Sample Form	liquid	liquid
Chemical Shift Resolution	< 20 ppb FWHM	< 40 ppb FWHM
Magnet	Rare Earth Permenent	Rare Earth Permenent
Sample Loop	400 μm Capillary ID	400 μm Capillary ID
Enviornmental	No Cryogens or Compressed Gases	No Cryogens or Compressed Gases
Interface	Ethernet: Direct Connection or LAN	Ethernet: Direct Connection or LAN
User Interface	Web Browser: Data Export; JCAMP-DX	Web Browser: Data Export; JCAMP-DX
Data Analysis	Mestrelab Mnova™	Mestrelab Mnova™

2.6 References

1. Shimadzu Corp. www.shimadzu.com (accessed September, 2019**)**.
2. Verplaetse, R.; Tytgat, J. *LC-MS/MS in forensic toxicology about matrix effects?*; TIAFT Bulletin: Cape Town, South Africa, 2011, *41*, 8-16.
3. PicoSpin product literature, ThermoFisher Scientific, 2019.
4. *Valve Sequence Programmer Instruction Manual*; *Valco Instruments Co. Inc: Houston, TX, 1993.*
5. Vollmer, M.; Nagele, E.; Rufer, A.; Zhang, K. *HPLC Solution for the Removal of High Abundance Proteins in Human Serum*; Application Note; Agilent Technologies: Santa Clara, CA, Nov 1, 2003.

CHAPTER 3. RESULTS AND DISCUSSION

3.1 Characterization of Novel Halogenated Alkylating Compounds by Liquid Chromatography Single Quadruple Mass Spectrometry

3.1.1 Mass Spectrometry Ionization Sources – An Overview of the Theory & Practice

Although there are several types of ionization modes available to use with MS analysis, the two types of ionization sources available on the instrument models used were electrospray ionization (ESI) and atmospheric pressure ionization (APCI), in addition to a dual mode setting that allows the option of both ionization modes used simultaneously. A diagram of depicting compound property and ionization source compatibility is shown in Figure 3-1 (1).

3.1.2 Method Optimization

Achieving ionization of halogenated compounds such as **1** and **2** requires the careful selection of ionization source as well as the optimization of the ionization source parameters, such as corona discharge needle distance from the corona needle. Typically, for ESI mode, it is favorable for ionization for the placement of the corona discharge needle to be further away from the cone while for APCI mode, it is more favorable to have the corona discharge needle closer to the cone. For dual ionization mode, a medium distance is best for a compromise between the two ionization settings, and though this allows for both ionization sources to be used simulatiously,

the signal produced by each respective ionization mode is weaker than if the ionization mode settings were optimized for individual ionization mode use.

Next the calculation for the gradient times (based on the column dimensions, column packing, and flow rate), is determined. This information is used to estimate the void volume and retention time to ensure that there is adequate time given for sample elution as well as column reequilibration. Figure 3-2a (2) defines the signals produced at critical time points of elution such as void time (t_m) and retention time (t_R) and Figure 3-2b shows these signals in an experimentally acquired chromatograph.

3.1.3 Characterization of Novel Compounds

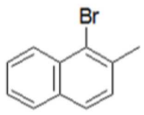

5

Calcd: ([M+1]+): 220.479

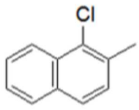

6

Calcd: ([M]+): 176.0280
Found: ([M]+): 176.150

Naphthalene precursors **5** and **6**

In order to qualitatively confirm a particular compound using MS analysis, it is important to determine the molecular mass/charge (m/z) as well as to predict the expected ionization and the peak ratio of isotopes. For example, in the case with **5**, the expected isotope peak pattern for a Br is about a 1:1 peak ratio (of $^{79}Br^+$:$^{81}Br^+$. For a compound with Br_2, the pattern would be expected to be about a 1:2:1 ratio of $^{79,81}Br^+$:$^{79,79}Br^+$:$^{81,81}Br^+$. Similarly, for chlorinated compound such as **6**, the isotope peak pattern is about 3:1 of ^{35}Cl and ^{37}Cl. For a compound with Cl_2, the pattern would be expected to be about a 9:6:1 ratio of $^{35,35}Br^+$:$^{35,37}Br^+$:$^{37,37}Br^+$.

The signal of the first sample, **6**, was detected on the PDA plot as seen on Figure 3-3a and the time point extracted on the MS spectrum (Figure 3-3b) based on the signal produced on the chromatogram. The results should have shown the ionization of the dimerized species at a 3:1 ratio, however this was not the case as the compound did not ionize. Retrospectively, after the successful ionization of similar compounds analyzed later, the most likely issue with the experiment was the low concentration (250 μM) of the compound in the injected sample, which may not have been sufficiently concentrated to produce a signal by MS analysis. Increasing the concentration to 1 mM and in addition, using dual or APCI mode of ionization with optimized corona discharge needle positioning would likely have resolved the ionization issue with **6**.

Upon making the described change in ionization mode (from ESI to APCI) and therefore also the corona discharge needle positioning (optimized to 10 mm), **6** was successfully ionized using simple flow injection (no column) and whist retaining the concentration of 250 μM used previously. In this manner, **6** was successfully detected in the MS spectrum Figure 3-3c (mass region of interest). After the ionization of **6** was established by flow injection, a column gradient method was executed once again confirming the compound as seen in the PDA plot and MS spectrum (Figures 3-4a and b, respectively).

As described above, for APCI analysis, the corona needle position was optimized to the 10 mm through a series of runs of the sample compound at various corona discharge needle positions. Spectra of corona needle positions by intervals of 1 mm are depicted in Figure 3-5 a-i. The setting of 10 mm produced the strongest and most abundant signal for the isotopic ratio of interest, under APCI mode, as seen from Figure 3-6, which summaries the signal intensity vs. corona discharge needle positioning.

Currently compounds **3** and **4,** which contain bromines**,** remain unsuccessfully analyzed

as mass spectrometry analysis was not successful with the brominated compound **5**. Future work can continue with instrumental conditions optimized for the ionization of such brominated naphthalene compounds and hence **3**, **4**, and **5**.

Methoxybenzene Analogues **7**, **8, 9**, and **10**

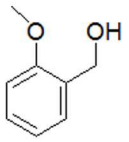

7

Calcd: ([M+1]+): 138.0681

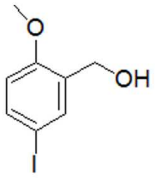

8

Calcd: ([M+]: 263.9637
Found: ([M-OH]+): 247.00

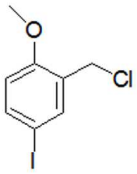

9

Calcd: ([M+1]+): 281.9308
Found: ([M+1]+): 282.00

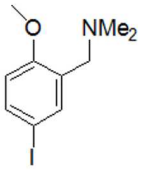

10

Calcd: ([M]+): 292.0120
Found: ([M]+): 292.10

Figure 3-7 a and b are the PDA plot and MS spectrum, respectively, of the uniodinated **10** starting material. Figure 3-8 a and b on the other hand are the PDA plot and MS spectrum respectively of **9**. Both the uniodinated and iodinated compounds ionize in the positive mode and lose an OH^- as evidence from the m/z of 121 for the uniodinated **9** and 247 for the iodinated **9**. Note that the I isotope peak produces a single peak and thus there is no peak ratio to evaluate. Lastly, both compounds ionized in APCI mode with the corona discharge needle optimized to 5 mm.

Compounds **7** and **8** were analyzed by first achieving a signal on the PDA spectrum as seen in Figures 3-9a. This was completed by increasing the concentration of the sample injected to 1.0 mM. Relaying this to the LC chromatogram and analyzing the MS spectrum (Figure 3-9 b) at about 2.9 min produced a 3:1 abundant peaks (76%:24%) for Cl at m/z = 282 and 284. The spectrum was also confirmed as it matched the predicted spectrum for the compound as seen in

Figure 3-10 (3).

Lastly is the analysis of **10** and an unknown sample. Attempting ESI mode as expected did not produce ionization. Two changes were made to remedy this issue. First the sample was dissolved in MeOH rather than ACN (and the mobile phase was also changed to MeOH), to better assist with ionization. Initially MeOH was avoided as the sample solvent due to potential solubility issues as compared to ACN however it was determined compatible. Secondly, switching the ionization mode to dual ESI/APCI modes and optimizing the corona needle position to be at 10 mm produced successful ionization of both compounds in the positive mode (Figure 3-11 a and b). The N on **10** (m/z = 291) is proposed to be protonated. Based on the structure of **10**, the unknown sample was determined to be a byproduct of the drug compound with an m/z = 221. Again, the I has a single abundant isotope (Figure 3-12 a and b).

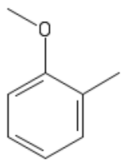

Found: ([M-1]-): 221.16

3.2 Analysis of In Vitro Microsomal Stability Assay

3.2.1 Method Optimization

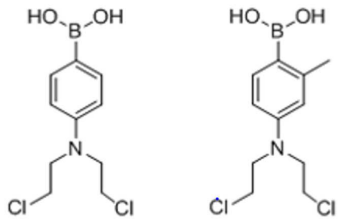

1, CWB-20145 **2,** FAN-NM-CH3

LC Gradient

First the transition ions are monitored in MRM mode for positive and negative ionization events (Figure 3-13 a and b) and the collision energy (CE) for these transition ions (Figure 3-14 a and b) in total and for positive mode, for **2** as determined by LabSolutions software. In addition, various LC gradient methods were attempted in order to balance both length of LC run as well as achieve sufficient separation and peak shape. These changes were established based on the determination of the void volume, which was calculated to be ~0.2 min (although the exact volume is difficult to calculate because the packing space is unknown). The spectrum for a blank ACN sample is depicted in Figure 3-3.This can be seen in Figures 3-(16-18) a-c with an improvement in peak resolution from gradient programming method 1 to 2 by amending the method to have a longer hold time and then a reduction in run time from 9 min to 4 min in gradient programming method 2 to 3 by delaying the gradient. Attempts shorter than 4 min resulted in a reduction in peak resolution so it was determined that method 3 was the optimized gradient programming method.

LC Peak Shape

As MeOH may cause adducts to form, seen in Figure 3-17a as the cause of tailing in the

spectra presented. Thus switched to an ACN as solvent system, while the sample solvent remained MeOH to assist with solubility, improved the peak shape distortion, this improvement seen in Figure 3-18 a and b. Also, peak shape distortions also appeared once again, as seen in Figure 3-19a, depicting the analysis of a 5 nM concentration of IS and 500 nM concentration of 6 in pure ACN. To resolve these peak, it was determined to be caused by solvent effects in the sample, therefore water was added to minimize these solvent effects. A clear improvement can be seen when the water:MeOH ratio of the same sample in a 1:3 water:MeOH, as seen in Figure 3-19b. However, one consideration worth noting for such a change is the stability of the compound in water. It was determined from previous studies by other investigators that **2** is not stable in water due to hydrolyzation, and so to prevent this, the samples were prepared the day of analysis.

Calibration Curve

For the calibration curve, initially standard samples were prepared of 5, 50, 500, 1000, and 5000 nM CP + 500 nM IS concentration, to encompass the calibration curve concentration requirements for both the microsomal stability assay as well as the pharmacokinetic study to come later. Such intervals of standard concentration to IS concentration proved to be too large and as a result the IS drowned the signal of the lower concentration CP, as seen in in the poor calibration curve fit in Figure 3-20 a-c. For this reason, it was decided to create two separate calibration curves, with the microsomal stability assay calibration curve using the concentrations of 1, 10, 50, 100, and 200 nM CP + 10 nM IS, the integration and manual calculations displayed for three trials of each standard concentration and the corresponding calculations as acquired from LabSolutions software in Figure 3-21a and the calibration curves displayed in Figure 3-21

b-d. The manual calculations that were completed confirmed the validity and accuracy of the calculations acquired from LabSolutions software for this particular calibration curve.

Concentrations/Injection Volume

Tailing was also present in the spectra and caused by injection volume (concentration). To amend this issue, the sample injection volume was increased from 20 µL to 50 µL, using the optimized sample preparation mentioned previously at concentrations of both 125 nM and 5 nM of CP. The peak shape improved from this concentration change as evidence in Figure 3-22 and 24, a-b. Most likely such tailing is due to poor signal resolution as a factor of sensitivity.

3.2.2 Calculations for the Determination of Drug Stability - An Overview of the Theory & Practice

The peak area ratios of the IS and test compound were calculated for every time point and the natural log of the ratio was then calculated and plotted as a function of time in order to determine the linear slope (k). The metabolic rate ($k*C_0/C$), half-life (0.693/k), and internal clearance (V*k) were also calculated, where k is the slope, C_0 is the initial concentration of test compound, C is the concentration of microsomes, and V is the volume of incubation (µL) per microsomal protein (mg). As the experiments were performed in triplicate, the values for each time point were averaged prior to the calculation.

For first-order kinetics, the slope eventually decreases to zero and the length of the half-life is constant, independent of concentration. The rate law for first-order kinetics is defined as

$$[A] = [A]_0 e^{-kt}$$

and rearranged to solve for the half-life ($t_{1/2}$) = ln/2 = 0.693/k.

Figure 3-24 (4) shows a graphical distinction between each half-life for first-order kinetics and in Figure 3-25 a and b, the experimental data for the stability assay is correlated to each respective half-life, which from the data, it can be determined that the $t_{1/2}$ exp for human microsomes was 77.06 min and the $t_{1/2}$ ln was 75.34 min. Meanwhile the $t_{1/2}$ exp for mouse microsomes was 33.00 min and the $t_{1/2}$ ln was 33.32 min.

3.3 Analysis of In Vivo Pharmacokinetic Studies

3.3.1 An Overview of the Theory & Practice

To better evaluate the stability and clearance of a drug in vitro and in vivo, several experiments were conducted to compare the parameters of **1** to those of **2**. Figure 3-26 a and b show the results of a pharmacokinetic study on plasma compound concentration (ng/mL) vs. time (min) for **1** and **2**, finding that **2** had about twice the length of half-life as that of **1**.These experiments for **1** were completed at an earlier time, therefore the analysis presented in this evaluation are primarily regarding **2**, however previous data is used in this presentation in a comparative manner. Several organs of the mouse model were harvested to better understand the distribution and clearance of the drug compound **2**. Although at this time not all information is conclusive, the data that has been established is promising.

3.3.2 Blood Plasma Sample Analysis

Figure 3-27 a and b plot the pharmacokinetic results for blood plasma in mice, and as shown with the two experimental trials, there is good reproducibility and in addition both compounds (**1** or **2**) were readily detected in plasma with a t_{max} value of ~3 min. Although both compounds showed rapid drug clearance, the introduction of a CH_3 in **2** greatly increased the duration time of the drug in the plasma with a $t_{1/2}$ of 8.84 min, which is almost two times that of **1** ($t_{1/2}$ = 4.92 min). The rate of elimination for **1** in the blood is considered fast (at a rate of E_{rate} = 0.141 min^{-1}), while the rate of elimination of **2** takes about twice as long (E_{rate} = 0.078 min^{-1}). **2** showed an area under the curve (AUC) of 16253 ng•min/mL, which is significantly higher than that of **1** (10883 ng•min/mL). These conclusions can be seen from Figures 31a and 31b.

3.3.3 Liver Sample Analysis

Figure 3-28 shows the pharmacokinetics results for liver, plotting the compound concentration (ng/mL) vs. time (min). The results show excellent reproducibility as seen by the minimal error bars (not including the first time point which is difficult to experimentally administer precisely. The decay also closely follows that of the plasma pharmacokinetic data, so again confirming reproducibility.

3.3.4 Brain Sample Analysis

Figure 3-29 shows the pharmacokinetics results for brain, plotting the compound concentration (ng/mL) vs. time (min). Interestingly, as there is a relatively high concentration of the CP in a non-targeted organ such as in this case, the brain, this brings into consideration

various adverse effects that may be a negative factor of the CP crossing the blood brain barrier (BBB). On the other hand, the ability of the CP to penetrate the BBB may bring rise to future studies on cancers that target the brain such as glioblastoma. Such a study could include similar stability and pharmacokinetic studies as well as the possibility for tissue imaging through MS-imaging methods such as MALDI (matrix assisted laser desorption ionization) imaging to better understand the drug distribution in the organ as well as to apply quantifiable measurements to these areas of drug distribution within the tissue sample.

3.4 Analysis of HPLC-UV-NMR Interfacing Scheme

3.4.1 HPLC, UV, and NMR - An Overview of the Theory and Practice

Interfacing HPLC to NMR is a powerful combination, particularly for pharmaceutical applications. First, it condenses three different techniques into a single, automated system that requires minimal sample preparation. Furthermore, detectors such as MS can be incorporated into the system because the NMR measurement is non-destructive. Many pharmaceutical approaches that traditionally rely on LC-MS analysis are not adequate for highly reactive or volatile metabolites. Moreover, the interfacing system is complimentary and provides structural information that when assessed together, one method alone could not achieve (*5*).

3.4.2 NMR Component Optimization

To allow for the optimization of each component of the system, spectra can be verified after each interfacing instrument. In the case of the NMR instrument, it was shimmed once a week at a minimum, using water (Figure 3-30). Figure 3-31 a and b are spectra of toluene (10 mM) in deuterated chloroform injected into the instrument after 64 and 512 scans, respectively. As expected, it can be seen from this scan study that more scans increase the S/N ratio. To confirm the acquired spectra, the shift values were compared to a table of published values. In Table I (*3*), shift values can be found for H-NMR for various solvents. In Figure 3-32, an impurity peak found in the spectrum (512 scans) is noted toluene in chloroform (10 mM). Based on Table I, it can be speculated that the peak defined in Figure 3-32 under the right arrow is most likely water (at a 4 ppm shift) and dichloromethane (at a 5.30 ppm shift). Lastly, the integrated spectrum (512 scans) of toluene (10 mM) in chloroform can be found in Figure 3-33 and matches the expected H ratio of 5:3 for CH_3:C_6H_5.

3.4.3 Interfacing LC-NMR: Flow Injection Manifold Design

Although there are several methods of coupling the various instruments, LC-NMR hyphenation typically includes capillary tubing, and a switching value interface (manual or automated). In addition, the interface may be a flow of the sample that is continuous, "on-flow," or "(direct) stop-flow" or the more advantageous "loop storage/loop transfer." The details of the various flow methods can be found in the Introduction chapter. And as mentioned previously, this work incorporates "on-flow," "stop-flow," a "loop transfer" in that the sample is captured the eluted from the NMR, the spectra is acquired in a static state while in the NMR cell, and the

remaining flow is diverted to waste (*6*). Such a LC-NMR system can allow for the analysis of a complex drug sample. Due to the efficient separation from the LC component, the NMR instrument can provide interference free data. In addition, NMR is non-destructive and it can also detect molecules with low molecular weights. NMR can provide both qualitative as well as quantitative information (as the spectral peaks can be integrated to the solvent shift) (*7-8*).

Adding an addition layer and coupling LC to both NMR and MS, whether in-series or in-parallel, offers the advantage of two complimentary and powerful tools in one system. However although there are significant advantages of LC-NMR-MS, one of the major concerns with such a hyphenation is the potential solvent suppression from the NMR signal if non-deuterated solvents are utilized or if this suppression is no resolve. Additionally, NMR is far less sensitive than the MS detector and also cannot detect NMR silent functional groups. Therefore, much research has occurred in the past several decades to interface NMR and MS and establish experimental conditions compatible to run using both detectors.

In recent times, groups have utilized LC-NMR-MS for the determination of endogenous drug metabolites, multiple generations of ion fragments, determination of the parent drug, and many other applications (*8*). As described in detail in the Introduction section, nearly all the historical improvements of LC-NMR were aimed at improvements to parameters such as sensitivity. This was first done by way of component design (thin-walled Teflon tubes and inserts) (1970s and 1980s) (*9-10*). From this point, attention was focused on column improvements (1990s -2000s) to amplify the analyte signal (*11-12*). In addition, flow cells were optimized to be smaller and be enabled for temperature control. Finally continuous flow development and throughput was fine-tuned (*13*).

Although data for the interfaced LC-NMR system is not presented at this time, the

previous portions have described the initial steps of optimization for the concept. In addition, further work can be done on the optimization of the HPLC-UV detector, which requires solvent gradient programming as presented in previous portions of this work, and timing studies to ensure that the sample is held in the NMR sample holding coil at the correct time, shortly after elution from the column. Furthermore, along with NMR, other detectors such as MS can be interfaced both in parallel by varying the widths of the lines to accommodate for varied sample volume required due to varying instrument sensitivity (*14*).

LC-NMR-MS is beneficial in that allows significant tools that not only expands the analysis of the sample, but also allows for high throughput analysis. The main benefit of hyphenating LC-MS is to extrapolatory information such as the sensitivity that MS offers and the structural information from both instrumental methods in a single experiment. As mentioned in the Introduction chapter, there are many varieties of flow for LC-NMR-MS hyphenation, including splitting the flow and coupling in-series preconcentration methods (SPE) and in-parallel analysis (LC-NMR coupled to UV, MS). In general, hyphenation presents issues such as ascribing results to a detector (if done in-series), pressure differences between detectors, and synchronization.

3.5 Figures and Tables

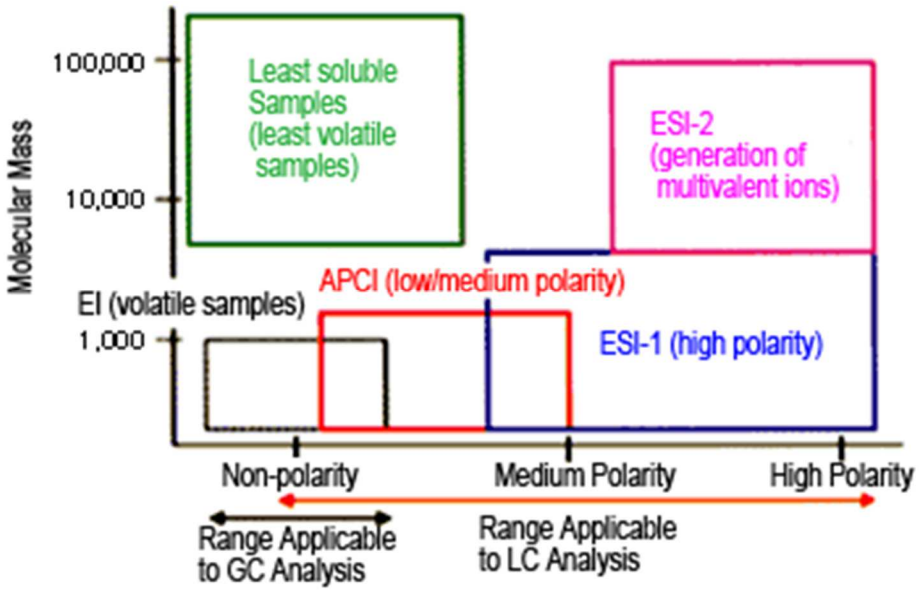

Figure 3-1. A diagram depicting compatible ionization sources for particular compound characteristics such as size molecular mass and polarity (*1*).

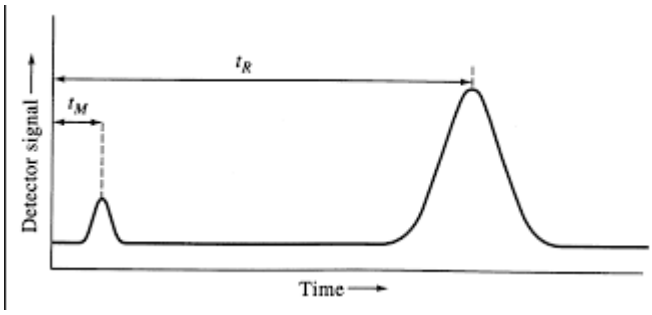

Figure 3-2a: A labeled chromatogram defining the signals produced at critical time points (t_m) and (t_R) (*2*).

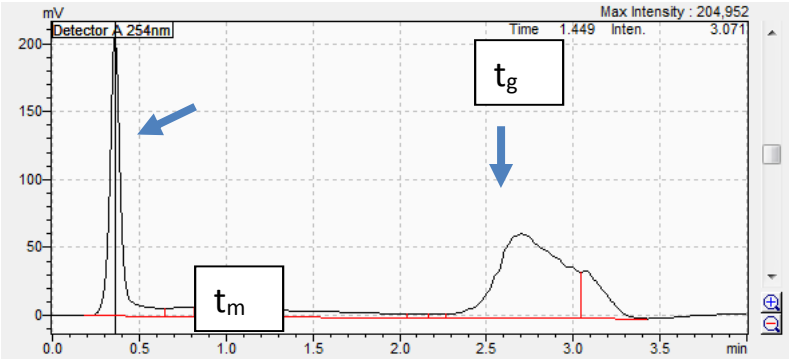

Figure 3-2b. An experimentally acquired chromatogram that labels the terms (t_m) and (t_R) as noted above.

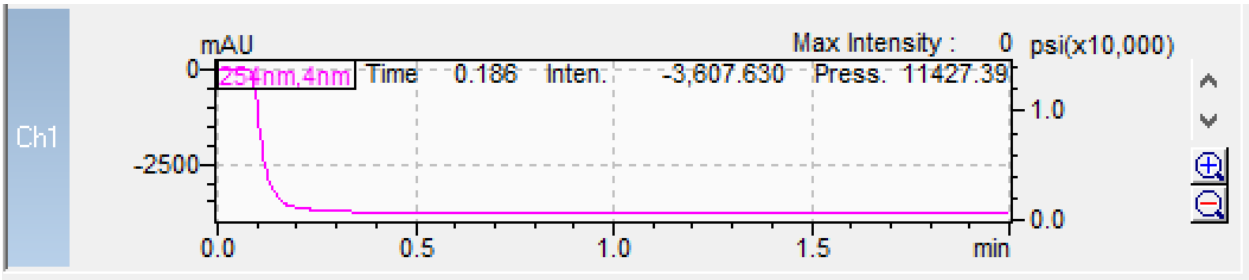

Figure 3-3a. PDA plot of compound 6 using a column, under APCI mode.

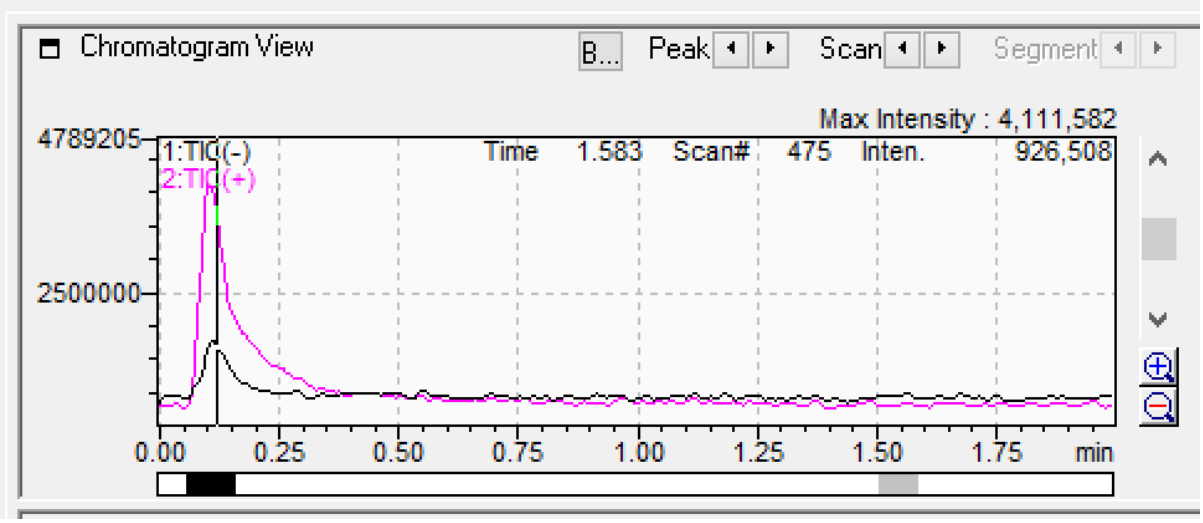

Figure 3-3b. MS spectrum of compound 6 by flow injection, under APCI mode.

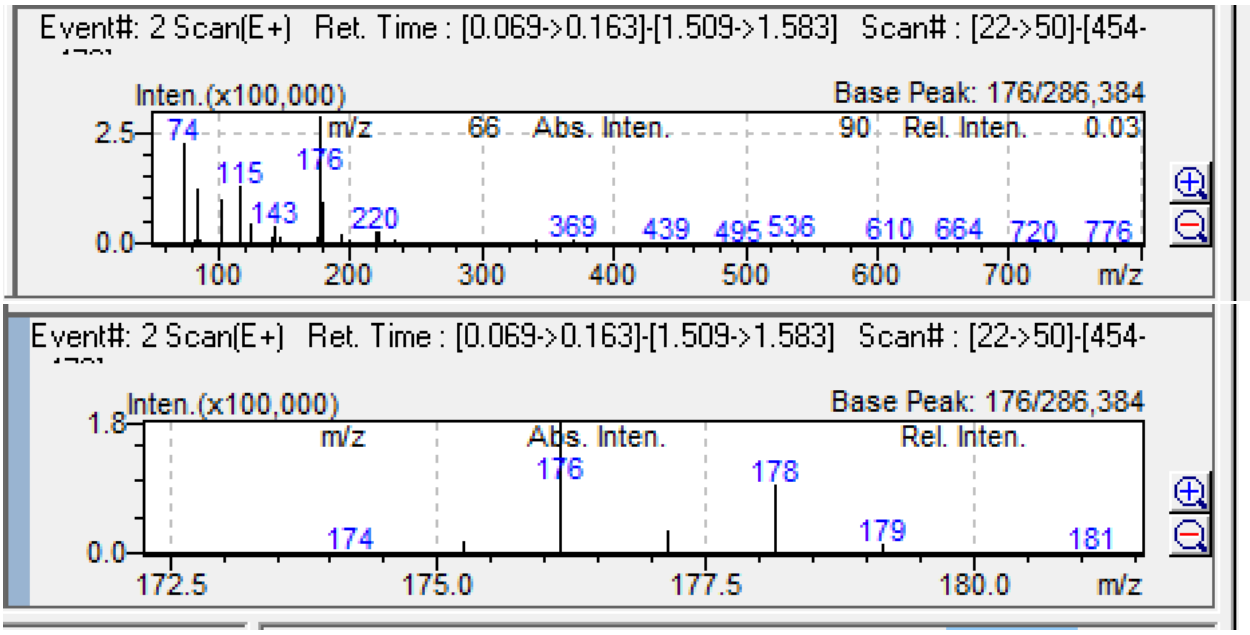

Figure 3-3c. MS spectrum region of interest for compound 6, depicting the Cl isotopic peaks of m/z = 176 and 178, at a 3:1 ratio, under APCI mode.

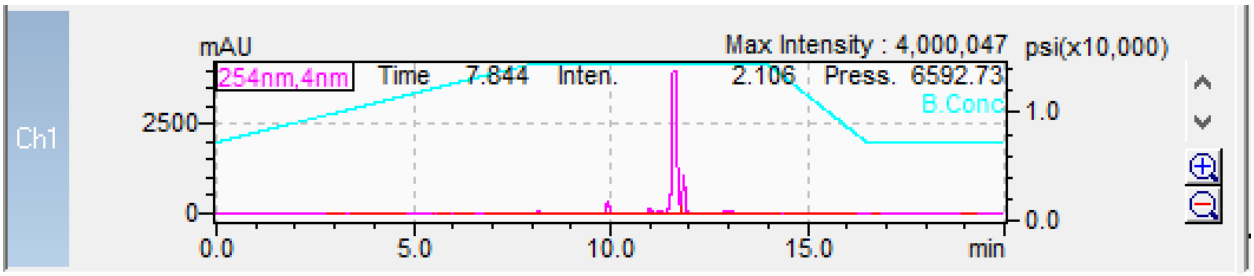

Figure 3-4a. PDA plot of compound 6 using a column, under APCI mode.

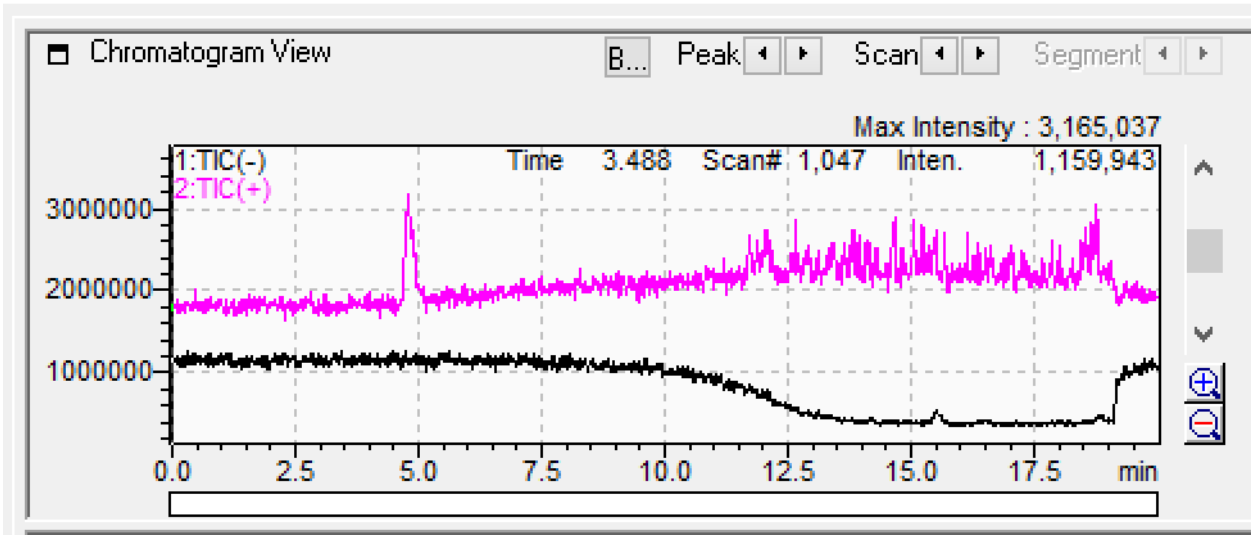

Figure 3-4b. MS spectrum of compound 6 by flow injection, under APCI mode.

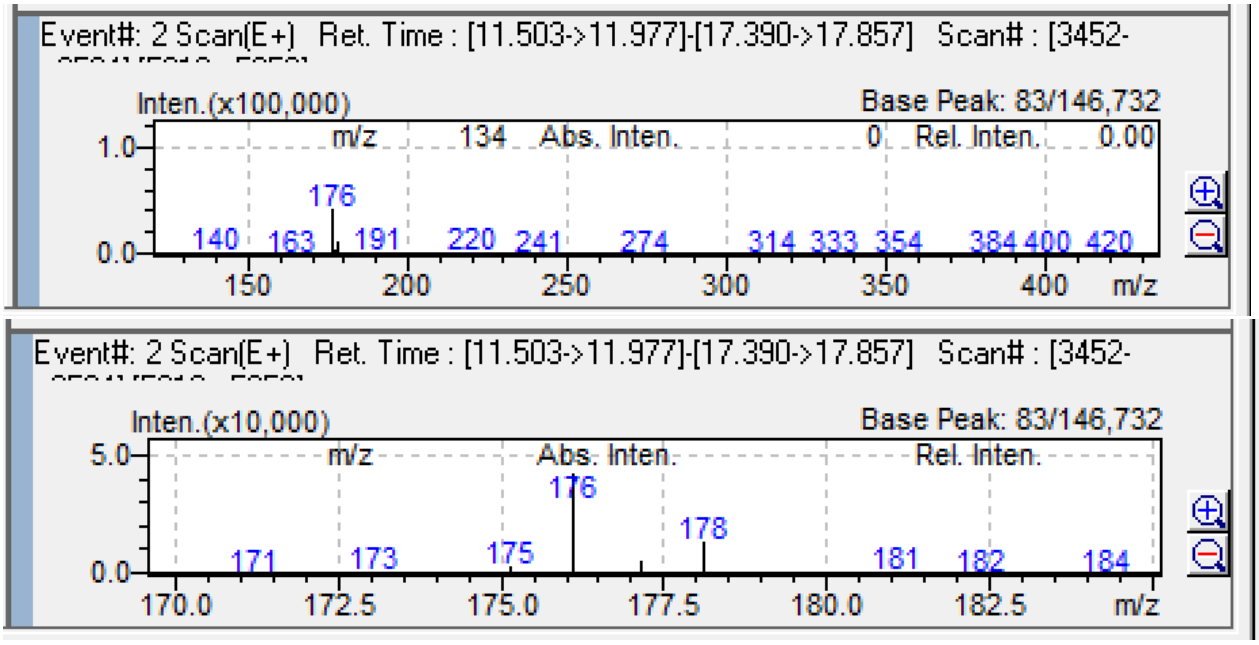

Figure 3-4c. MS spectrum region of interest for compound 6, depicting the Cl isotopic peaks of m/z = 176 and 178, at a 3:1 ratio, under APCI mode.

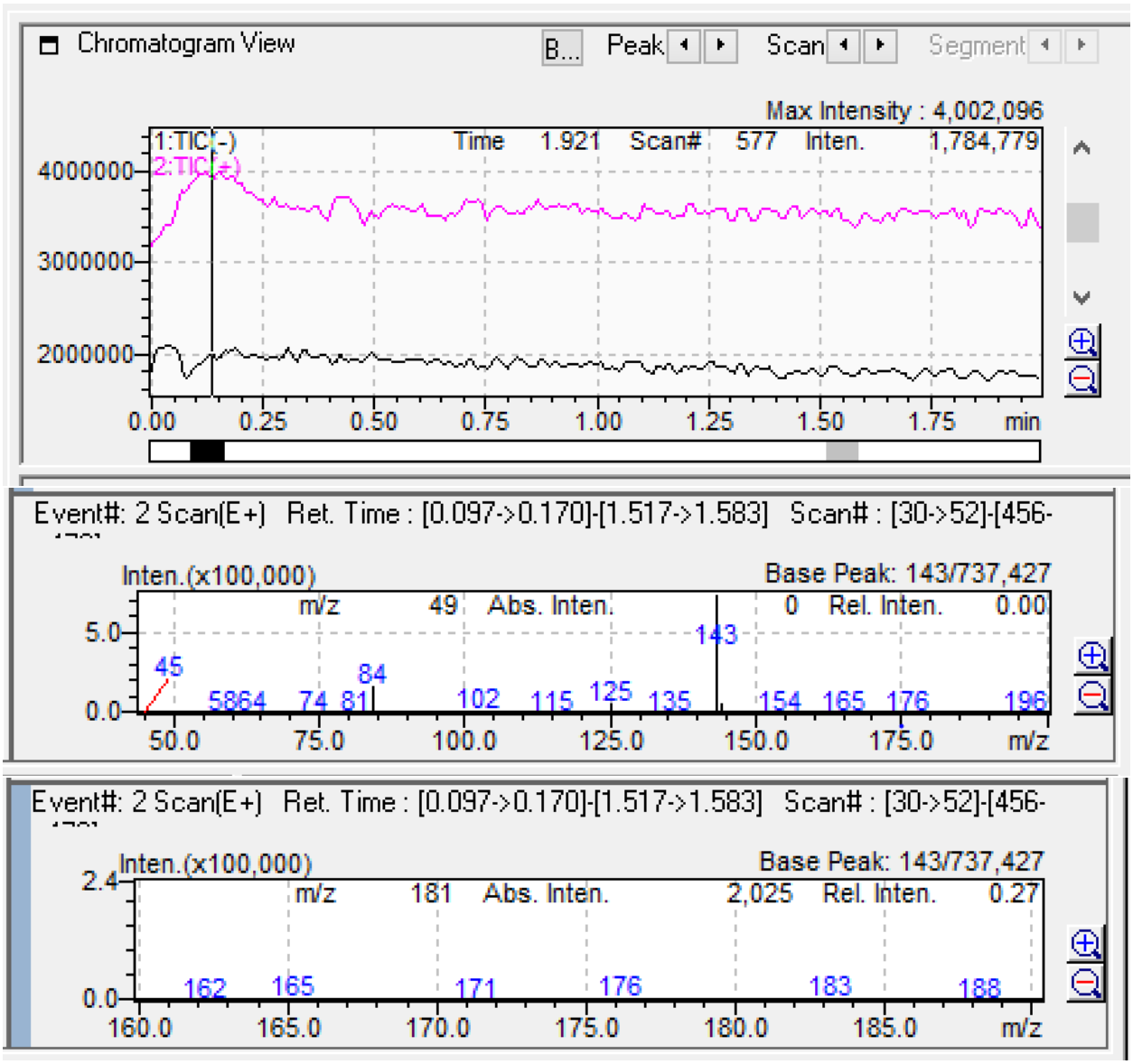

Figure 3-5a. Mass spectrum chromatograph and MS spectrum in APCI mode with corona discharge needle set to 2 mm.

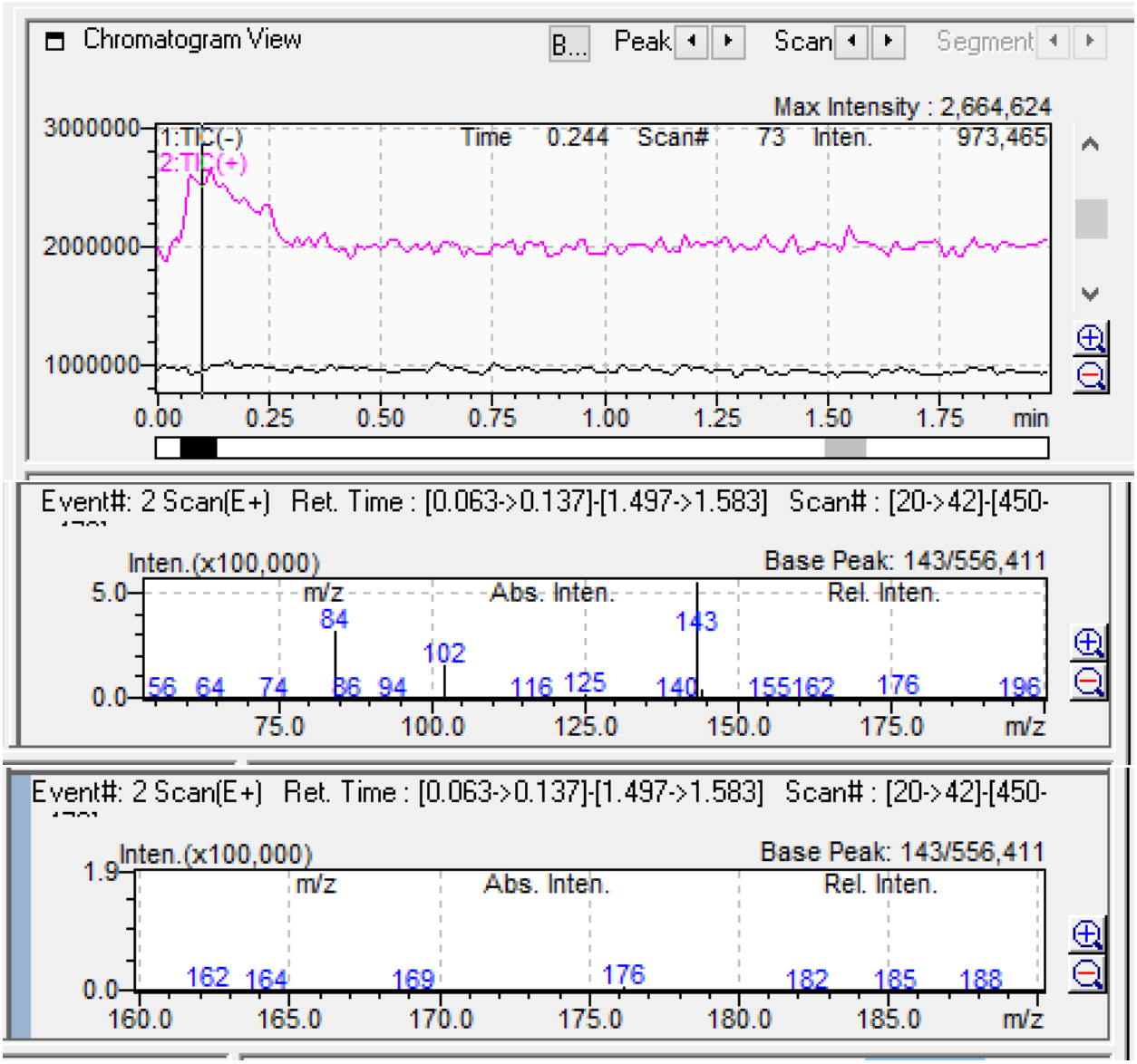

Figure 3-5b. Flow injection chromatograph and MS spectrum in APCI mode with corona discharge needle set to 3 mm.

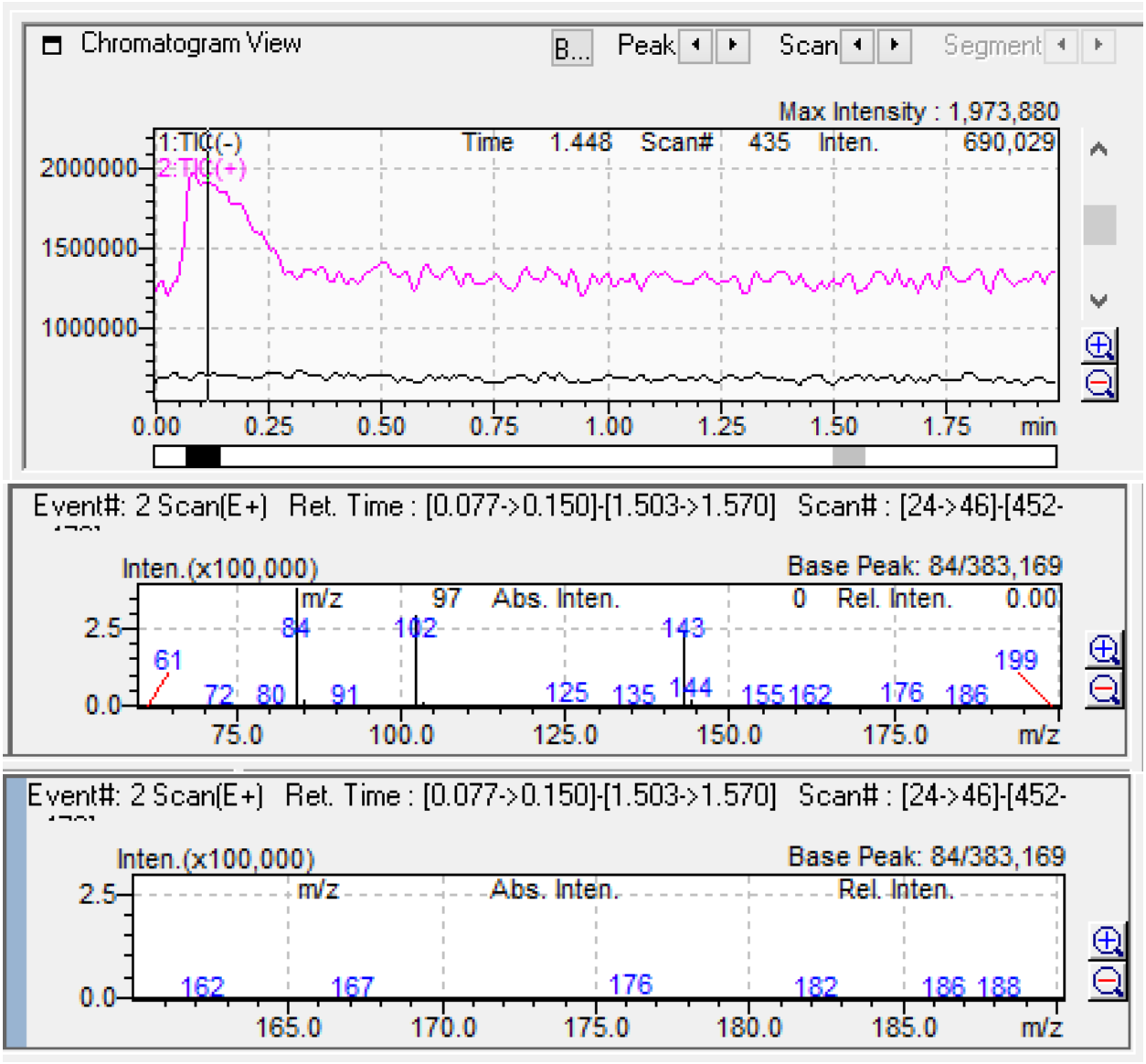

Figure 3-5c. Flow injection chromatograph and MS spectrum in APCI mode with corona discharge needle set to 4 mm.

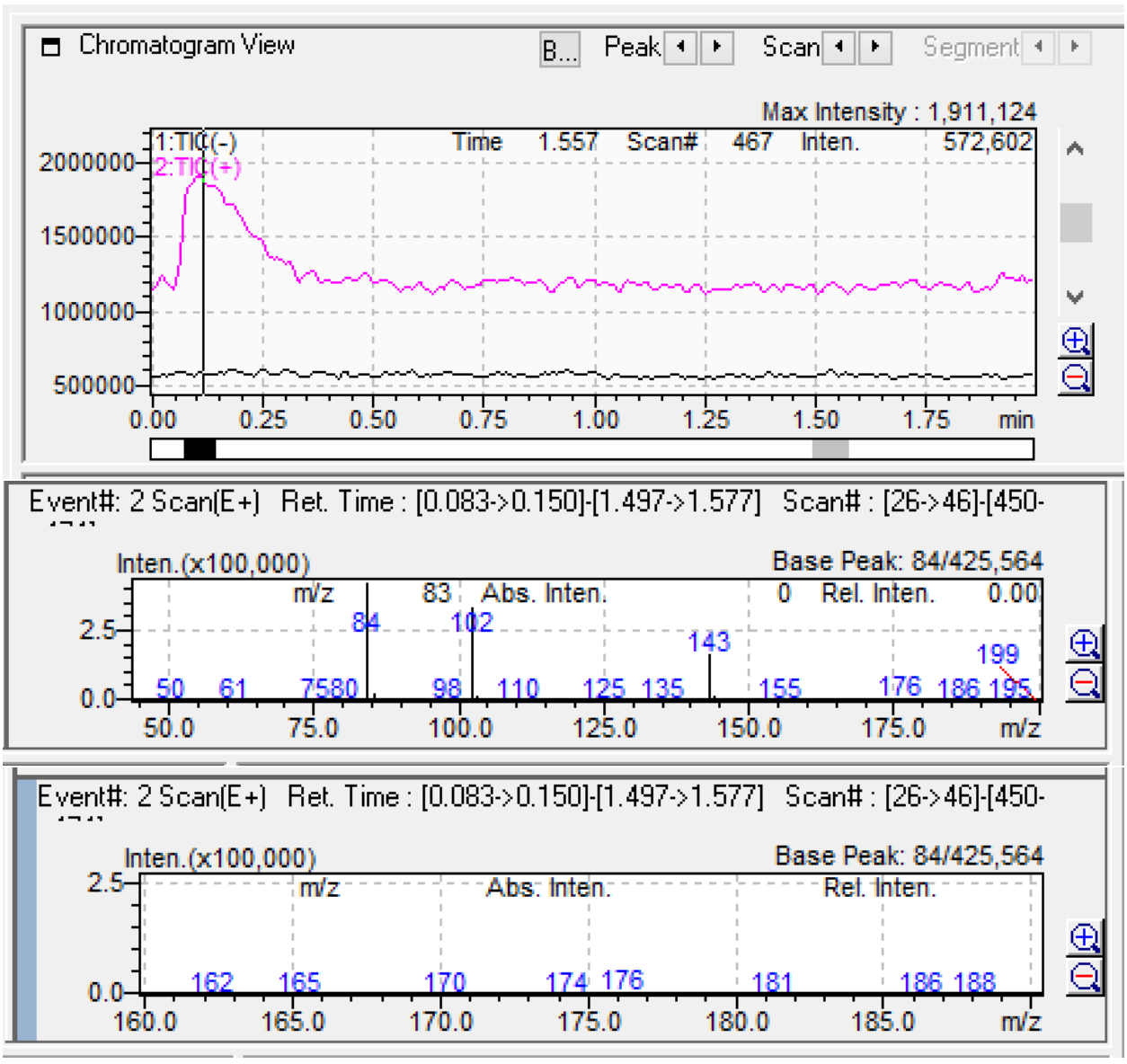

Figure 3-5d. Flow injection chromatograph and MS spectrum in APCI mode with corona discharge needle set to 5 mm.

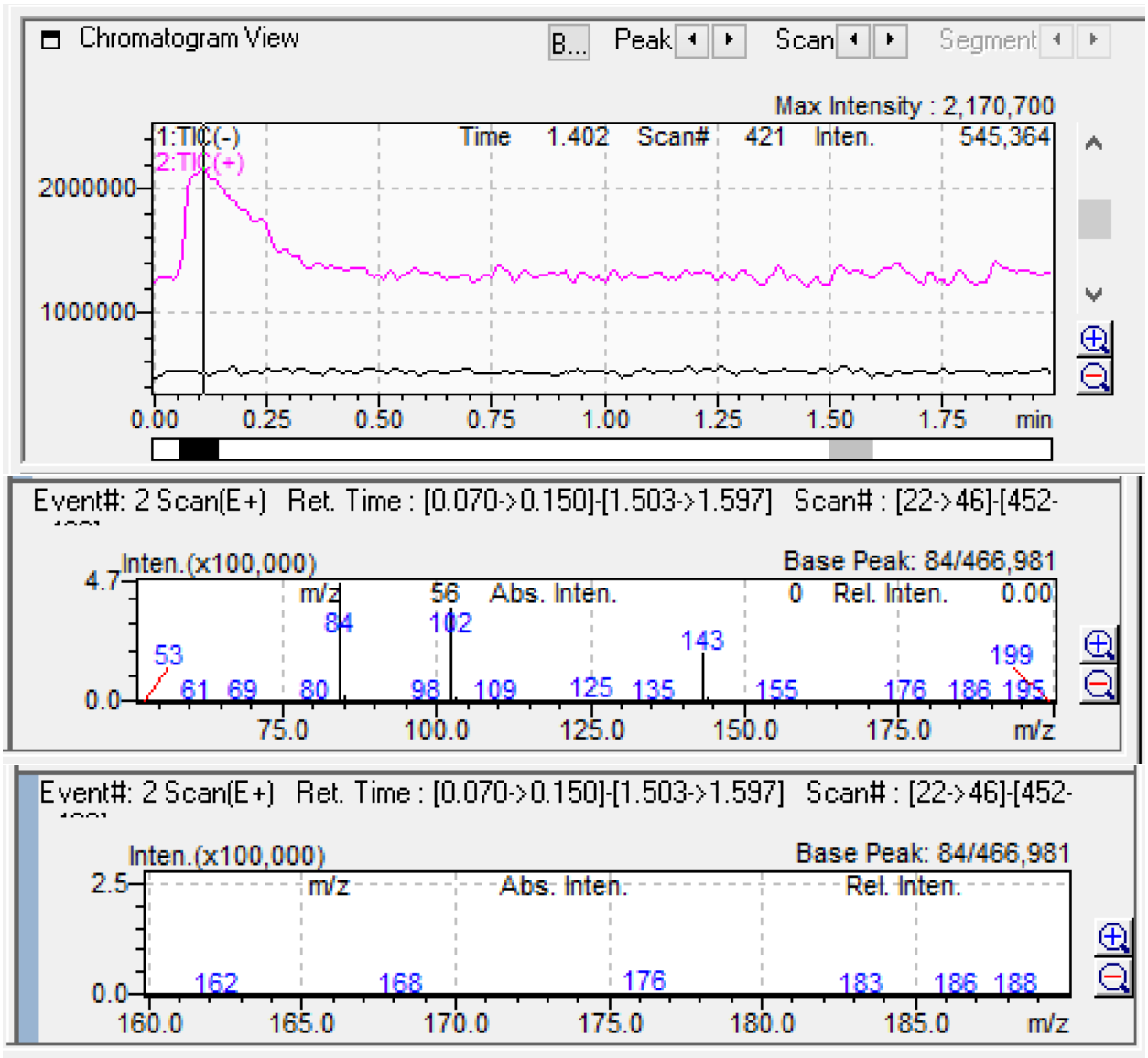

Figure 3-5e. Flow injection chromatograph and MS spectrum in APCI mode with corona discharge needle set to 6 mm.

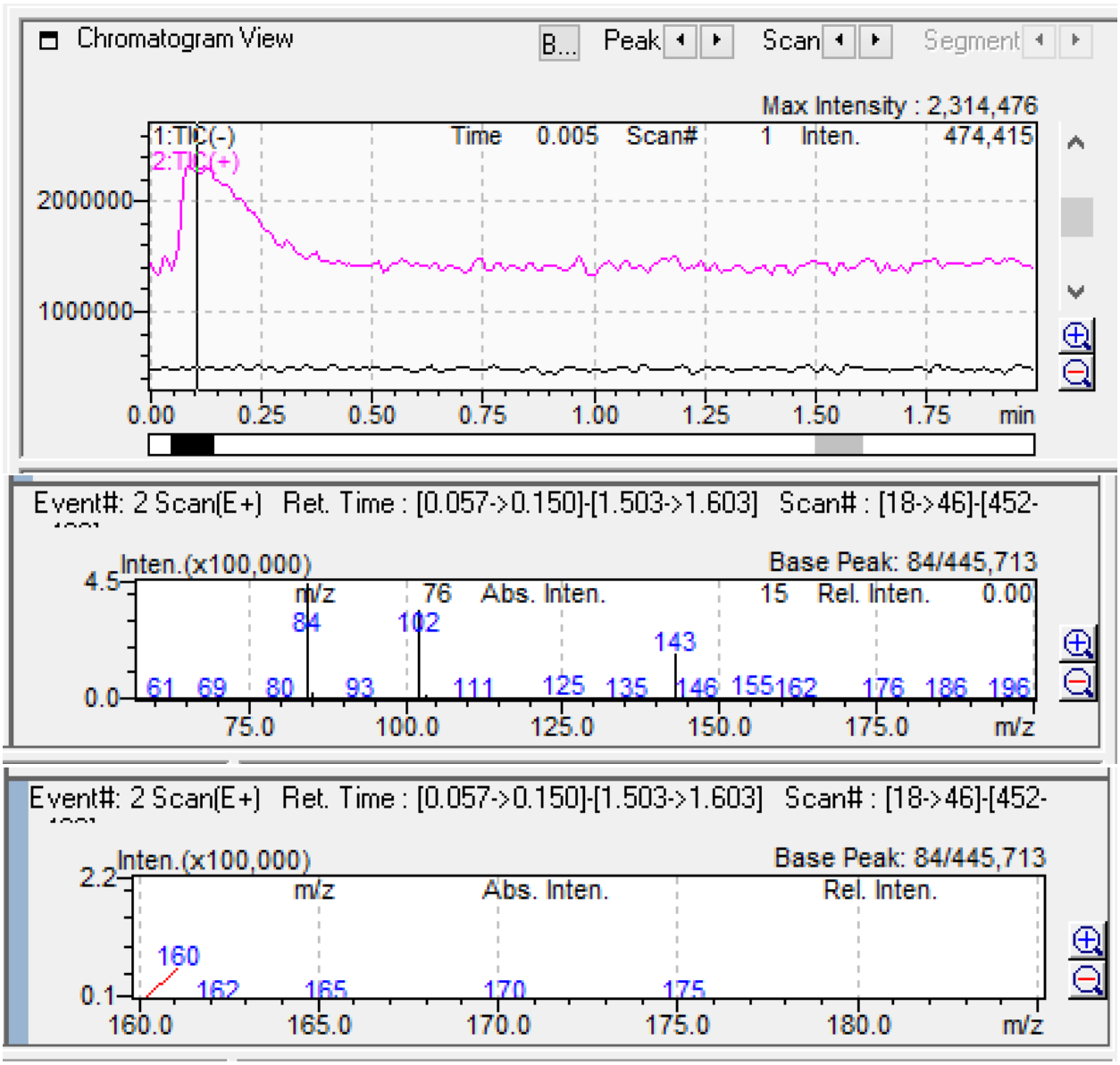

Figure 3-5f. Flow injection chromatograph and MS spectrum in APCI mode with corona discharge needle set to 7 mm.

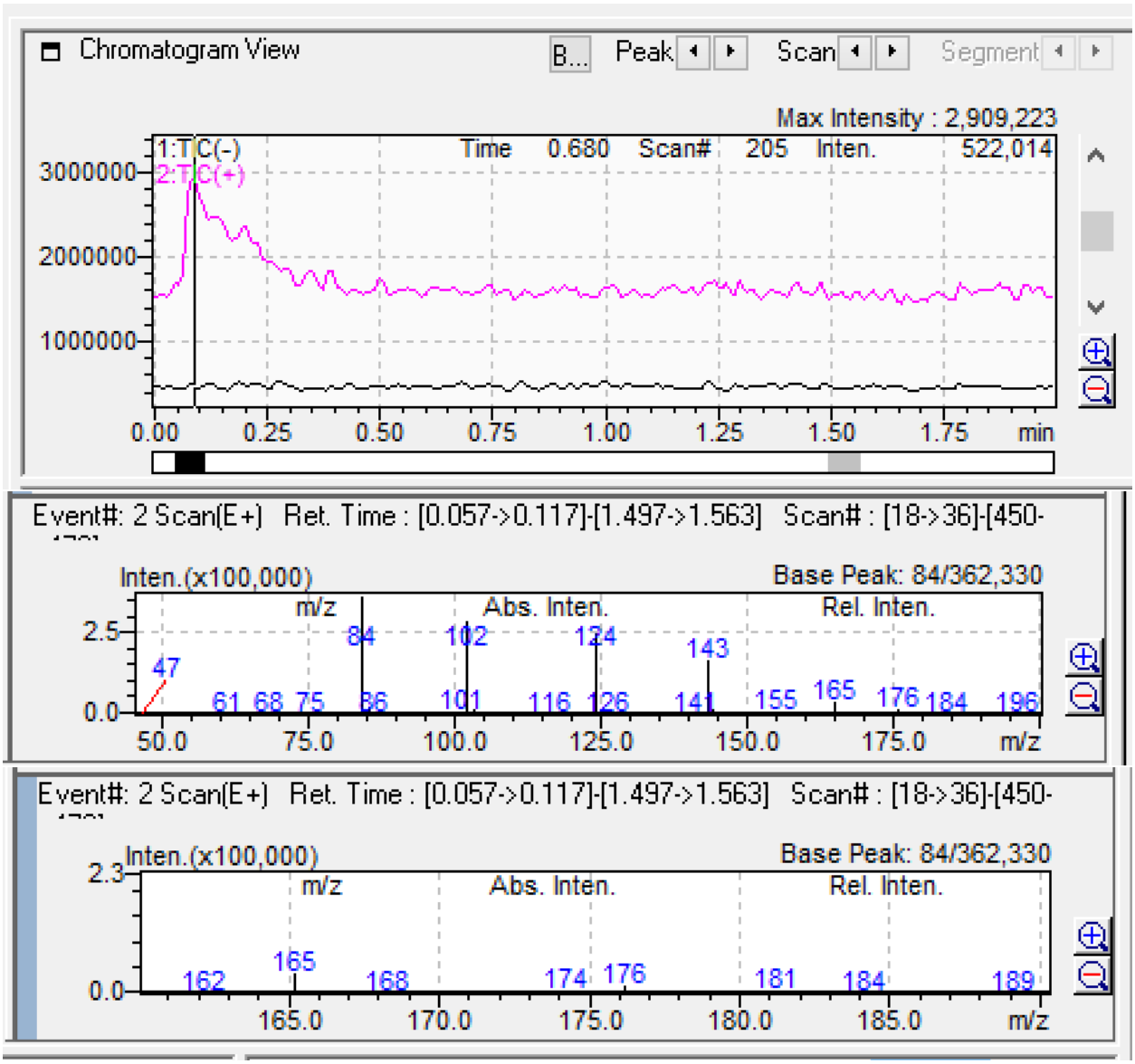

Figure 3-5g. Flow injection chromatograph and MS spectrum in APCI mode with corona discharge needle set to 8 mm.

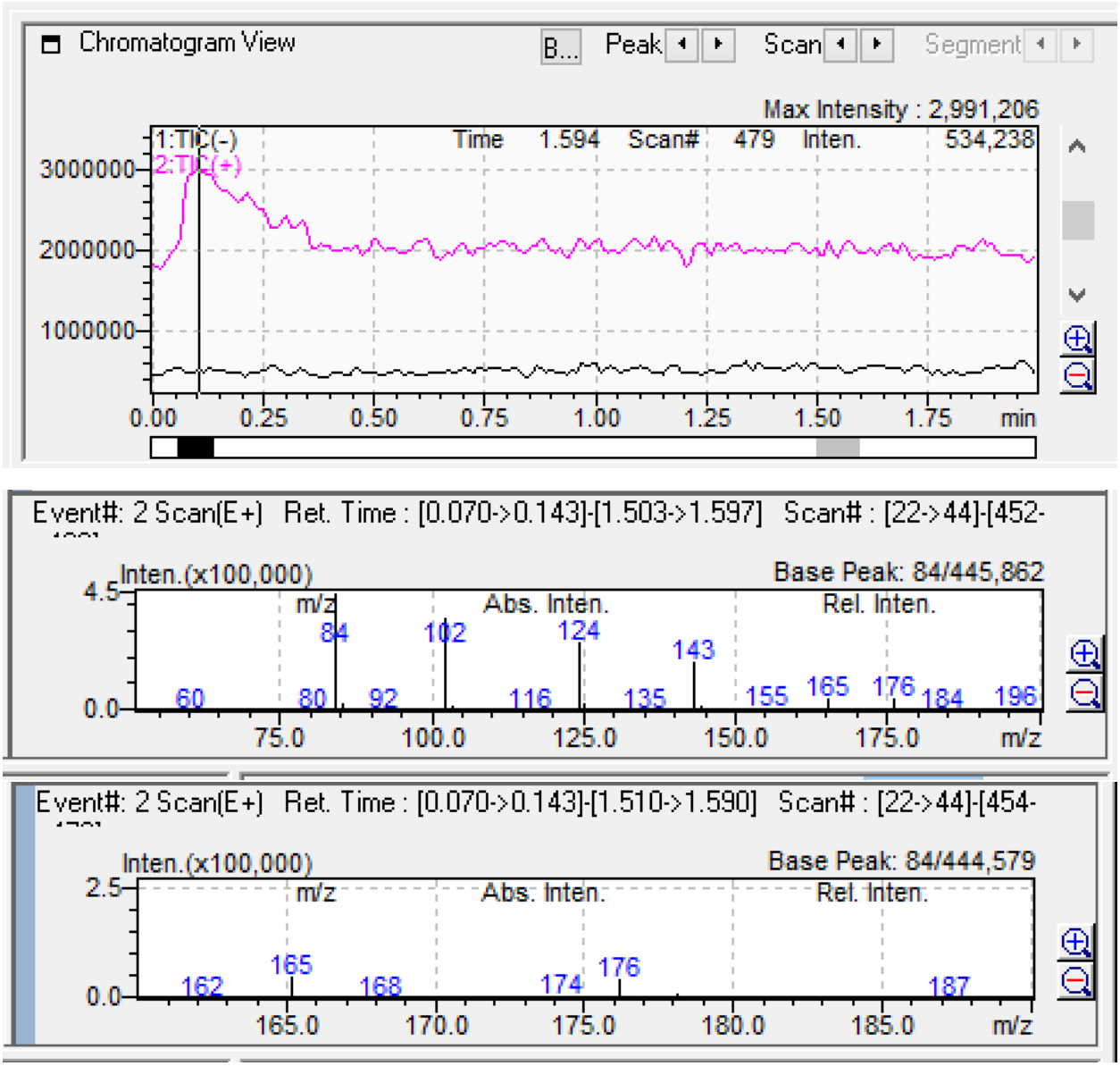

Figure 3-5h. Flow injection chromatograph and MS spectrum in APCI mode with corona discharge needle set to 9 mm.

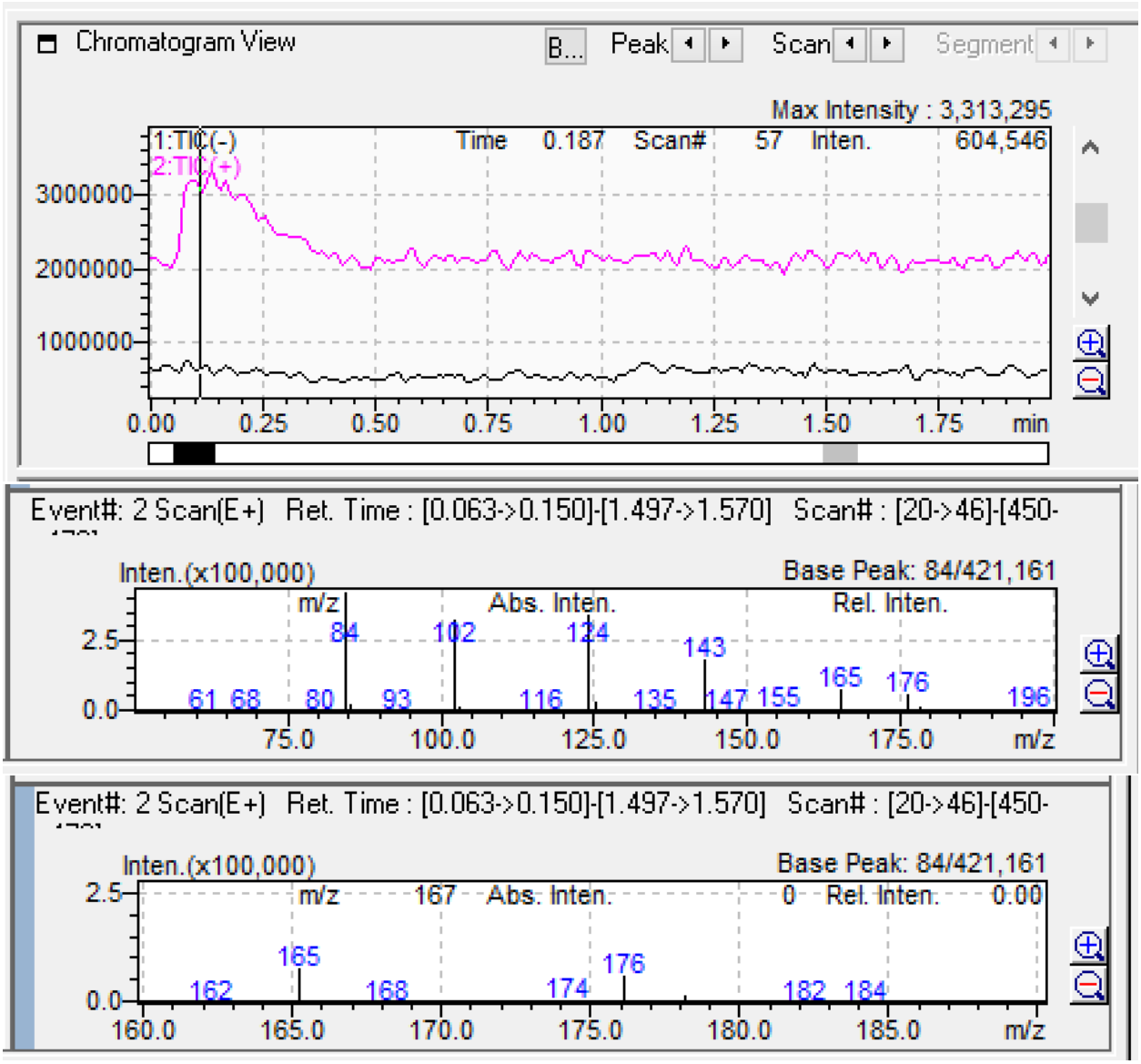

Figure 3-5i. Flow injection chromatograph and MS spectrum in APCI mode with corona discharge needle set to 10 mm.

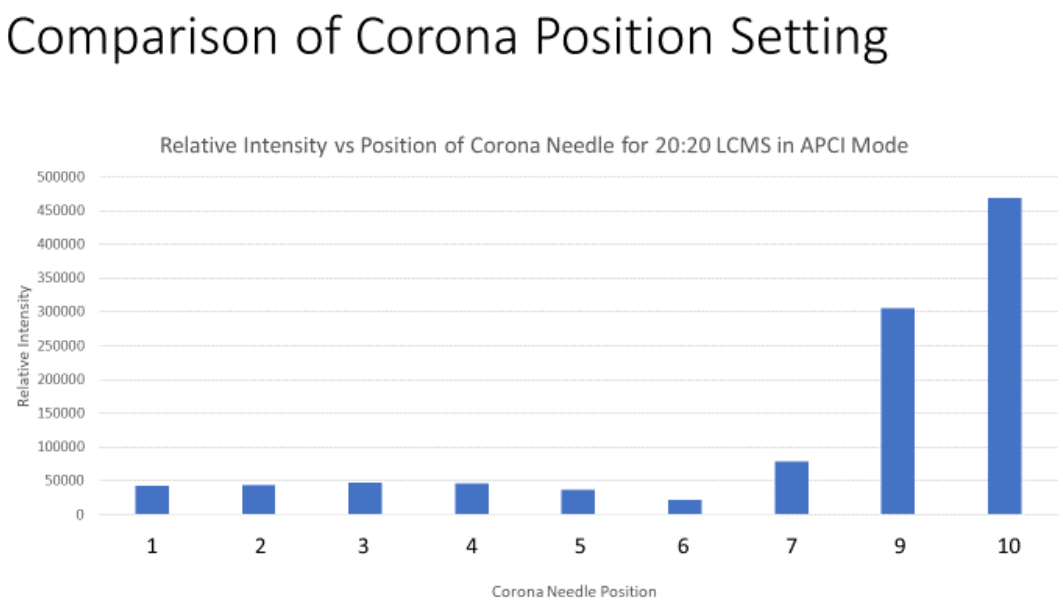

Figure 3-6. A summary of the relative signals produced at different corona discharge needle settings in APCI mode for compound 6.

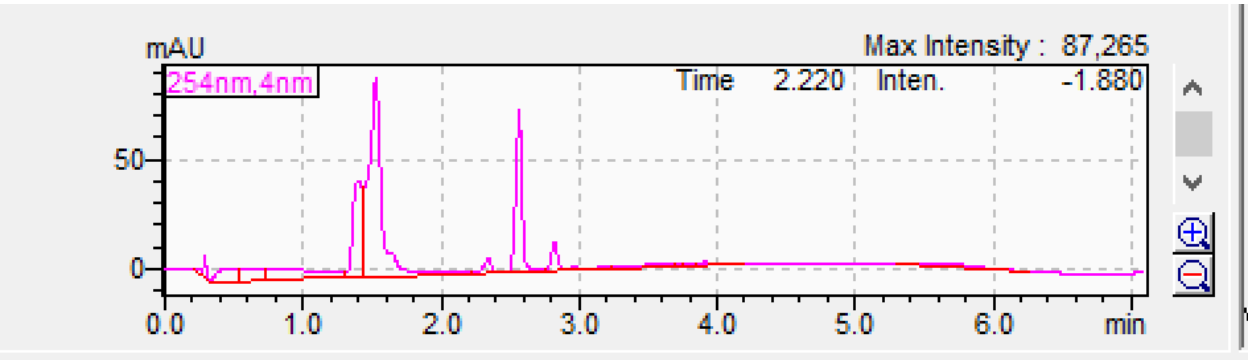

Figure 3-7a. PDA plot of uniodinated compound 7.

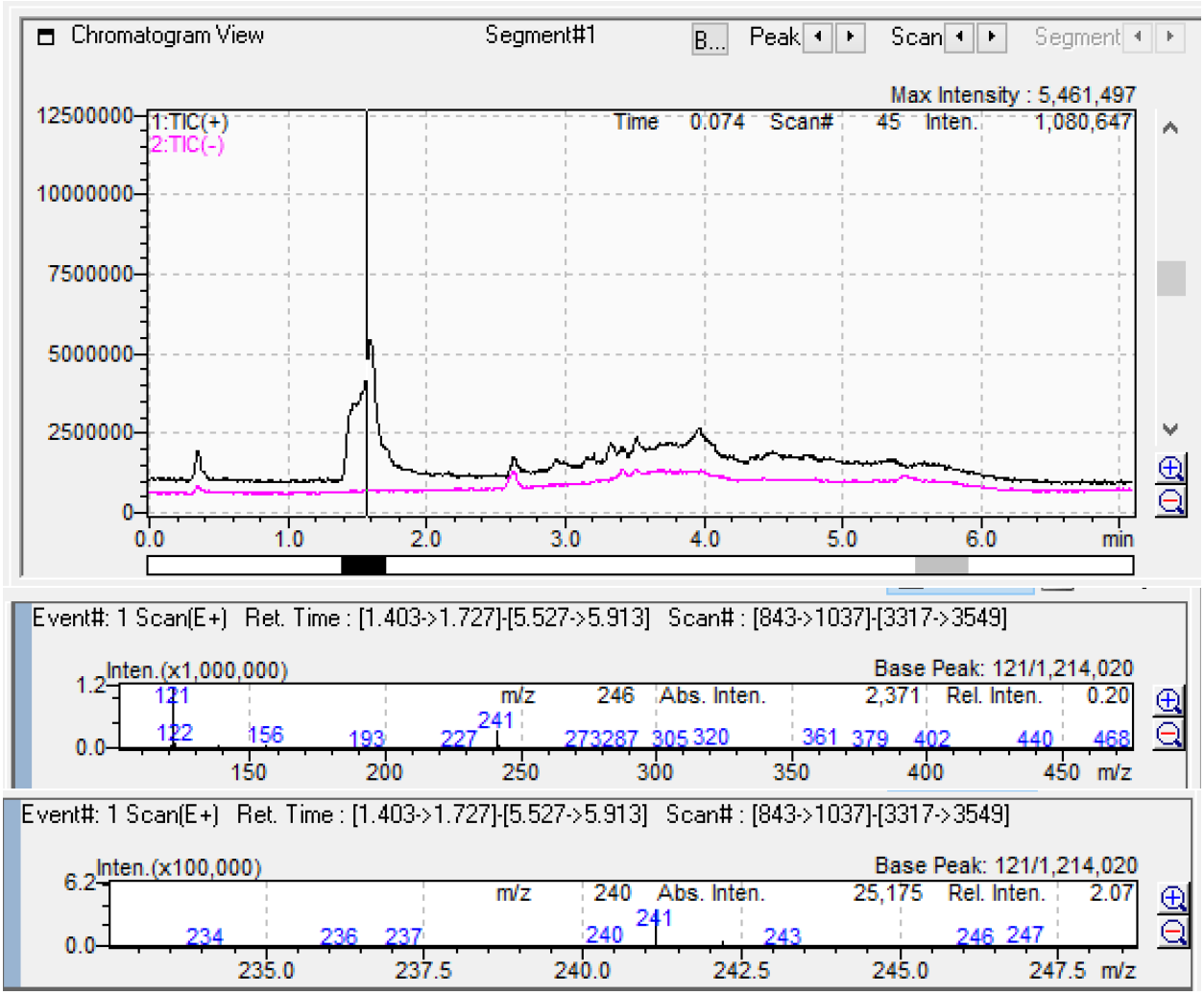

Figure 3-7b. An MS spectrum of uniodinated compound 7, in APCI mode with the corona discharge needle set to 5 mm.

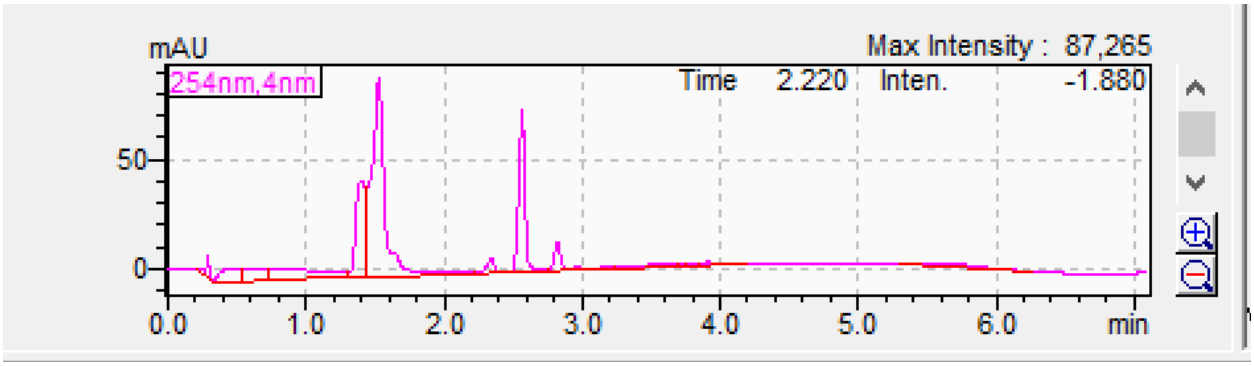

Figure 3-8a. PDA plot of iodinated compound 8.

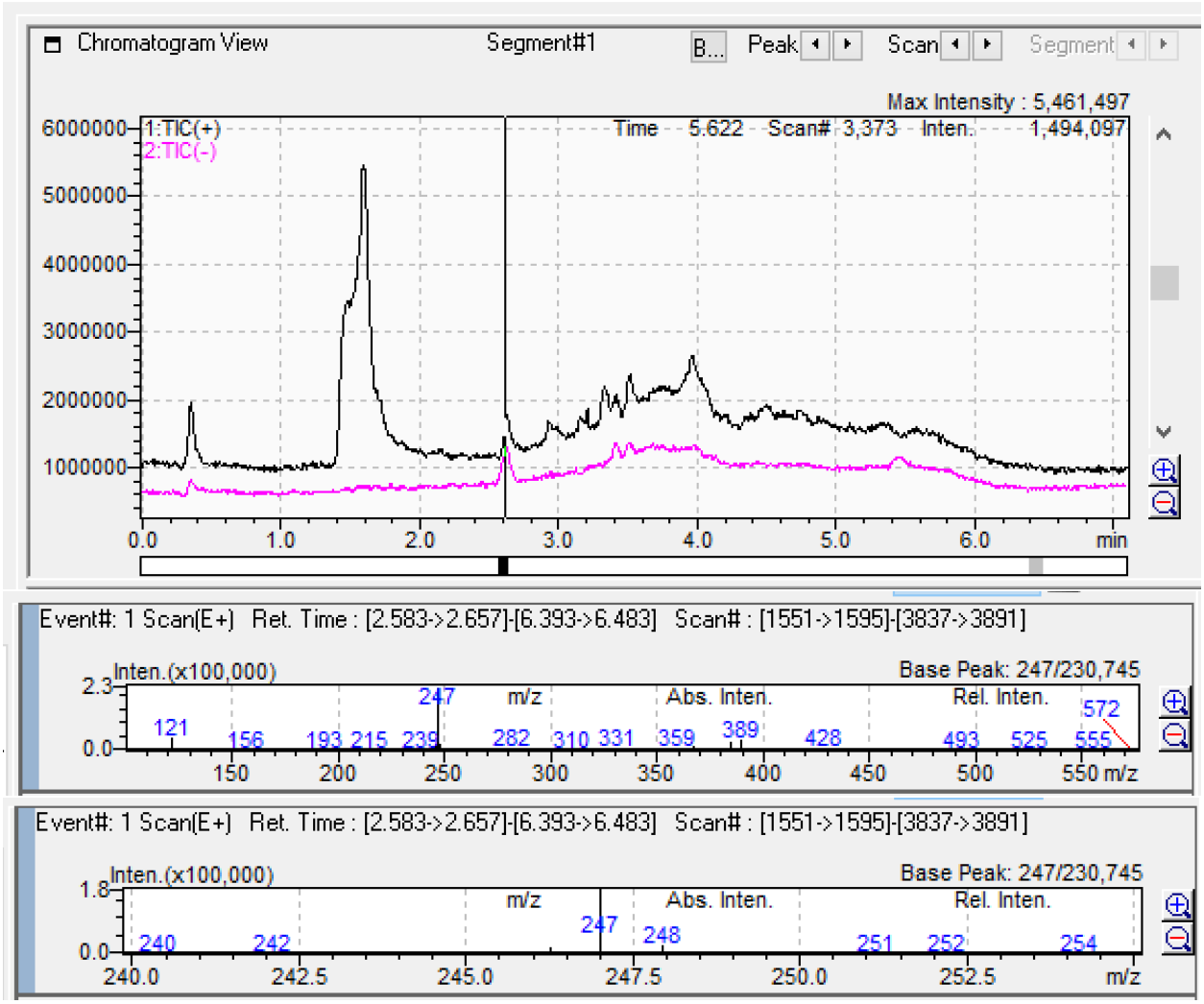

Figure 3-8b. An MS spectrum of iodinated compound 8, in APCI mode with the corona discharge needle set to 5 mm.

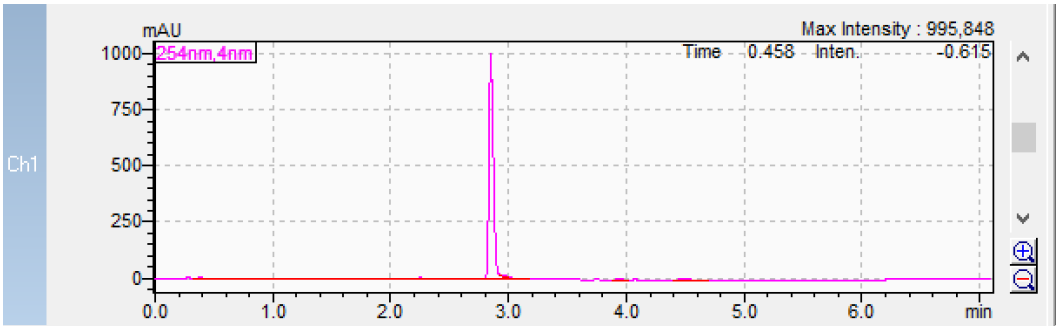

Figure 3-9a. A chromatograph of compound 8.

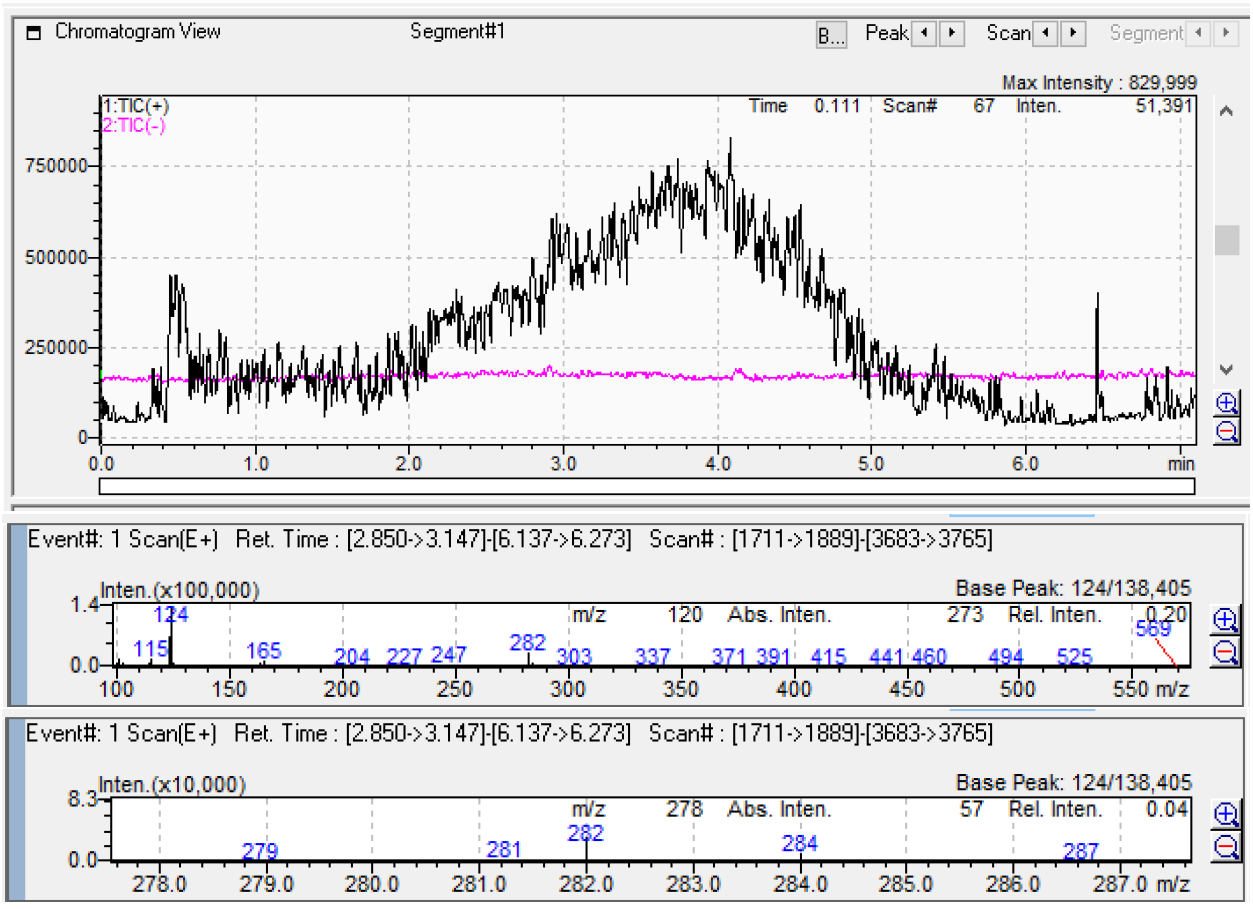

Figure 3-9b. An MS spectrum of compound 9, in APCI mode with the corona discharge needle set to 10 mm.

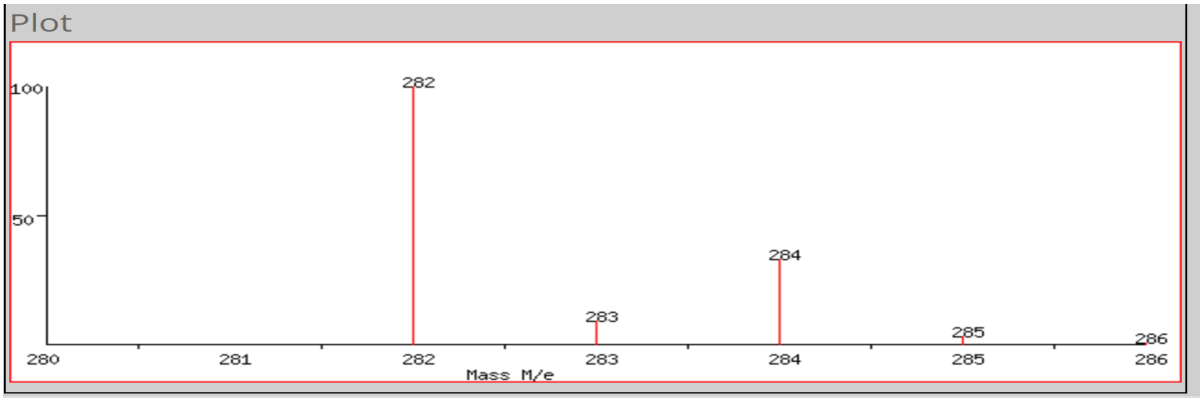

Figure 3-10. An expected MS spectrum, with emphasis on the isotopic peak ratio for compound 9 (3).

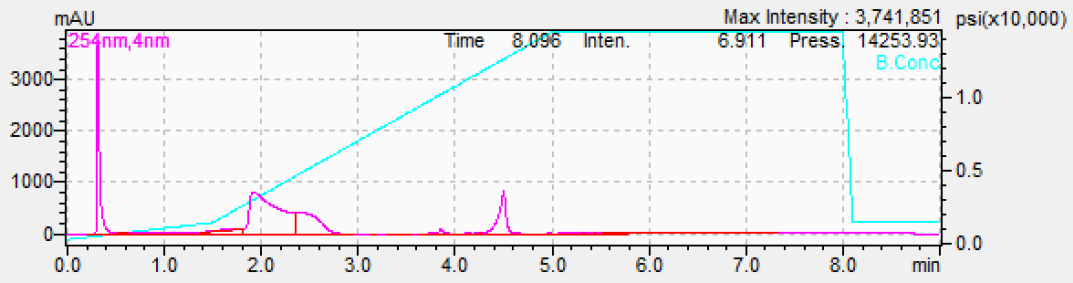

Figure 3-11a. A chromatograph of compound 10.

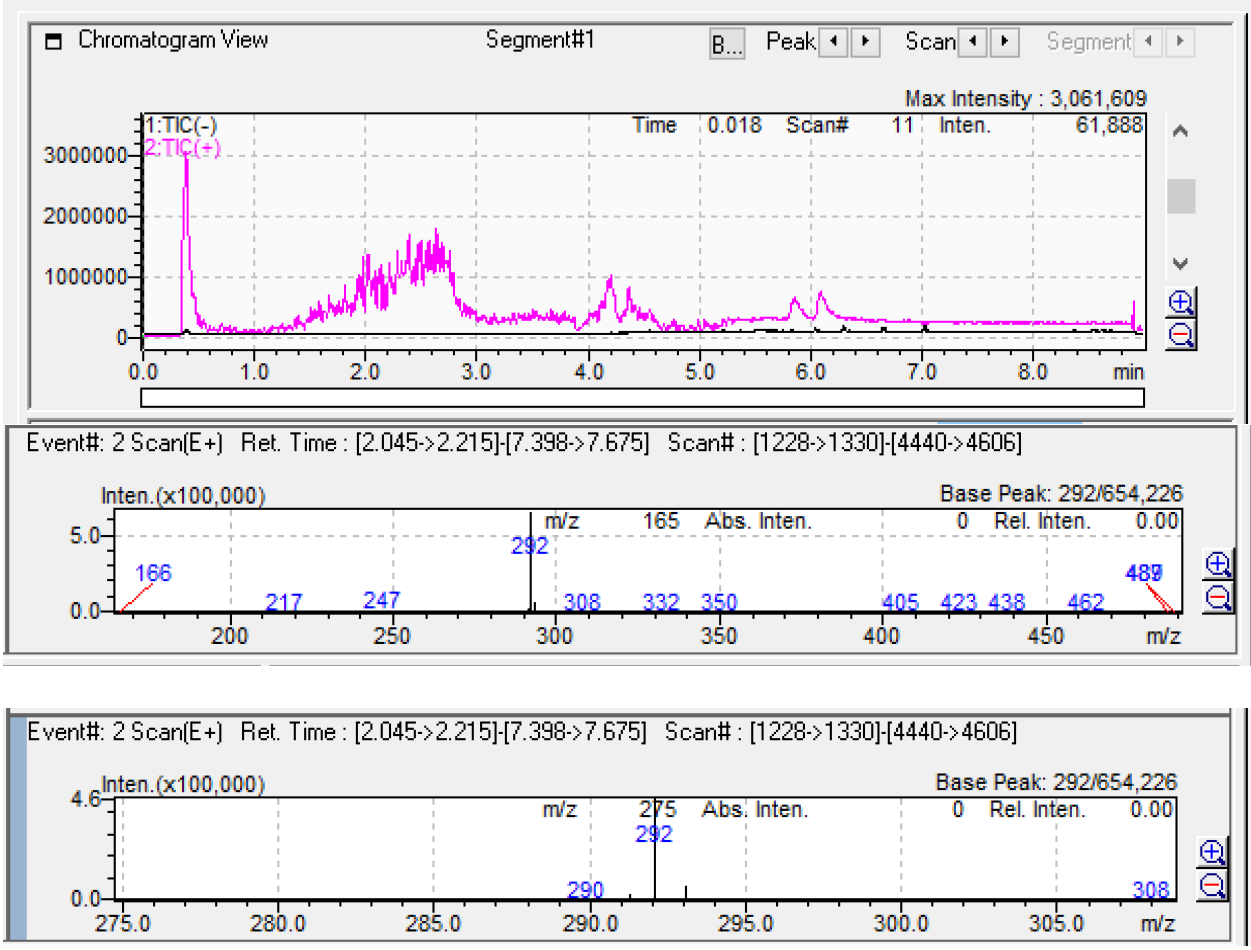

Figure 3-11b. An MS spectrum of compound 10, in dual ionization mode with the corona discharge needle set to 10 mm.

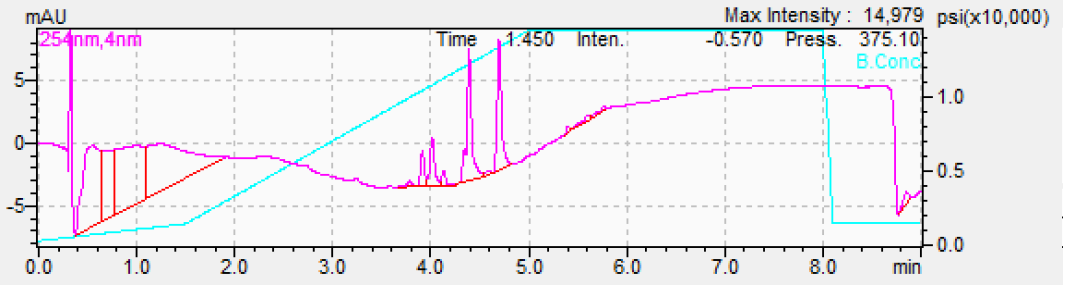

Figure 3-12a. A chromatograph of unknown compound.

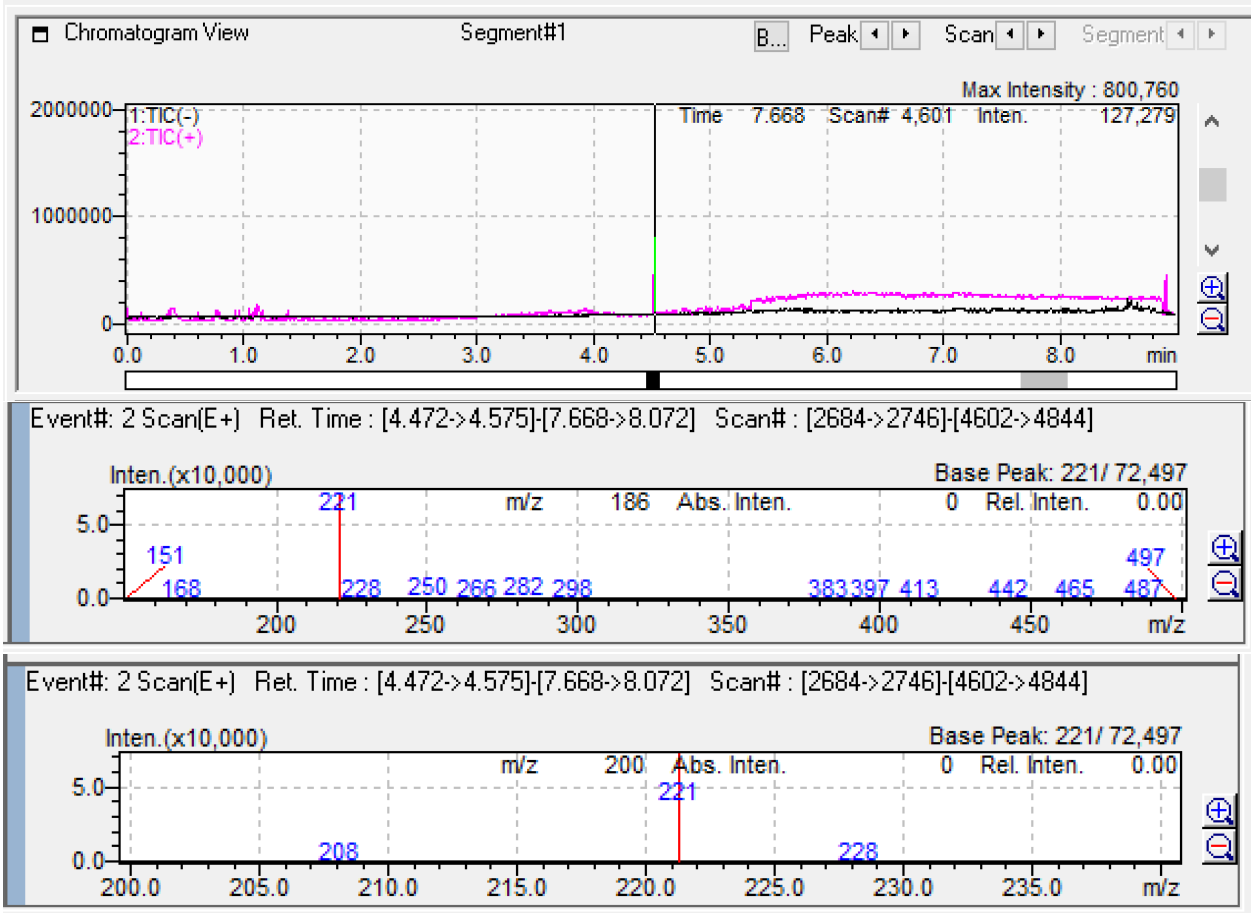

Figure 3-12b. An MS spectrum of unknown compound, in dual ionization mode with the corona discharge needle set to 10 mm.

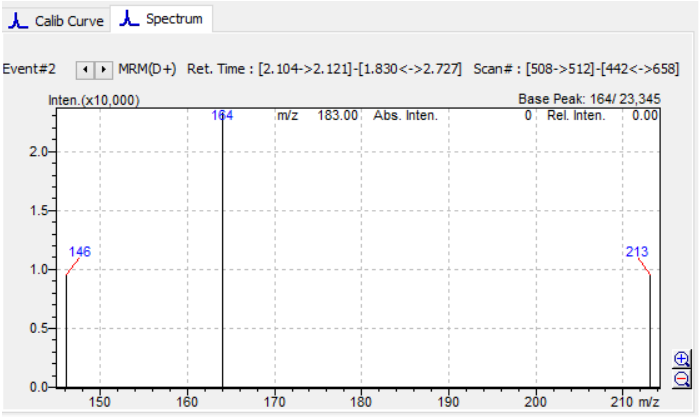

Figure 3-13a. MRM spectrum for compound 2, in positive mode.

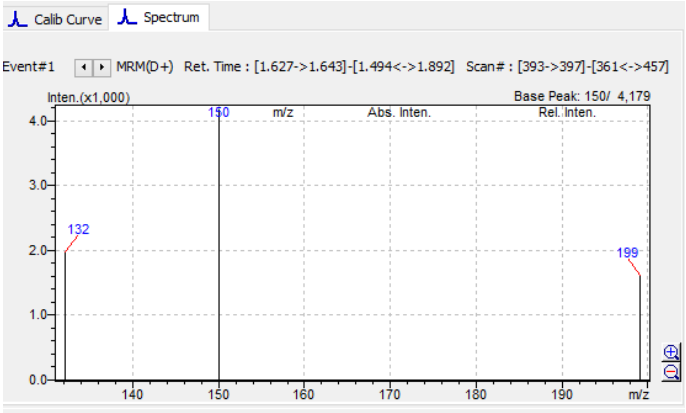

Figure 3-13b. MRM spectrum for compound 2, in negative mode.

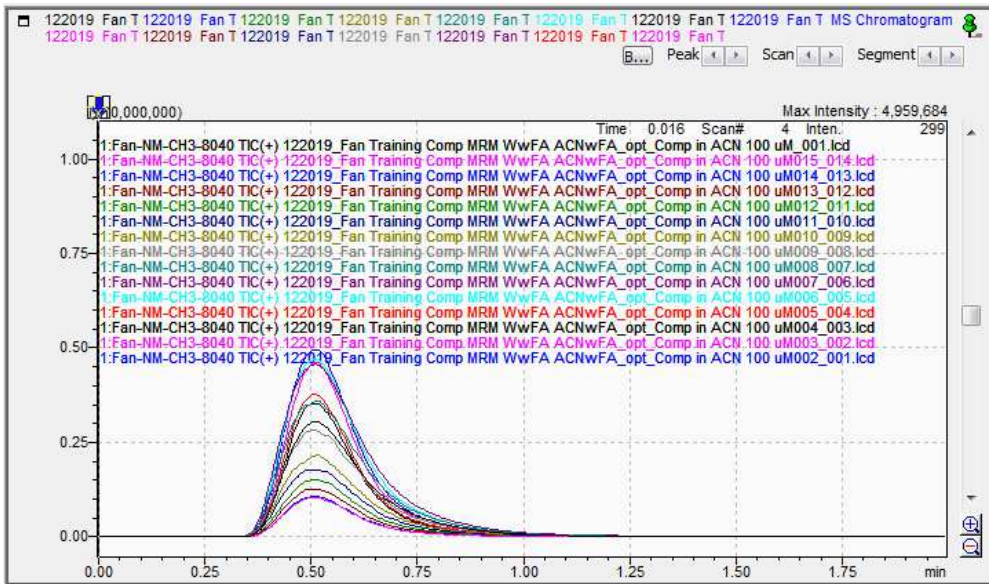

Figure 3-14a. Total CE optimization for compound 2 under MRM.

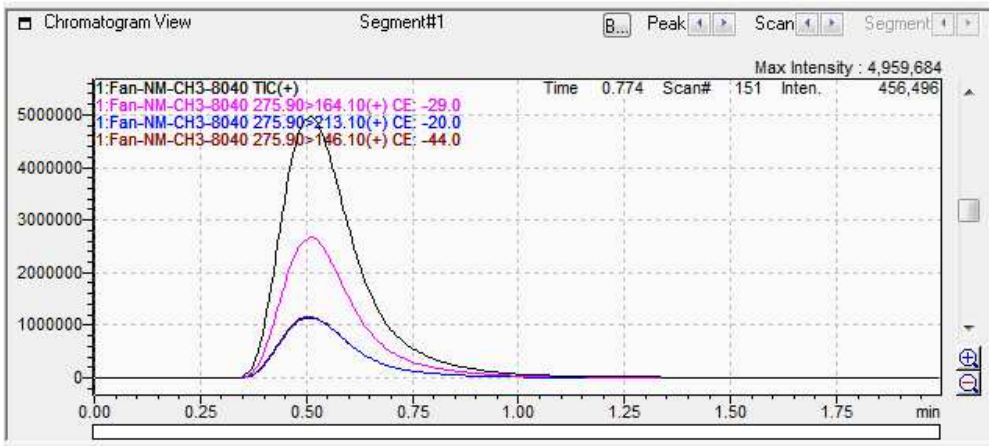

Figure 3-14b. CE optimization for compound 2 under MRM, in positive mode.

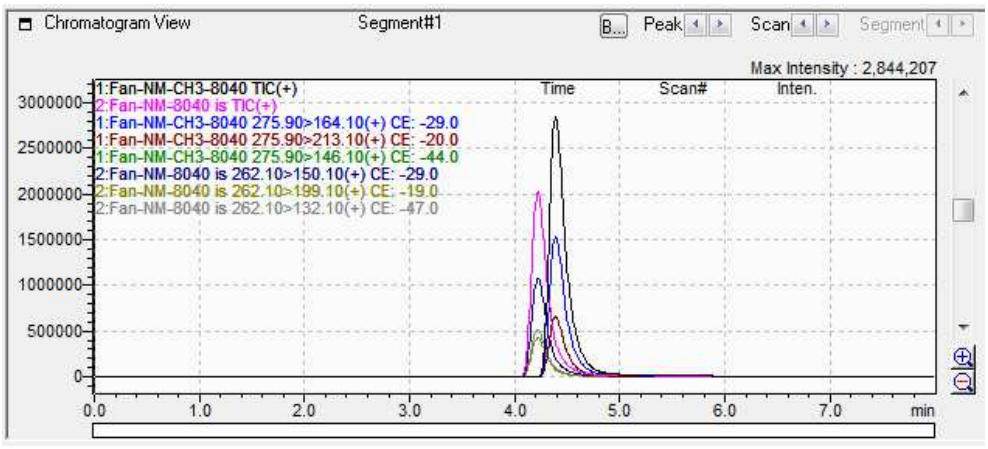

Figure 3-15a. Chromatograph of first attempt at gradient programming, with an 8 min column run.

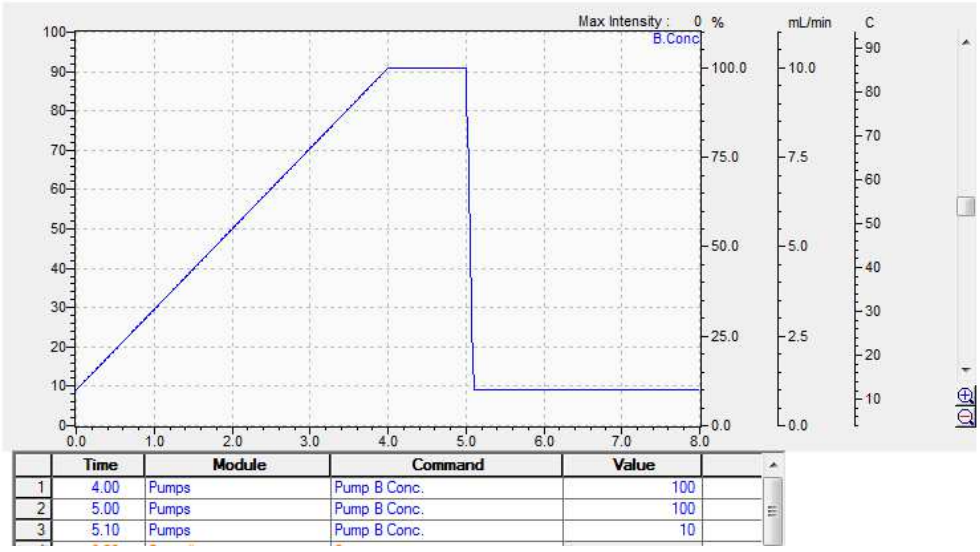

	Time	Module	Command	Value
1	4.00	Pumps	Pump B Conc.	100
2	5.00	Pumps	Pump B Conc.	100
3	5.10	Pumps	Pump B Conc.	10

Figure 3-15b. The gradient programing time events for the first method for gradient programming, with an 8 min column run.

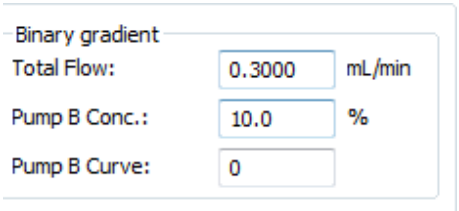

Figure 3-15c. Gradient conditions for the first method for gradient programming.

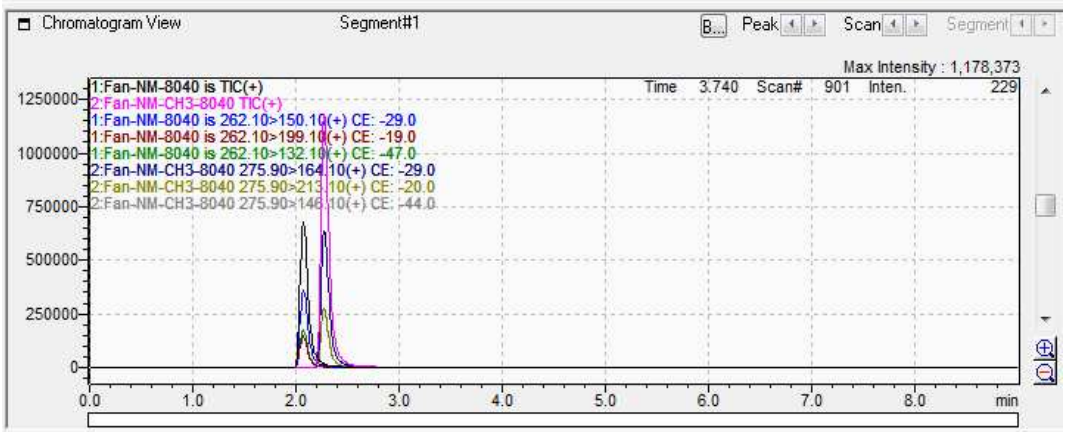

Figure 3-16a. Chromatograph of second method at gradient programming, with a 9 min column run.

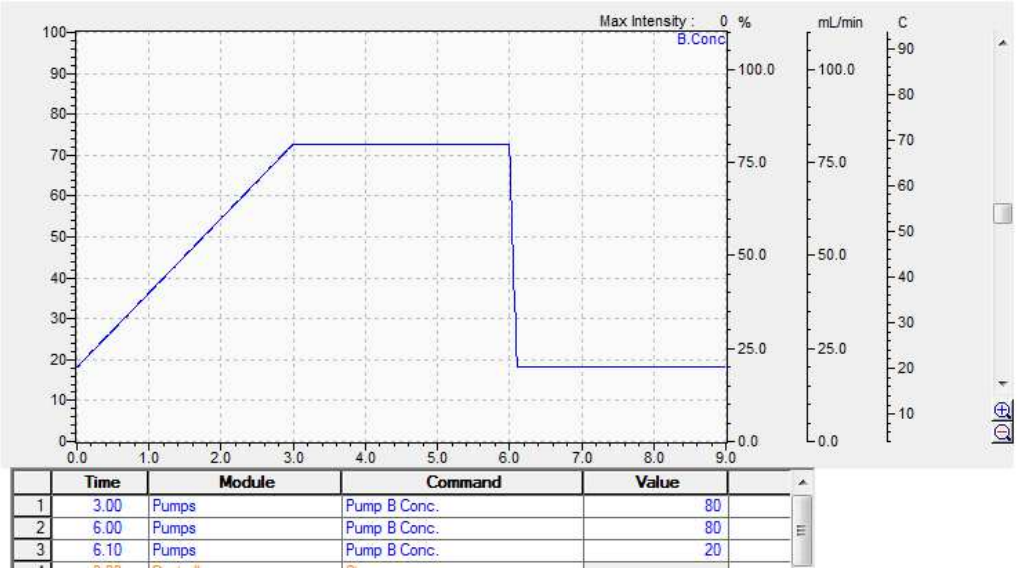

	Time	Module	Command	Value
1	3.00	Pumps	Pump B Conc.	80
2	6.00	Pumps	Pump B Conc.	80
3	6.10	Pumps	Pump B Conc.	20

Figure 3-16b. The gradient programing time events for the first method for gradient programming, with a 9 min column run.

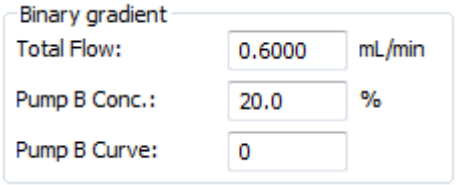

Figure 3-16c. Gradient conditions for the second method for gradient programming.

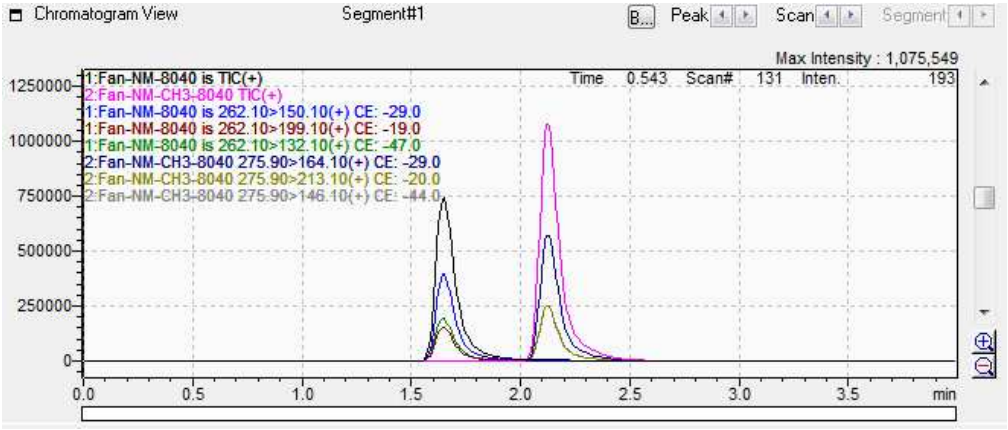

Figure 3-17a. Chromatograph of third method at gradient programming, with a 4 min column run.

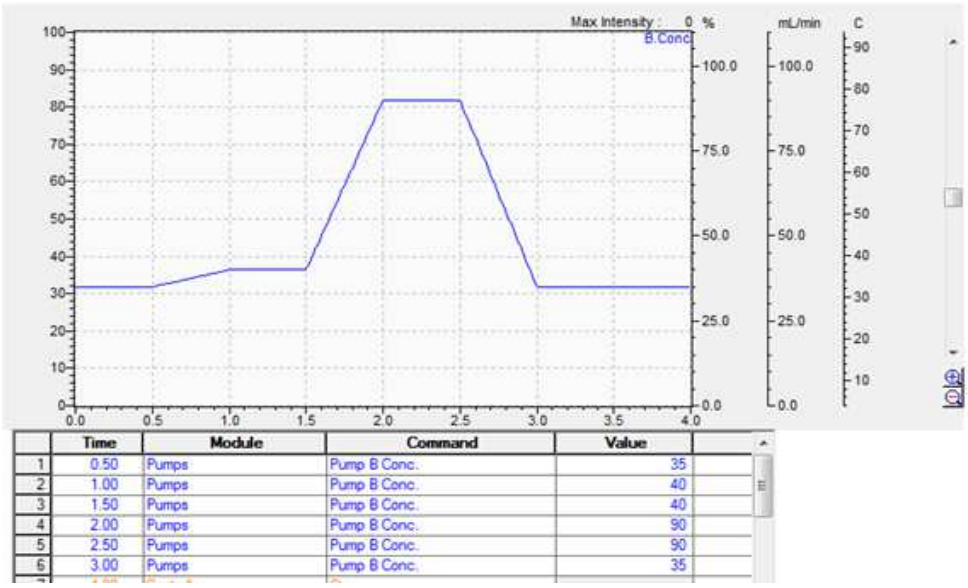

	Time	Module	Command	Value
1	0.50	Pumps	Pump B Conc.	35
2	1.00	Pumps	Pump B Conc.	40
3	1.50	Pumps	Pump B Conc.	40
4	2.00	Pumps	Pump B Conc.	90
5	2.50	Pumps	Pump B Conc.	90
6	3.00	Pumps	Pump B Conc.	35

Figure 3-17b. The gradient programing time events for the third method for gradient programming, with a 9 min column run.

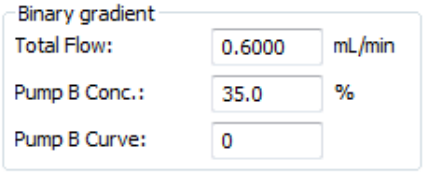

Figure 3-17c. Gradient conditions for the third method for gradient programming.

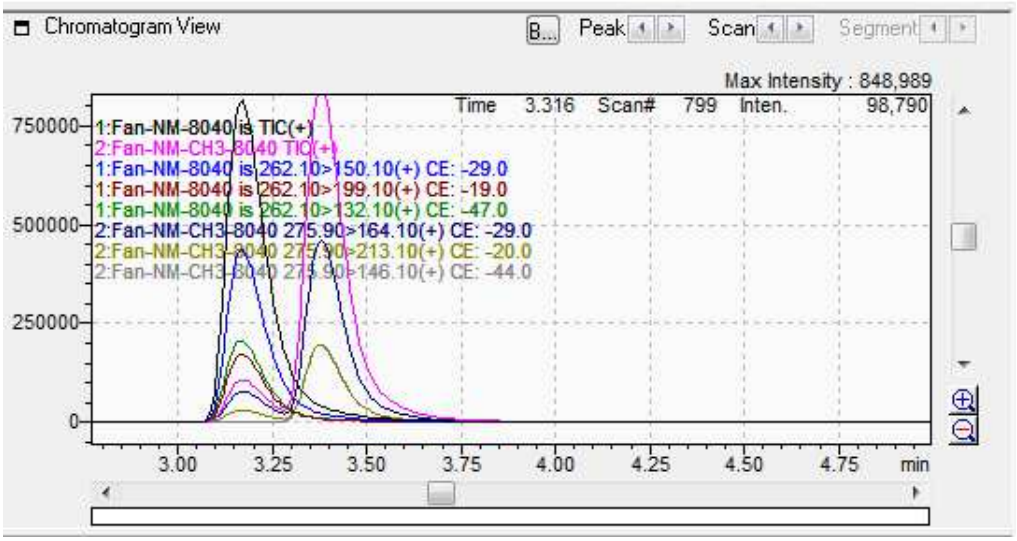

Figure 3-18a. Chromatograph depicting peaks detected using a MeOH organic mobile phase.

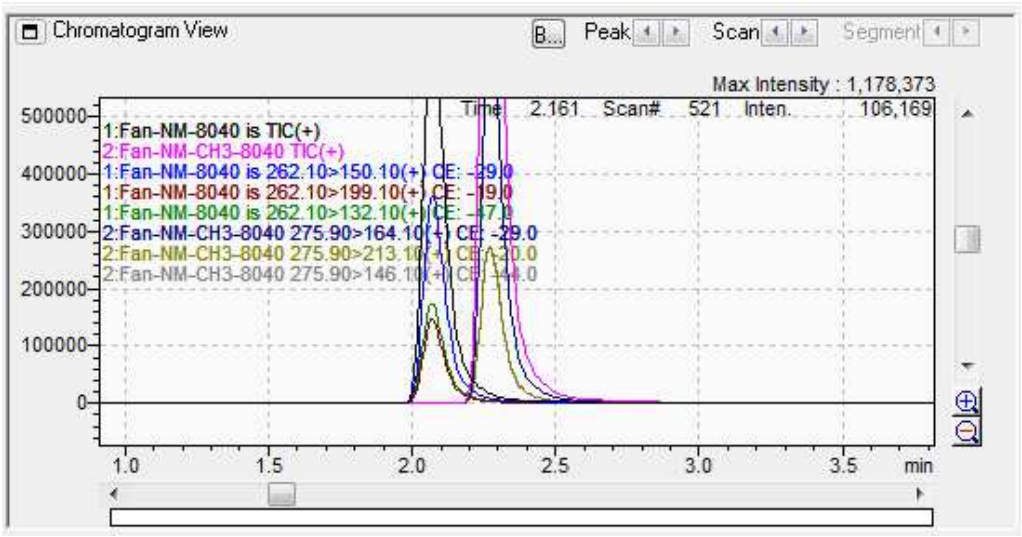

Figure 3-18b. Chromatograph depicting peaks detected after switching to ACN as the organic mobile phase.

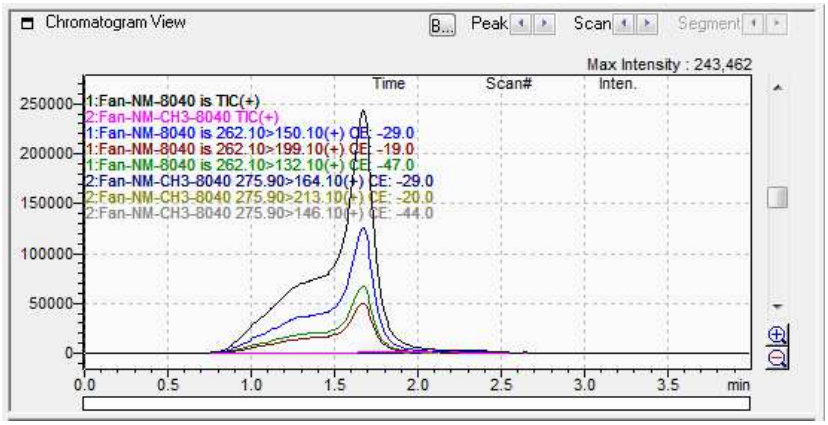

Figure 3-19a. 5 nM IS + 500 nM IS compound prepared in MeOH, no water.

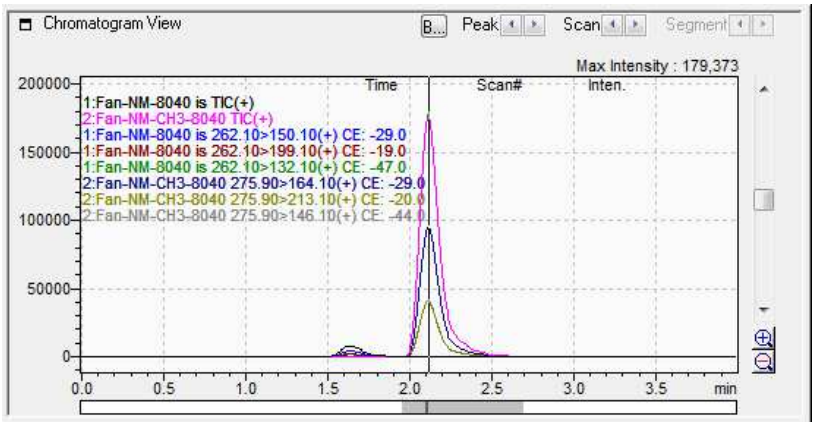

Figure 3-19b. 5 nM IS + 500 nM compound prepared in 1:3 water:MeOH.

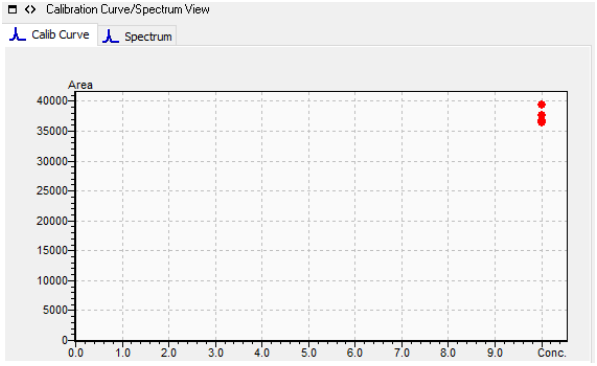

Figure 3-20a. Precision of the IS concentration added to each standard for the microsomal stability assay calibration curve.

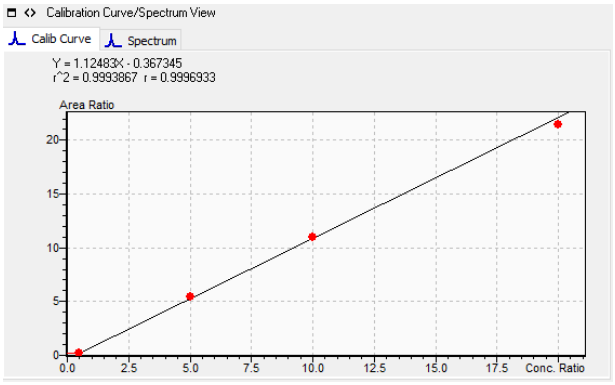

Figure 3-20b. A calibration curve with compound 2 and no IS.

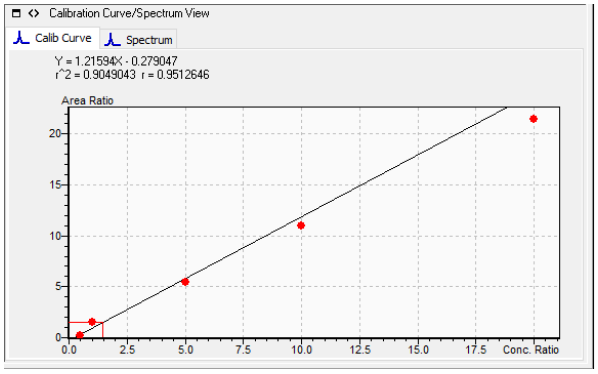

Figure 3-20c. A calibration curve with compound 2 and 10 nM IS.

	1 nm	10 nm	50 nm	100 nm	200 nm
	1.0	10.5	49.7	100.1	192.9
	1.0	10.7	47.7	97.0	202.1
	1.0	9.9	48.6	103.2	201.4
MEAN	**1.0**	**10.4**	**48.7**	**100.1**	**198.8**
STD	**0.0**	**0.4**	**1.0**	**3.1**	**5.1**

Quantitative Results View ID# 1 Fan-NM-CH3-8040

Data#	Data File	Area	Conc. (ppb)	Std. Conc.	Accuracy[%]	Cal. Point
1	1292019_F	957,512	201.4	200	100.7	☑
2	1292019_F	473,128	103.2	100	103.2	☑
3	1292019_F	226,671	48.6	50	97.2	☑
4	1292019_F	46,494	9.9	10	98.8	☑
5	1292019_F	5,300	1.0	1	100.1	☑

Figure 3-21a. The microsomal stability assay calibration curve standard concentrations and respective concentrations for three trials, mean and standard deviation as determined by manual calculation by comparison of area integration and the calculations as acquired from LabSolutions software.

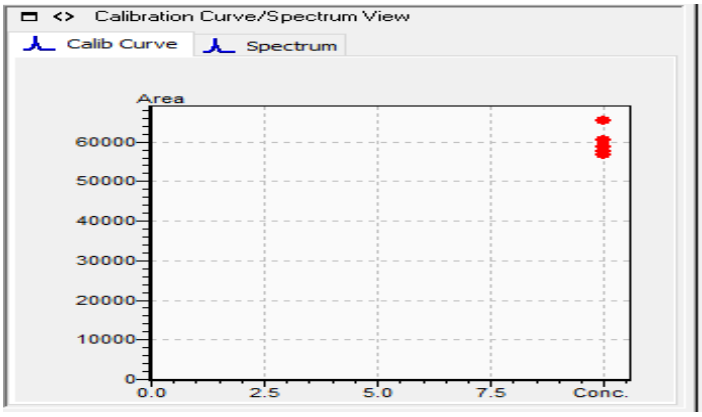

Figure 3-21b. Precision of the IS concentration added to each standard for the microsomal stability assay calibration curve as established by using the amended standard concentrations.

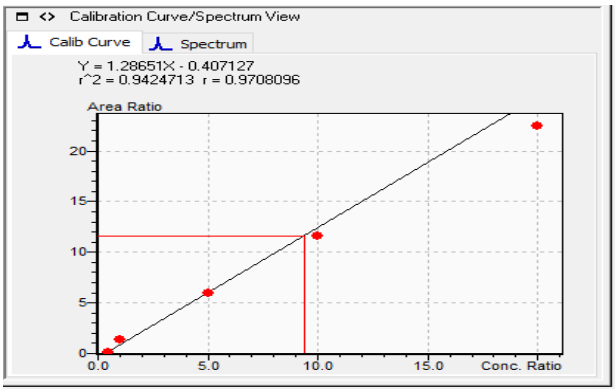

Figure 3-21c. A microsomal stability study calibration curve with the amended standard concentrations with compound 2 and no IS.

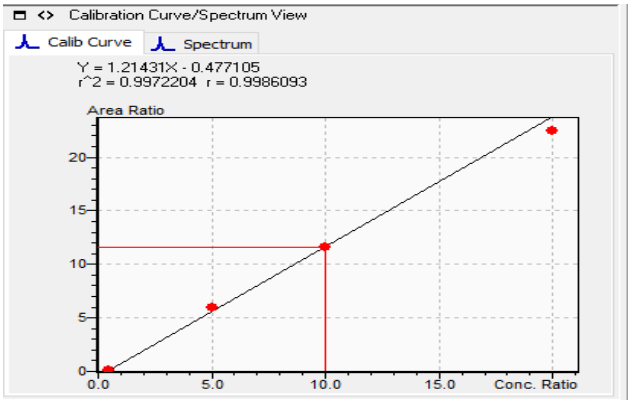

Figure 3-21d. A microsomal stability study calibration curve with the amended standard concentrations with compound 2 and 10 nM IS.

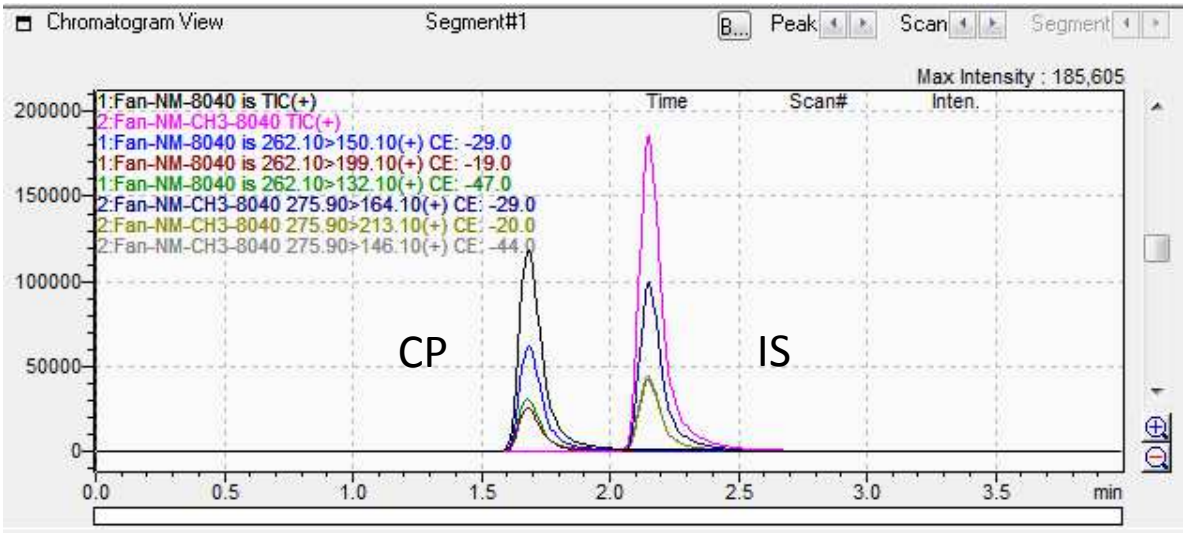

Figure 3-22a. 125 nM compound 2 + IS with an injection volume of 50 uL.

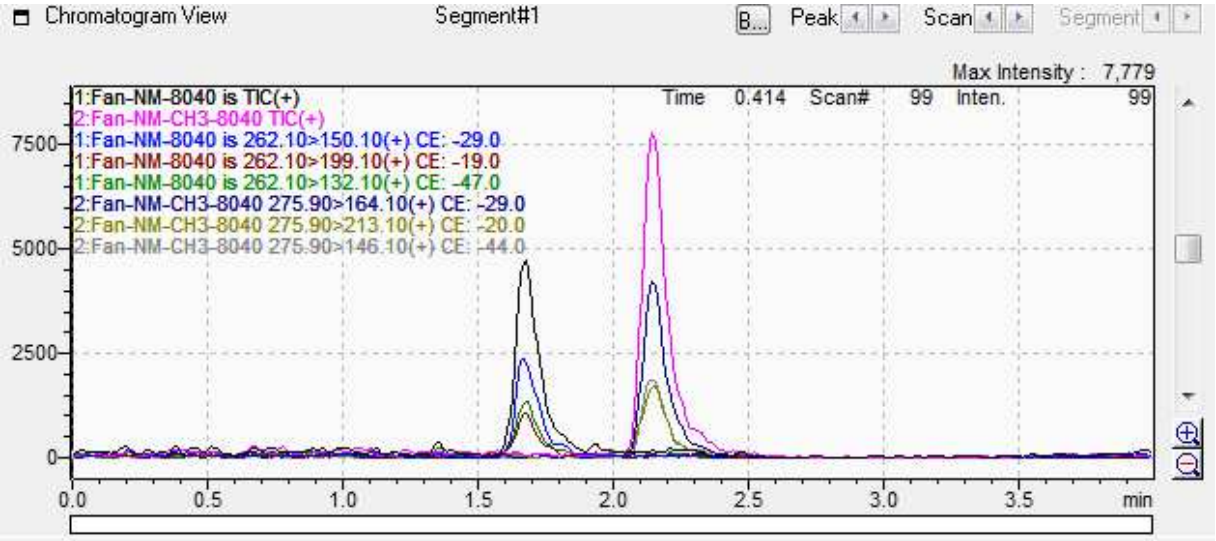

Figure 3-22b. 5 nM compound 2 + IS with an injection volume of 50 uL.

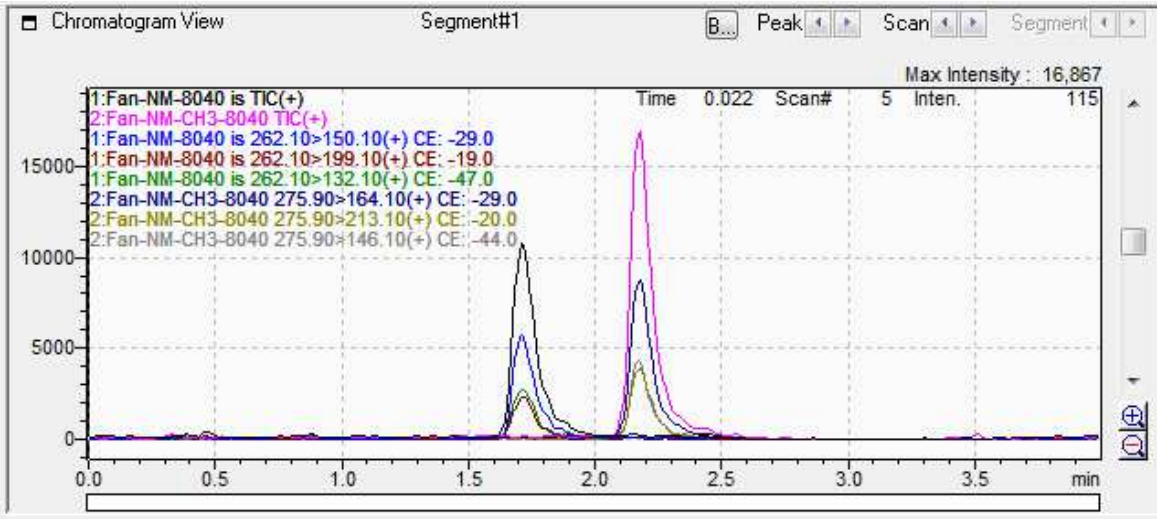

Figure 3-23a. 125 nM compound 2 + IS with an injection volume of 20 uL.

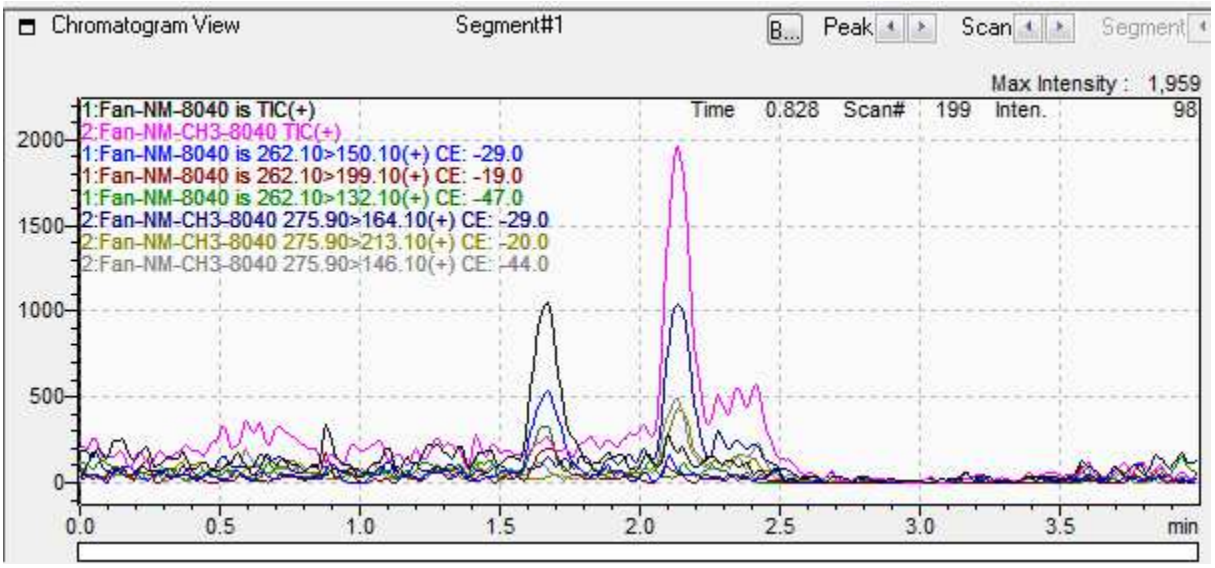

Figure 3-23b. 5 nM compound 2 + IS with an injection volume of 20 uL.

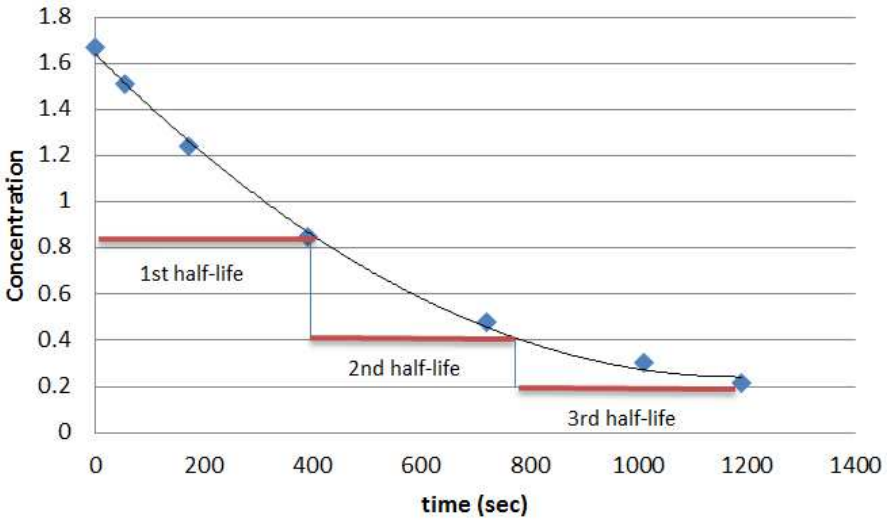

Figure 3-24. A depiction of graphical half-life determination for first-order kinetics (4).

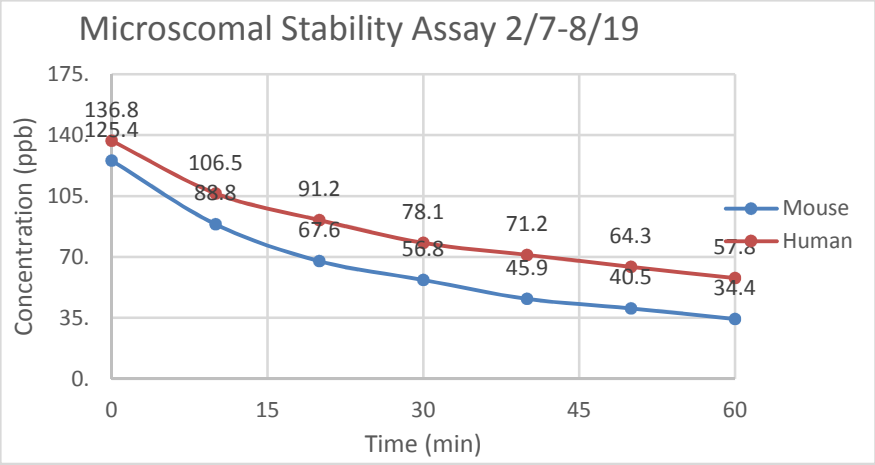

Figure 3-25a. Microsomal stability assay for compound 2 results depicting concentration (ppb) at various time points min, for human and mouse microsomes.

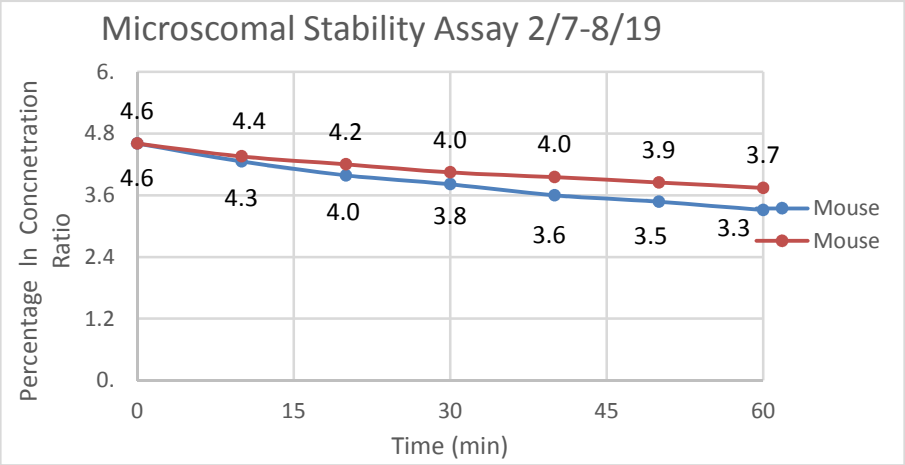

Figure 3-25b. Microsomal stability assay for compound 2 results depicting percentage ln concentration ratio at various time points min, for human and mouse microsomes.

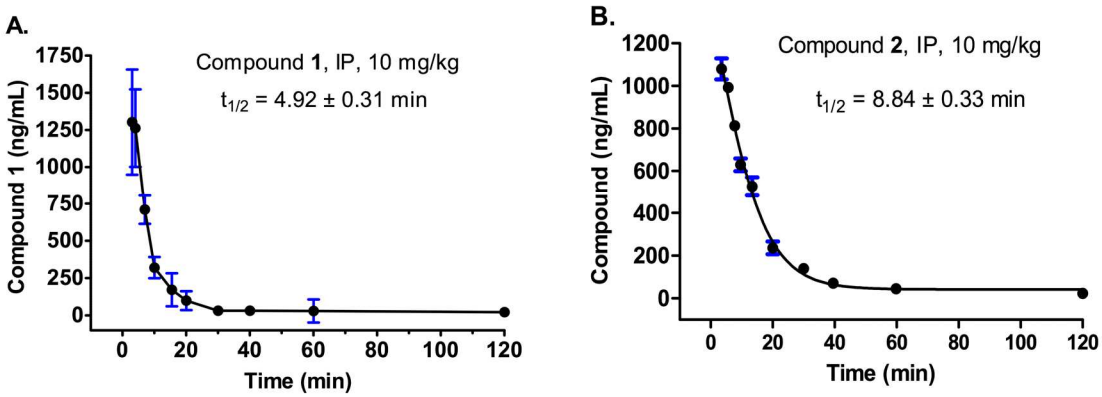

Figure 3-26a and b. Graph of pharmacokinetic study on plasma compound concentration (ng/mL) vs. time (min) for compound 1 (A.) and compound 2 (B).

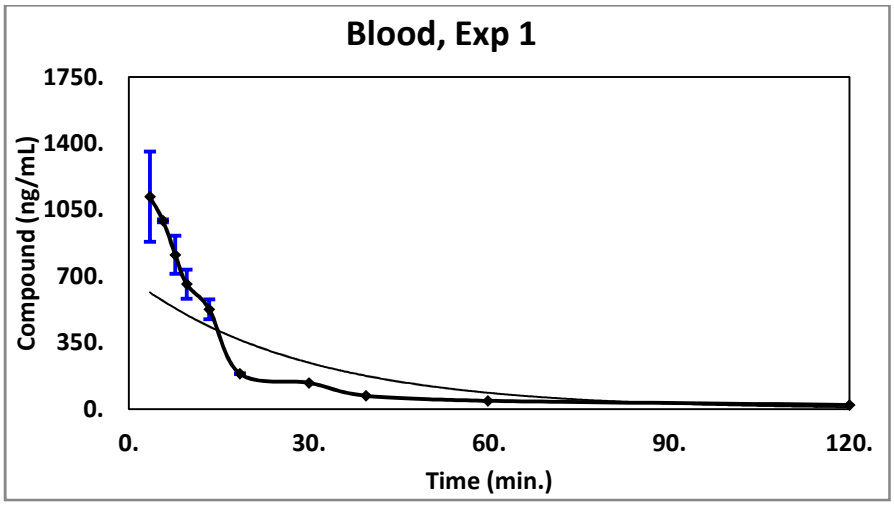

Figure 3-27a. Graph of pharmacokinetic study on plasma compound concentration (ng/mL) vs. time (min), experiment 1.

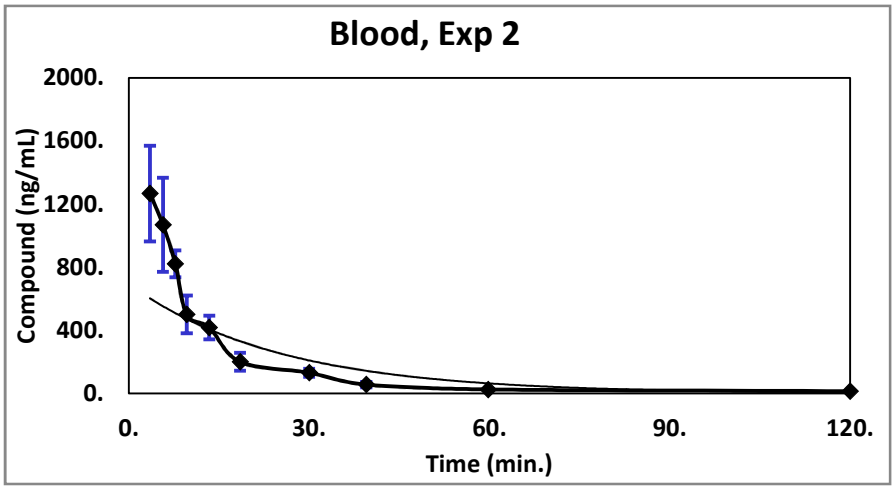

Figure 3-27b. Graph of pharmacokinetic study on plasma compound concentration (ng/mL) vs. time (min), experiment 2.

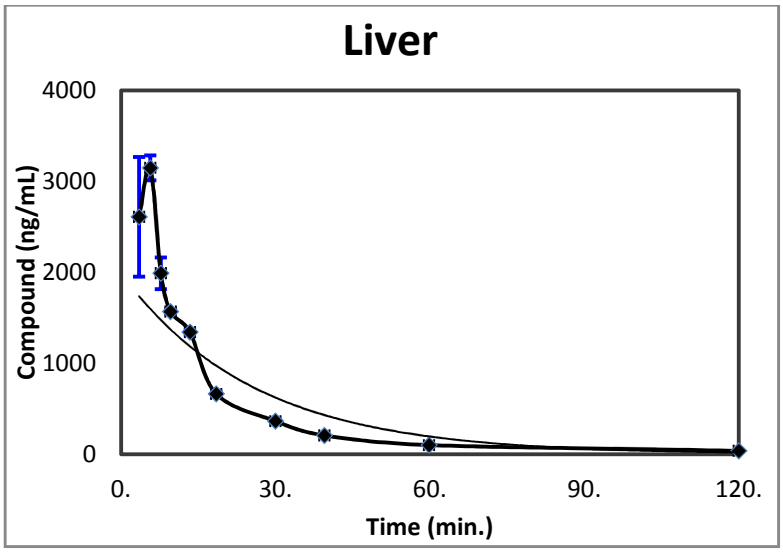

Figure 3-28. Graph of pharmacokinetic study on liver compound concentration (ng/mL) vs. time (min).

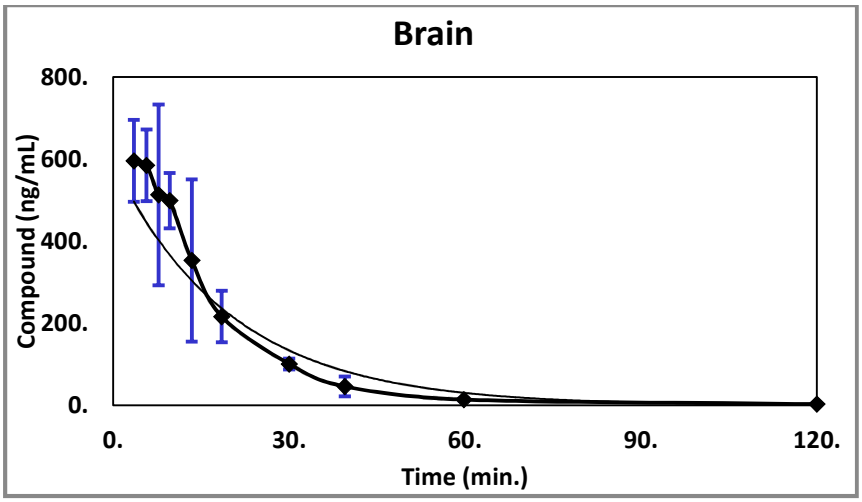

Figure 3-29. Graph of pharmacokinetic study on brain compound concentration (ng/mL) vs. time (min).

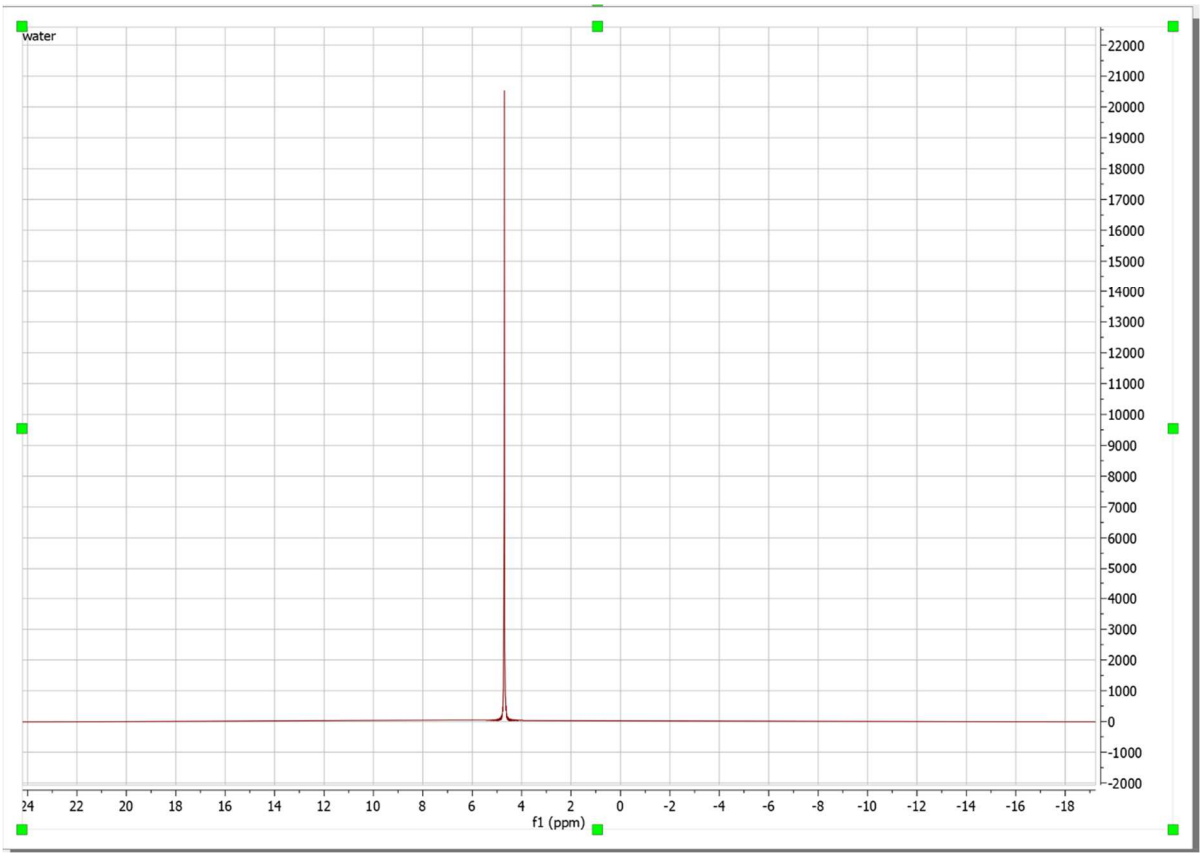

Figure 3-30. An NMR spectrum of a water peak injected into the NMR instrument and analyzed at 62 scans.

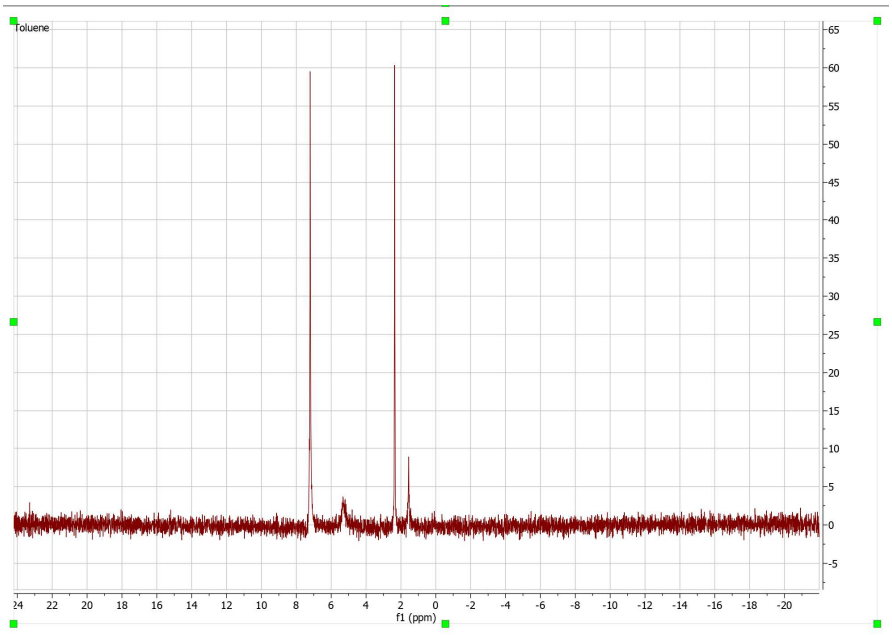

Figure 3-31a. An NMR spectrum of a 10 mM sample of toluene in deuterated chloroform injected into the NMR instrument and analyzed at 62 scans.

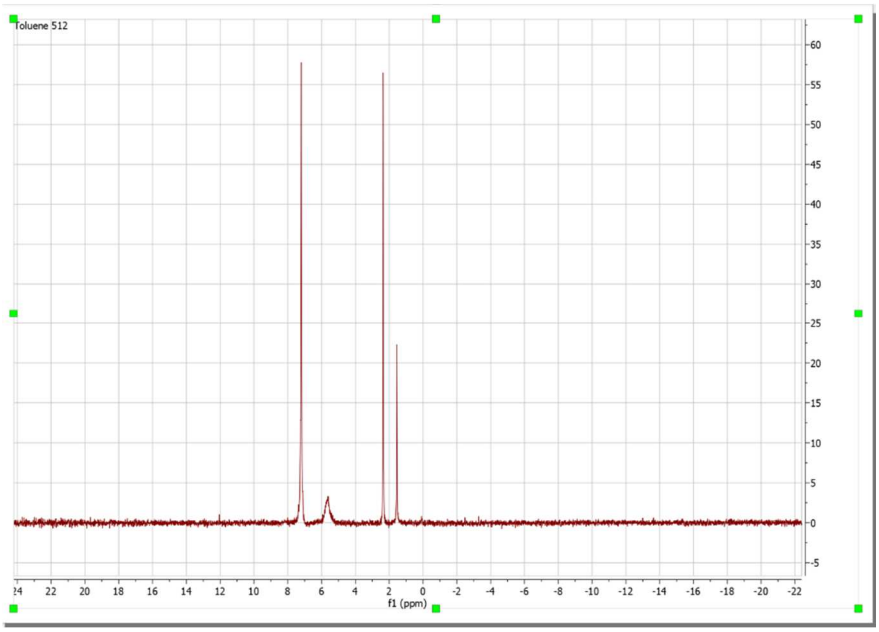

Figure 3-31b. An NMR spectrum of a 10 mM sample of toluene injected into the NMR instrument and analyzed at 512 scans.

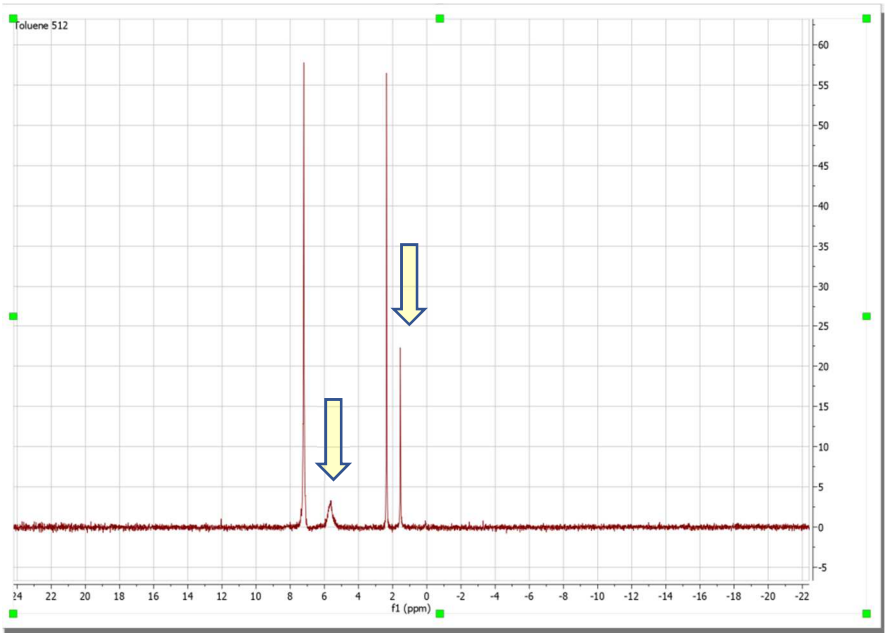

Figure 3-32. An NMR spectrum (512 scans) of toluene (10 mM) in chloroform with two impurities defined.

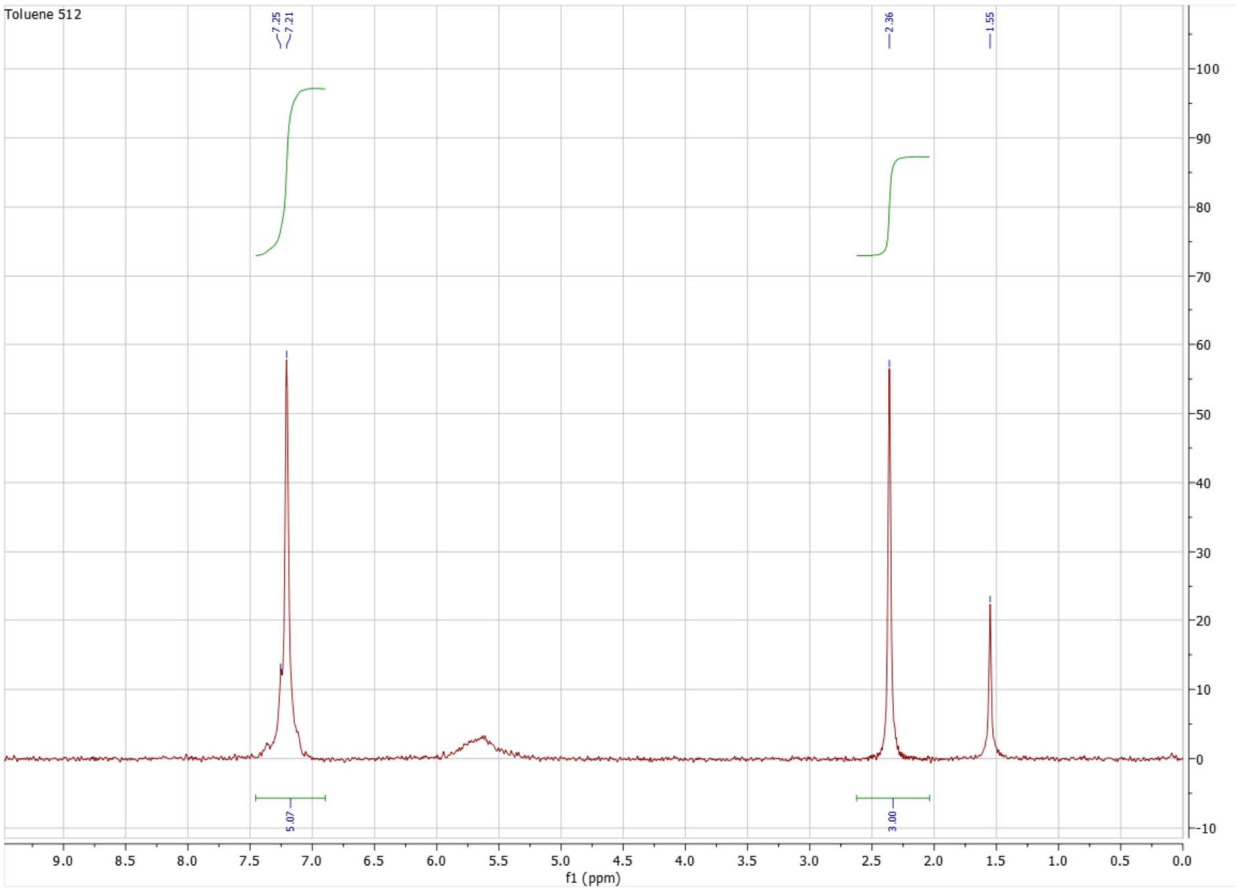

Figure 3-33. An integrated NMR spectrum (512 cans) of chloroform (10 mM) in toluene.

Table I. A table of H-NMR shifts for various solvents (*3*).

Table 1. ^{1}H NMR Data

	proton	mult	$CDCl_3$	$(CD_3)_2CO$	$(CD_3)_2SO$	C_6D_6	CD_3CN	CD_3OD	D_2O
solvent residual peak			7.26	2.05	2.50	7.16	1.94	3.31	4.79
H_2O		s	1.56	2.84[a]	3.33[a]	0.40	2.13	4.87	
acetic acid	CH_3	s	2.10	1.96	1.91	1.55	1.96	1.99	2.08
acetone	CH_3	s	2.17	2.09	2.09	1.55	2.08	2.15	2.22
acetonitrile	CH_3	s	2.10	2.05	2.07	1.55	1.96	2.03	2.06
benzene	CH	s	7.36	7.36	7.37	7.15	7.37	7.33	
tert-butyl alcohol	CH_3	s	1.28	1.18	1.11	1.05	1.16	1.40	1.24
	OH[c]	s			4.19	1.55	2.18		
tert-butyl methyl ether	CCH_3	s	1.19	1.13	1.11	1.07	1.14	1.15	1.21
	OCH_3	s	3.22	3.13	3.08	3.04	3.13	3.20	3.22
BHT[b]	ArH	s	6.98	6.96	6.87	7.05	6.97	6.92	
	OH[c]	s	5.01		6.65	4.79	5.20		
	$ArCH_3$	s	2.27	2.22	2.18	2.24	2.22	2.21	
	$ArC(CH_3)_3$	s	1.43	1.41	1.36	1.38	1.39	1.40	
chloroform	CH	s	7.26	8.02	8.32	6.15	7.58	7.90	
cyclohexane	CH_2	s	1.43	1.43	1.40	1.40	1.44	1.45	
1,2-dichloroethane	CH_2	s	3.73	3.87	3.90	2.90	3.81	3.78	
dichloromethane	CH_2	s	5.30	5.63	5.76	4.27	5.44	5.49	
diethyl ether	CH_3	t, 7	1.21	1.11	1.09	1.11	1.12	1.18	1.17
	CH_2	q, 7	3.48	3.41	3.38	3.26	3.42	3.49	3.56
diglyme	CH_2	m	3.65	3.56	3.51	3.46	3.53	3.61	3.67
	CH_2	m	3.57	3.47	3.38	3.34	3.45	3.58	3.61
	OCH_3	s	3.39	3.28	3.24	3.11	3.29	3.35	3.37
1,2-dimethoxyethane	CH_3	s	3.40	3.28	3.24	3.12	3.28	3.35	3.37
	CH_2	s	3.55	3.46	3.43	3.33	3.45	3.52	3.60
dimethylacetamide	CH_3CO	s	2.09	1.97	1.96	1.60	1.97	2.07	2.08
	NCH_3	s	3.02	3.00	2.94	2.57	2.96	3.31	3.06
	NCH_3	s	2.94	2.83	2.78	2.05	2.83	2.92	2.90
dimethylformamide	CH	s	8.02	7.96	7.95	7.63	7.92	7.97	7.92
	CH_3	s	2.96	2.94	2.89	2.36	2.89	2.99	3.01
	CH_3	s	2.88	2.78	2.73	1.86	2.77	2.86	2.85
dimethyl sulfoxide	CH_3	s	2.62	2.52	2.54	1.68	2.50	2.65	2.71
dioxane	CH_2	s	3.71	3.59	3.57	3.35	3.60	3.66	3.75
ethanol	CH_3	t, 7	1.25	1.12	1.06	0.96	1.12	1.19	1.17
	CH_2	q, 7[d]	3.72	3.57	3.44	3.34	3.54	3.60	3.65
	OH	s[c,d]	1.32	3.39	4.63		2.47		
ethyl acetate	CH_3CO	s	2.05	1.97	1.99	1.65	1.97	2.01	2.07
	CH_2CH_3	q, 7	4.12	4.05	4.03	3.89	4.06	4.09	4.14
	CH_2CH_3	t, 7	1.26	1.20	1.17	0.92	1.20	1.24	1.24
ethyl methyl ketone	CH_3CO	s	2.14	2.07	2.07	1.58	2.06	2.12	2.19
	CH_2CH_3	q, 7	2.46	2.45	2.43	1.81	2.43	2.50	3.18
	CH_2CH_3	t, 7	1.06	0.96	0.91	0.85	0.96	1.01	1.26
ethylene glycol	CH	s[e]	3.76	3.28	3.34	3.41	3.51	3.59	3.65
"grease"[f]	CH_3	m	0.86	0.87		0.92	0.86	0.88	
	CH_2	br s	1.26	1.29		1.36	1.27	1.29	
n-hexane	CH_3	t	0.88	0.88	0.86	0.89	0.89	0.90	
	CH_2	m	1.26	1.28	1.25	1.24	1.28	1.29	
HMPA[g]	CH_3	d, 9.5	2.65	2.59	2.53	2.40	2.57	2.64	2.61
methanol	CH_3	s[h]	3.49	3.31	3.16	3.07	3.28	3.34	3.34
	OH	s[c,h]	1.09	3.12	4.01		2.16		
nitromethane	CH_3	s	4.33	4.43	4.42	2.94	4.31	4.34	4.40
n-pentane	CH_3	t, 7	0.88	0.88	0.86	0.87	0.89	0.90	
	CH_2	m	1.27	1.27	1.27	1.23	1.29	1.29	
2-propanol	CH_3	d, 6	1.22	1.10	1.04	0.95	1.09	1.50	1.17
	CH	sep, 6	4.04	3.90	3.78	3.67	3.87	3.92	4.02
pyridine	CH(2)	m	8.62	8.58	8.58	8.53	8.57	8.53	8.52
	CH(3)	m	7.29	7.35	7.39	6.66	7.33	7.44	7.45
	CH(4)	m	7.68	7.76	7.79	6.98	7.73	7.85	7.87
silicone grease[i]	CH_3	s	0.07	0.13		0.29	0.08	0.10	
tetrahydrofuran	CH_2	m	1.85	1.79	1.76	1.40	1.80	1.87	1.88
	CH_2O	m	3.76	3.63	3.60	3.57	3.64	3.71	3.74
toluene	CH_3	s	2.36	2.32	2.30	2.11	2.33	2.32	
	CH(*o*/*p*)	m	7.17	7.1–7.2	7.18	7.02	7.1–7.3	7.16	
	CH(*m*)	m	7.25	7.1–7.2	7.25	7.13	7.1–7.3	7.16	
triethylamine	CH_3	t,7	1.03	0.96	0.93	0.96	0.96	1.05	0.99
	CH_2	q, 7	2.53	2.45	2.43	2.40	2.45	2.58	2.57

3.6 References

1. Introduction to LC-MS. https://www.shimadzu.com/an/hplc/support/lib/lctalk/47/47intro.html (accessed 4AD).
2. Skoog, D. A.; Holler, F. J.; Crouch, S. R. *Principles of instrumental analysis*; Cengage Learning: Boston, MA, 2018.
3. https://www.sisweb.com/mstools.htm (accessed 4AD).
4. Libretexts. Half-lives. https://chem.libretexts.org/Bookshelves/Physical_and_Theoretical_Chemistry_Textbook_Maps Supplemental_Modules_(Physical_and_Theoretical_Chemistry)/Kinetics/Reaction_Rates/Half-lives_and_Pharmacokinetics (accessed 4AD).
5. Scarfe, G. B.; Wilson, I. D.; Spraul, M.; Hofmann, M.; Braumann, U.; Lindon, J. C.; Nicholson, J. K. Application of directly coupled high-performance liquid chromatography-nuclear magnetic resonance-mass spectrometry to the detection and characterization of the metabolites of 2-bromo-4-(trifluoromethyl)aniline in rat urine. *Anal. Commun.* **1997**, *34*, 37-39.
6. Elipe, M. V. S. *LC-NMR and other hyphenated NMR techniques overview and applications*; Wiley: Hoboken, NJ, 2012.
7. Corcoran, O.; Spraul, M. LC–NMR–MS in Drug Discovery. *Drug Discovery Today* **2003**, *8* (14), 624–631.
8. Down, S. A Primer on LC/NMR/MS. https://www.spectroscopynow.com/details/education/sepspec10145education/A-Primer on-LCNMRMS.html?1,1=& (accessed Nov 11, 2019).
9. Tabei, K.; Siegel, M. M. 47th ASMS Conference on Mass Spectrometry, 1999, Dallas, TX, June 13-17, 1999, NO 234.
10. Watanabe, N.; Niki, E. Direct-Coupling of FT-NMR to High Performance Liquid Chromatography, *Proc. Jpn. Acad. Ser. B. Phys. Biol. Sci.* **1978**, *54* 194–199.
11. Haw, J.; Glass, T.; Dorn, H. Continuous Flow High Field Nuclear Magnetic Resonance Detector for Liquid Chromatographic Analysis of Fuel Samples. *Analytical Chemistry* **1981**, *53* (14), 2327–2332.
12. Laude, D.; Wilkins, C. Direct-Linked Analytical Scale High-Performance Liquid Chromatography/Nuclear Magnetic Resonance Spectrometry. *Analytical Chemistry* **1984**, *56* (13), 2471–2475.
13. Subramanian, R.; Kelley, W. P.; Floyd, P. D.; Tan, Z. J.; Webb, A. G.; Sweedler, J. V. A Microcoil NMR Probe for Coupling Microscale HPLC with On-Line NMR Spectroscopy, *Anal. Chem.* **1999**, *71*, 5335–5339.
14. Andes, D.; Marchillo, K.; Stamstad, T.; Conklin, R. In Vivo Pharmacokinetics and Pharmacodynamics of a New Triazole, Voriconazole, in a Murine Candidiasis Model. *Antimicrobial Agents and Chemotherapy* **2003**, *47* (10), 3165–3169.

CHAPTER 4. CONCLUSION

There were several objectives of this thesis. The first was to successfully ionize the halogenated compounds in order to characterize them by mass spectrometry (MS) (single quadrupole). This allows for the compound to be confirmed during the synthesis process and allows for the quantification of the compound in later stages of research and development. The second goal included the quantification of a drug compound which included an animal study, assay development, and finally the optimization of MS/MS instrument parameters (triple quadrupole).

To achieve efficient ionization of the halogenated alkylating agents, electrospray ionization (ESI), atmospheric pressure chemical ionization (APCI), and dual mode ionization combining the two ionization modes (DUIS) were applied. It was determined that efficient ionization and highest signal intensity were obtained for the compounds when APCI mode was set at an optimized corona needle position of 10 mm. This work suggested that these halogenated alkylating agents could be best analyzed using APCI ionization mode and at the optimized instrumental conditions. Finally, we successfully analyzed compounds **3-10** by mass spectrometry.

For the pharmacokinetic study, we first optimized the instrument parameters for signal intensity and established calibration curve for the proceeding studies. Then, we carried out an in-vitro stability assay where the samples were quantitatively characterized by MS/MS. Compound **2** showed a $t_{1/2}$ of 77.06 min in the presence of human microsomes and a $t_{1/2}$ of 33.00 min in the presence of mouse microsomes.

Followed by microsome stability study, we determined pharmacokinetic parameters of compound **2**. The mice were injected with compound **2** at different time point, sacrificed, and their blood, liver, and brain organs harvested. The organs were then homogenized, samples processed, and quantified by MS/MS. Our data showed that introduction of a CH_3 group (**2)** greatly increased the duration time of the drug in the plasma with a $t_{1/2}$ of 8.84 min, which is almost two times that of the parent compound **1** ($t_{1/2}$ = 4.92 min). The rate of elimination for **1** (E_{rate} = 0.141 min^{-1}) in the blood is faster that of **2** (E_{rate} = 0.078 min^{-1}). Compound **2** showed an area under the curve (AUC) of 16253 ng•min/mL, which is significantly higher than that of **1** (10883 ng•min/mL). The half-life of compound **2** in mice liver and brain is 17.769 min and 13.86 min, respectively.

Future work includes modification of the parent compound **2** by introducing more lipophilic substituents to further improve the in vivo duration time and characterization of modified compounds with MS, including pharmacokinetic assays and quantifications. The pharmacokinetic data of compound **2** indicated a relatively high concentration of the compound in mice brain, which suggested that **2** is able to cross the blood brain barrier (BBB). Thus, **2** can be a potential candidate for further research towards brain cancers, including glioblastoma. We would also consider tissue imaging through MS-imaging methods such as MALDI (matrix assisted laser desorption ionization) imaging to better understand the drug distribution in different organs as well as to apply quantifiable measurements to determine drug distribution within different tissue samples.